

5-2019

# Multi-Scale, Multi-Criteria Design of Meta-Materials with Offset Periodicity

Rushabh Rajesh Sadiwala

Clemson University, rsadiwala95@gmail.com

Follow this and additional works at: [https://tigerprints.clemson.edu/all\\_theses](https://tigerprints.clemson.edu/all_theses)

---

## Recommended Citation

Sadiwala, Rushabh Rajesh, "Multi-Scale, Multi-Criteria Design of Meta-Materials with Offset Periodicity" (2019). *All Theses*. 3056.  
[https://tigerprints.clemson.edu/all\\_theses/3056](https://tigerprints.clemson.edu/all_theses/3056)

This Thesis is brought to you for free and open access by the Theses at TigerPrints. It has been accepted for inclusion in All Theses by an authorized administrator of TigerPrints. For more information, please contact [kokeefe@clemson.edu](mailto:kokeefe@clemson.edu).

MULTI-SCALE, MULTI-CRITERIA DESIGN OF META-MATERIALS  
WITH OFFSET PERIODICITY

---

A Thesis  
Presented to  
the Graduate School of  
Clemson University

---

In Partial Fulfillment  
of the Requirements for the Degree  
Master of Science  
Mechanical Engineering

---

by  
Rushabh Rajesh Sadiwala  
May 2019

---

Accepted by:  
Dr. Georges Fadel, Committee Chair  
Dr. Gang Li  
Dr. Nicole Coutris

# Abstract

Meta-materials are a class of artificial materials with a wide range of bulk properties, completely different from the base material they are made of. Some notable examples include negative Poisson's ratio materials, materials designed for specific electromagnetic, acoustic, or thermal properties. The term meta-material in the context of this research refers to a continuous, heterogeneous structure with prescribed elastic properties. Such meta-materials are designed using Topology Optimization (TO). Tools like SIMP interpolation, mesh filtering and continuation methods are used to address the numerical issues with Topology Optimization.

The most popular tool to design such materials is Asymptotic Homogenization. However, it has its limitations. Homogenization requires the meta-material to obey periodicity and scaling requirements. Dr. Chris Czech in his Ph.D. dissertation proposes a way to design meta-materials that may, due to manufacturing limitations, break the scaling requirements. Using Volume Averaging, he designs thin-layered meta-materials for use in the shear beam of a non-pneumatic wheel. By offsetting the said meta-material layers by a half-width of the Unit Cell, auxetic honeycomb-like geometry was obtained. This was the first time such a shape was observed as the result of Topology Optimization targeting the effective shear modulus.

This research will further study the offset periodicity by considering offsets other than just zero or half-widths. The same shear beam of a non-pneumatic wheel is designed using such offsets.

The optimization formulations in literature and the ones proposed by Dr. Czech

have been extensively studied and used for single-criteria design problems. This research demonstrates the use of those formulations for the design of meta-materials with multiple prescribed elastic properties, such as prescribed behaviors in shear and in tension or compression.

This research also identifies a possible physical limitation in the combinations of elastic properties that can be achieved for meta-materials when designed using Topology Optimization.

# Dedication

To my parents for their constant love and support.

# Acknowledgments

I would like to thank my parents, Sunita and Rajesh Sadiwala for their constant support both in my education and my life. I would like to thank my friends and family for their support outside my research work.

A special thanks for my advisor Dr. Georges Fadel, for imparting his knowledge and constant guidance throughout my entire research. A special thanks to Dr. Nicole Coutris and Dr. Gang Li for acting as my co-advisors. Thanks to Dr. Li for helping me with his expertise in Finite Element Analysis and other numerical methods, and Thanks to Dr. Coutris for helping me with her expertise in Continuum Mechanics and Elasticity Theory.

Thank You, Clemson University for the generous allotment of resources and computation time on your High Performance Computing(HPC) platform, the Palmetto Cluster. This research would not have been possible without access to it.

# Table of Contents

<b>Title Page</b> . . . . .	<b>i</b>
<b>Abstract</b> . . . . .	<b>ii</b>
<b>Dedication</b> . . . . .	<b>iv</b>
<b>Acknowledgments</b> . . . . .	<b>v</b>
<b>List of Tables</b> . . . . .	<b>viii</b>
<b>List of Figures</b> . . . . .	<b>xii</b>
<b>1 Introduction</b> . . . . .	<b>1</b>
1.1 Meta-Material Design using Topology Optimization . . . . .	1
1.2 Numerical Issues with Topology Optimization . . . . .	8
1.3 Asymptotic Homogenization (Homogenization) . . . . .	13
1.4 Field Homogenization (Volume Averaging) . . . . .	15
<b>2 Motivation and Research Questions</b> . . . . .	<b>20</b>
2.1 Hypothesis and Research Questions . . . . .	22
<b>3 Meta-materials with Offset Periodicity</b> . . . . .	<b>24</b>
3.1 Overview of the Problem . . . . .	26
3.2 Comparison between Volume Averaging and Homogenization for Offset Pe- riodicity . . . . .	29
3.3 Example Optimization for Different Offsets . . . . .	32
3.4 Optimization of the Shear Beam for a Pon-Pneumatic Wheel . . . . .	53
3.5 Summary . . . . .	67
<b>4 Multi-criteria design of meta-materials</b> . . . . .	<b>68</b>
4.1 Optimization Formulation Studies . . . . .	68
4.2 Range of Obtainable Moduli . . . . .	78
4.3 Summary . . . . .	85
<b>5 Concluding Remarks</b> . . . . .	<b>87</b>
5.1 Answering Research Questions . . . . .	87
5.2 Contributions . . . . .	89

5.3 Future Research . . . . .	89
<b>Appendices . . . . .</b>	<b>92</b>
<b>A Code Development and Validation . . . . .</b>	<b>93</b>
A.1 Program development . . . . .	93
A.2 Validation of Modulus for non-offset Meta-Materials. . . . .	95
A.3 Validation of Modulus for offset Meta-Materials. . . . .	96
<b>B Geometric Results - Shear Beam of a Non-Pneumatic Wheel . . . . .</b>	<b>99</b>
<b>C Numerical Results - Shear Beam of a Non-Pneumatic Wheel . . . . .</b>	<b>132</b>
<b>References . . . . .</b>	<b>148</b>



# List of Tables

3.1	Numerical results for $E_{11}^t = 3$ GPa using volume averaging analysis for RVE containing 6x2 unit cells . . . . .	32
3.2	Numerical results for $E_{11}^t = 9$ GPa using volume averaging analysis for RVE containing 6x2 unit cells . . . . .	33
3.3	Numerical results for $E_{11}^t = 15$ GPa using volume averaging analysis for RVE containing 6x2 unit cells . . . . .	34
3.4	Numerical results for $E_{11}^t = 21$ GPa using volume averaging analysis for RVE containing 6x2 unit cells . . . . .	35
3.5	Graphical results when targeting normal moduli, using volume averaging analysis for RVE containing 6x2 unit cells. . . . .	36
3.6	Numerical results for $E_{12}^t = 1$ GPa using volume averaging analysis for RVE containing 6x2 unit cells . . . . .	37
3.7	Numerical results for $E_{12}^t = 4$ GPa using volume averaging analysis for RVE containing 6x2 unit cells . . . . .	38
3.8	Numerical results for $E_{12}^t = 5$ GPa using volume averaging analysis for RVE containing 6x2 unit cells . . . . .	39
3.9	Numerical results for $E_{12}^t = 7$ GPa using volume averaging analysis for RVE containing 6x2 unit cells . . . . .	40
3.10	Graphical results when targeting shear moduli, using volume averaging analysis for RVE containing 6x2 unit cells. . . . .	41
3.11	Numerical results for $E_{11}^t = 3$ GPa using volume averaging analysis for RVE containing 3x3 unit cells . . . . .	42
3.12	Numerical results for $E_{11}^t = 9$ GPa using volume averaging analysis for RVE containing 3x3 unit cells . . . . .	43
3.13	Numerical results for $E_{11}^t = 15$ GPa using volume averaging analysis for RVE containing 3x3 unit cells . . . . .	44
3.14	Numerical results for $E_{11}^t = 21$ GPa using volume averaging analysis for RVE containing 3x3 unit cells . . . . .	45
3.15	Graphical results when targeting normal moduli, using volume averaging analysis for RVE containing 3x3 unit cells. . . . .	46
3.16	Numerical results for $E_{12}^t = 1$ GPa using volume averaging analysis for RVE containing 3x3 unit cells . . . . .	47
3.17	Numerical results for $E_{12}^t = 4$ GPa using volume averaging analysis for RVE containing 3x3 unit cells . . . . .	48
3.18	Numerical results for $E_{12}^t = 5$ GPa using volume averaging analysis for RVE containing 3x3 unit cells . . . . .	49

3.19	Numerical results for $E_{12}^t = 7$ GPa using volume averaging analysis for RVE containing 3x3 unit cells . . . . .	50
3.20	Graphical results when targeting shear moduli, using volume averaging analysis for RVE containing 3x3 unit cells. . . . .	51
3.21	Optimization results for $sl_{Thk} = 6$ mm, initial point A. . . . .	57
3.22	Optimization results for $sl_{Thk} = 7$ mm, initial point A. . . . .	58
3.23	Optimization results for $sl_{Thk} = 12$ mm, initial point A. . . . .	59
3.24	Optimization results for $sl_{Thk} = 5$ mm, initial point B. . . . .	60
3.25	Optimization results for $sl_{Thk} = 7$ mm, initial point B. . . . .	61
3.26	Optimization results for $sl_{Thk} = 8$ mm, initial point B. . . . .	62
3.27	Optimization results for $sl_{Thk} = 12$ mm, initial point B. . . . .	63
3.28	Optimization results for $sl_{Thk} = 5$ mm, initial point C. . . . .	64
3.29	Optimization results for $sl_{Thk} = 8$ mm, initial point C. . . . .	65
4.1	Numerical results for multi-criteria design, formulation 1, using Homogenization	70
4.2	Numerical results for multi-criteria design, formulation 2, $\delta = 0.1$ , using Homogenization . . . . .	70
4.3	Numerical results for multi-criteria design, formulation 2, $\delta = 1$ , using Homogenization . . . . .	71
4.4	Numerical results for multi-criteria design, formulation 2, $\delta = 10$ , using Homogenization . . . . .	71
4.5	Graphical results for multi-criteria design, formulation 1, using Homogenization	72
4.6	Graphical results for multi-criteria design, formulation 2, $\delta = 0.1$ , using Homogenization . . . . .	72
4.7	Graphical results for multi-criteria design, formulation 2, $\delta = 1$ , using Homogenization . . . . .	73
4.8	Graphical results for multi-criteria design, formulation 2, $\delta = 10$ , using Homogenization . . . . .	73
4.9	Numerical results for multi-criteria design, formulation 1, using Volume Averaging . . . . .	74
4.10	Numerical results for multi-criteria design, formulation 2, $\delta = 0.1$ , using Volume Averaging . . . . .	74
4.11	Numerical results for multi-criteria design, formulation 2, $\delta = 1$ , using Volume Averaging . . . . .	75
4.12	Numerical results for multi-criteria design, formulation 2, $\delta = 10$ , using Volume Averaging . . . . .	75
4.13	Graphical results for multi-criteria design, formulation 1, using Volume Averaging . . . . .	76
4.14	Graphical results for multi-criteria design, formulation 2, $\delta = 0.1$ , using Volume Averaging . . . . .	76
4.15	Graphical results for multi-criteria design, formulation 2, $\delta = 1$ , using Volume Averaging . . . . .	77
4.16	Graphical results for multi-criteria design, formulation 2, $\delta = 10$ , using Volume Averaging . . . . .	77

A.1	Relative difference between displacements for meta-material and corresponding homogeneous material . . . . .	98
B.1	Optimization results for $sl_{Thk} = 5$ mm, initial point A. . . . .	100
B.2	Optimization results for $sl_{Thk} = 6$ mm, initial point A. . . . .	101
B.3	Optimization results for $sl_{Thk} = 7$ mm, initial point A. . . . .	102
B.4	Optimization results for $sl_{Thk} = 8$ mm, initial point A. . . . .	103
B.5	Optimization results for $sl_{Thk} = 9$ mm, initial point A. . . . .	104
B.6	Optimization results for $sl_{Thk} = 10$ mm, initial point A. . . . .	105
B.7	Optimization results for $sl_{Thk} = 11$ mm, initial point A. . . . .	106
B.8	Optimization results for $sl_{Thk} = 12$ mm, initial point A. . . . .	107
B.9	Optimization results for $sl_{Thk} = 5$ mm, initial point B. . . . .	108
B.10	Optimization results for $sl_{Thk} = 6$ mm, initial point B. . . . .	109
B.11	Optimization results for $sl_{Thk} = 7$ mm, initial point B. . . . .	110
B.12	Optimization results for $sl_{Thk} = 8$ mm, initial point B. . . . .	111
B.13	Optimization results for $sl_{Thk} = 9$ mm, initial point B. . . . .	112
B.14	Optimization results for $sl_{Thk} = 10$ mm, initial point B. . . . .	113
B.15	Optimization results for $sl_{Thk} = 11$ mm, initial point B. . . . .	114
B.16	Optimization results for $sl_{Thk} = 12$ mm, initial point B. . . . .	115
B.17	Optimization results for $sl_{Thk} = 5$ mm, initial point C. . . . .	116
B.18	Optimization results for $sl_{Thk} = 6$ mm, initial point C. . . . .	117
B.19	Optimization results for $sl_{Thk} = 7$ mm, initial point C. . . . .	118
B.20	Optimization results for $sl_{Thk} = 8$ mm, initial point C. . . . .	119
B.21	Optimization results for $sl_{Thk} = 9$ mm, initial point C. . . . .	120
B.22	Optimization results for $sl_{Thk} = 10$ mm, initial point C. . . . .	121
B.23	Optimization results for $sl_{Thk} = 11$ mm, initial point C. . . . .	122
B.24	Optimization results for $sl_{Thk} = 12$ mm, initial point C. . . . .	123
B.25	Optimization results for $sl_{Thk} = 5$ mm, initial point D. . . . .	124
B.26	Optimization results for $sl_{Thk} = 6$ mm, initial point D. . . . .	125
B.27	Optimization results for $sl_{Thk} = 7$ mm, initial point D. . . . .	126
B.28	Optimization results for $sl_{Thk} = 8$ mm, initial point D. . . . .	127
B.29	Optimization results for $sl_{Thk} = 9$ mm, initial point D. . . . .	128
B.30	Optimization results for $sl_{Thk} = 10$ mm, initial point D. . . . .	129
B.31	Optimization results for $sl_{Thk} = 11$ mm, initial point D. . . . .	130
B.32	Optimization results for $sl_{Thk} = 12$ mm, initial point D. . . . .	131
C.1	Numerical results for $sl_{Thk} = 5$ mm, initial point A. . . . .	132
C.2	Numerical results for $sl_{Thk} = 6$ mm, initial point A. . . . .	133
C.3	Numerical results for $sl_{Thk} = 7$ mm, initial point A. . . . .	133
C.4	Numerical results for $sl_{Thk} = 8$ mm, initial point A. . . . .	134
C.5	Numerical results for $sl_{Thk} = 9$ mm, initial point A. . . . .	134
C.6	Numerical results for $sl_{Thk} = 10$ mm, initial point A. . . . .	135
C.7	Numerical results for $sl_{Thk} = 11$ mm, initial point A. . . . .	135
C.8	Numerical results for $sl_{Thk} = 12$ mm, initial point A. . . . .	136
C.9	Numerical results for $sl_{Thk} = 5$ mm, initial point B. . . . .	136

C.10 Numerical results for $sl_{Thk} = 6$ mm, initial point B. . . . .	137
C.11 Numerical results for $sl_{Thk} = 7$ mm, initial point B. . . . .	137
C.12 Numerical results for $sl_{Thk} = 8$ mm, initial point B. . . . .	138
C.13 Numerical results for $sl_{Thk} = 9$ mm, initial point B. . . . .	138
C.14 Numerical results for $sl_{Thk} = 10$ mm, initial point B. . . . .	139
C.15 Numerical results for $sl_{Thk} = 11$ mm, initial point B. . . . .	139
C.16 Numerical results for $sl_{Thk} = 12$ mm, initial point B. . . . .	140
C.17 Numerical results for $sl_{Thk} = 5$ mm, initial point C. . . . .	140
C.18 Numerical results for $sl_{Thk} = 6$ mm, initial point C. . . . .	141
C.19 Numerical results for $sl_{Thk} = 7$ mm, initial point C. . . . .	141
C.20 Numerical results for $sl_{Thk} = 8$ mm, initial point C. . . . .	142
C.21 Numerical results for $sl_{Thk} = 9$ mm, initial point C. . . . .	142
C.22 Numerical results for $sl_{Thk} = 10$ mm, initial point C. . . . .	143
C.23 Numerical results for $sl_{Thk} = 11$ mm, initial point C. . . . .	143
C.24 Numerical results for $sl_{Thk} = 12$ mm, initial point C. . . . .	144
C.25 Numerical results for $sl_{Thk} = 5$ mm, initial point D. . . . .	144
C.26 Numerical results for $sl_{Thk} = 6$ mm, initial point D. . . . .	145
C.27 Numerical results for $sl_{Thk} = 7$ mm, initial point D. . . . .	145
C.28 Numerical results for $sl_{Thk} = 8$ mm, initial point D. . . . .	146
C.29 Numerical results for $sl_{Thk} = 9$ mm, initial point D. . . . .	146
C.30 Numerical results for $sl_{Thk} = 10$ mm, initial point D. . . . .	147
C.31 Numerical results for $sl_{Thk} = 11$ mm, initial point D. . . . .	147
C.32 Numerical results for $sl_{Thk} = 12$ mm, initial point D. . . . .	148

# List of Figures

1.1	Compliant design of a beam using Topology Optimization . . . . .	1
1.2	Topology Optimization of a Cantilever Beam in a 3D domain . . . . .	2
1.3	Meta-Material Design Process . . . . .	3
1.4	Periodicity conditions require functions to be identical at each point P in the domain . . . . .	4
1.5	Micro-cells with rectangular holes . . . . .	5
1.6	Micro-cells with layered materials . . . . .	5
1.7	Solutions of minimum compliant cantilever beam problem for different penalties	6
1.8	Numerical Issues with Topology Optimization . . . . .	9
1.9	Defined neighborhood for mesh-filtering . . . . .	10
1.10	Local Design Domain for Homogenization . . . . .	13
1.11	Representative Volume Element (RVE) . . . . .	16
1.12	Single/Multiple Unit Cells deformed in normal loading using displacement(top) and traction(bottom) BCs . . . . .	17
1.13	Single/Multiple Unit Cells deformed in shear loading using displacement(top) and traction(bottom) BCs . . . . .	18
1.14	A meta-material which violates the homogenization requirements in the vertical direction . . . . .	19
2.1	Example meso-structures using parallelogram unit cells . . . . .	21
2.2	Left: Regular periodic unit cells; Right: Irregular periodic unit cells . . . .	21
3.2	Meta-material designed using square unit cells offset by their half-widths . .	24
3.1	Meta-materials designed using parallelogram unit cells for different parallelogram angles $\alpha$ . . . . .	25
3.3	Square UC w/ offset tessellation . . . . .	26
3.4	RUC with modified offset periodicity conditions in the three modes of deformation: Tension in $Y_2$ , Tension in $Y_1$ and Shear . . . . .	27
3.5	Rectangular RVE generated using partial unit cells . . . . .	28
3.6	RVE with modified offset periodicity in the three modes of deformation, with the original shape shown in red . . . . .	28
3.7	Geometry A, for comparison between Homogenization and Volume Averaging for Offset Meta-Materials . . . . .	30
3.8	Normalized moduli for geometry A . . . . .	30
3.9	Comparison between homogenization and volume averaging for geometry A	30

3.10	Geometry B, for comparison between Homogenization and Volume Averaging for Offset Meta-Materials . . . . .	31
3.11	Normalized moduli for geometry B . . . . .	31
3.12	Comparison between homogenization and volume averaging for geometry B . . . . .	31
3.13	Two-level optimization process used for meta-material design of the shear beam of the non-pneumatic wheel . . . . .	53
3.14	Solution to the top-level optimization for design of the shear beam of the non-pneumatic wheel . . . . .	54
3.15	Different initial points used for the Topology Optimization of the shear beam of the non-pneumatic wheel . . . . .	55
3.16	Selected solutions to Topology Optimization of the shear beam of the non-pneumatic wheel as produced by Dr. Czech . . . . .	56
4.1	Bounds on the Elastic and Shear Moduli . . . . .	79
4.2	Bounds on moduli, plotted against each other . . . . .	79
4.3	Obtained bounds for 20x20 mesh, 3x3 UCs, 0 offset problem . . . . .	81
4.4	Obtained bounds for different mesh sizes . . . . .	82
4.5	Elastic modulus for different RVEs (NxN), as calculated by Dr. czech . . . . .	83
4.6	Obtained bounds for different RVEs (NxN) . . . . .	84
4.7	Obtained bounds for different RVEs . . . . .	84
4.8	Obtained bounds for different offsets . . . . .	85
A.1	Flow of data between Matlab's fmincon, volume and analysis functions. . . . .	94
A.2	Geometry evaluated [1] . . . . .	95
A.3	Validation analysis for elastic modulus; here $d_E$ is the vertical displacement of the top edge . . . . .	96
A.4	Validation analysis for shear modulus; here $d_S$ is the horizontal displacement of the top edge . . . . .	97

# Chapter 1

## Introduction

### 1.1 Meta-Material Design using Topology Optimization

Topology Optimization (TO) is a structural optimization tool used to find the optimal distribution of material in a design space subjected to certain stimuli (such as structural loading, heat input, electromagnetic field etc.). Topology Optimization helps to solve a broad set of design problems from different engineering disciplines.

The most common problems are minimum compliance and minimum weight problems. Other problems include maximum heat transfer rate, maximum porosity, etc. Figures 1.1 and 1.2 show compliant design of some structures using topology optimization [2].

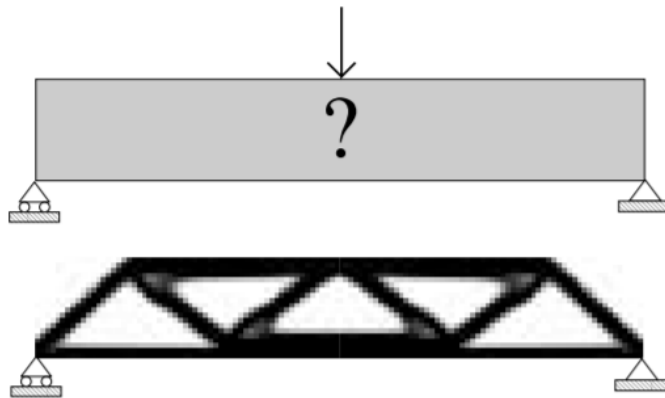


Figure 1.1: Compliant design of a beam using Topology Optimization [2]

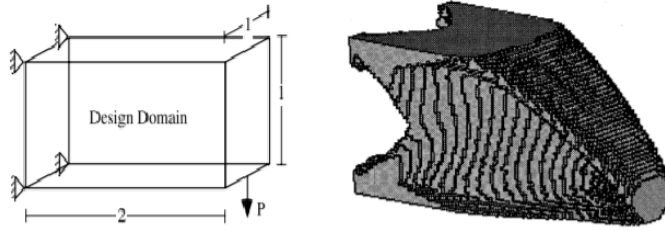


Figure 1.2: Topology Optimization of a Cantilever Beam in a 3D domain [3]

Meta-material design is one such problem that can be solved using topology optimization. Meta-materials are a class of artificial materials which are designed to achieve a set of properties which are very different from the base material they are made of. Such meta-materials can also achieve properties which are not found in any traditional, homogeneous material. The term “Meta-Material” was first used by Rodger M. Walser in 2001 to describe the design of materials with electromagnetic properties beyond those of natural or conventional composite materials [4]. In the context of this research, meta-materials are heterogeneous, periodic structures, designed to achieve a specific elastic behavior. For example, meta-materials can be designed to mimic the elastic behavior of elastomers such as rubber, without their hysteretic loss effect [5].

Meta-material design is a two-step optimization problem with the overall objective of optimizing the material distribution in a design space to achieve a global objective such as minimum compliance or minimum weight, while subjected to the loads and constraints of the system.

The first step optimizes the system in which the meta-material is to be used. The system optimization problem is typically a standard minimum compliance or minimum weight problem, where a homogeneous material with properties  $E_{ij}^*$ , is used in place of the meta-material. The properties  $E_{ij}^*$  are optimized to achieve the objectives and constraints of the system optimization problem.

The second step uses topology optimization to find the optimal material distribution with  $E_{ij}^*$  as its effective elastic behavior. This research primarily focuses on the second step of the meta-material design process.



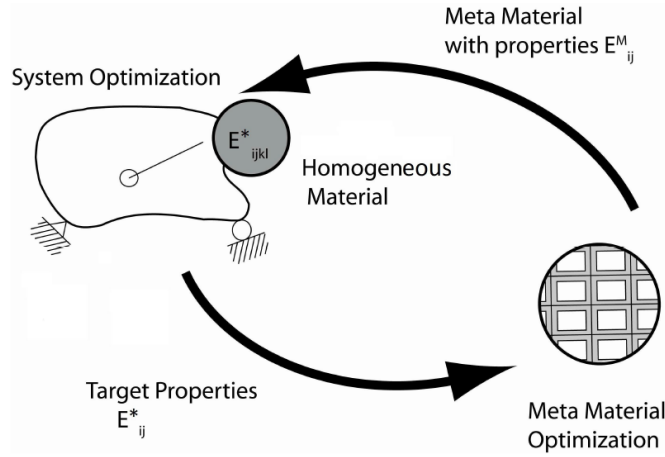


Figure 1.3: Meta-Material Design Process [6]

Meta-material design typically uses the mathematical Asymptotic Homogenization theory to evaluate the effective elastic property ( $E_{ij}^M$ ) of a given meta-material. The assumptions of the mathematical tool require the meta-material to be  $Y$ -periodic, where the domain  $Y$ , is far smaller in size than the global design space. This limits the applicability of asymptotic homogenization in the design of meta-material components.

Field homogenization, also called Volume Averaging is another analytical tool that can be used to evaluate the elastic properties of a material distribution. Volume averaging was originally developed to evaluate the global properties of composite materials. It was previously demonstrated by Chris Czech that this tool can be used to solve meta-material design problems where asymptotic homogenization could not be used [6], such as when the domain is not  $Y$ -periodic (non-simple or offset geometry), and when designing a meta-material outside the scaling limit of asymptotic homogenization.

The design domain  $Y$  is said to be  $Y$ -periodic if some physical property of the domain follows the periodicity equation within the domain:

$$f(x + nY_1 + mY_2) = f(x)$$

Where,

$x$  is the position of any given point in the design domain,

$n, m$  are arbitrary integers, and

$Y$  is the domain bound by the vectors  $Y_1$  and  $Y_2$

For meta-materials, the periodic function is the material tensors  $C_{ijkl}(x)$  at a given point  $x$ . This means  $C_{ijkl}$  at any point in the UC is equivalent to  $C_{ijkl}$  at the corresponding point in any other cell in the global design domain.

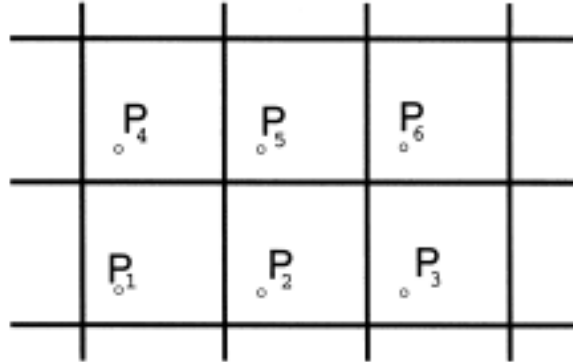


Figure 1.4: Periodicity conditions require functions to be identical at each point  $P$  in the domain [7].

To satisfy the  $Y$ -periodic conditions, the global design domain is discretized into smaller, periodic unit cells with the same material distribution. This discretization is known as the meso-structure of the design domain. The topological connectivity of the meso-structure can have a significant impact on the final optimized meta-material bulk behavior.

Each cell in the meso-structure is further discretized into a number of finite elements (referred as elements in this thesis). This discretization serves two purposes: firstly, this discretization will be used for any finite element analysis required for the evaluation of the meta-material, and lastly to approximate the density function.

A density function,  $\rho(x)$ , is used to quantify the material distribution. For simplicity, the density function is approximated as being constant within each element  $e$ . i.e.  $\rho(x) = \rho_e$ . The constant densities  $\rho_e$  are then chosen as the design variables for topology optimization.

A material model is required to translate these densities to a real physical quantity such as the elastic modulus. The three commonly used models are micro-cells with rectangular holes, layered materials, and artificial materials.

The micro-structure for the rectangular hole model consists of infinitesimal holes. The variables  $a(x)$  and  $b(x)$  define the size of the hole at point  $x$ . The densities  $\rho_e$  are then interpreted as a function of the size of the microscopic holes,  $\rho(a, b)$  [8].

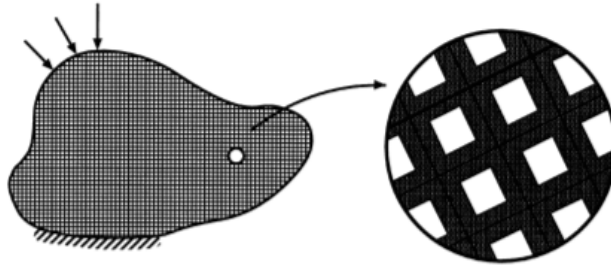


Figure 1.5: Micro-cells with rectangular holes [8].

The layered material model is made of infinitesimal layers of material and void, similar to the layers of a composite material. The variable  $\gamma$  defines the width of the material layer, and  $\theta$  defines the orientation of the layer. The densities  $\rho_e$  are interpreted as a function of the width and orientation of the material layer,  $\rho(\gamma, \theta)$  [8].

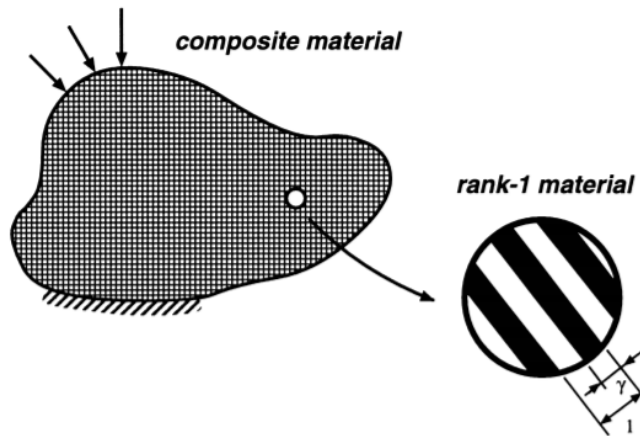


Figure 1.6: Micro-cells with layered materials [8].

For an artificial material model,  $\rho_e$  ranges from 0(void) to 1(material).  $\rho_e$  can be a discrete (black or white) or a continuous (gray) variable. A discrete design variable will require a discrete optimization such as integer programming, which is computationally costly and is NP-complete (no guaranteed convergence). Unlike in micro-cell models, intermediate

values of design variables lack any physical interpretation. Hence this model is called an "artificial" material model. A material interpolation scheme is required to translate the "artificial" variables to a real material property. In the context of this research, the densities  $\rho_e$  are translated into the elastic tensor  $C_e$  using Solid Isotropic Material with Penalization (SIMP) interpolation [9].

The elastic tensor of element  $e$ , is given by:

$$C_e = \rho_e^s \cdot C_0$$

Where,

$C_e$  is the material tensor for the element  $e$ .

$\rho_e$  is the artificial density for the element  $e$ .

$C_0$  is the material tensor for the base material.

$s$  is the penalty exponent applied.

The penalty,  $s$ , is an arbitrary constant that penalizes intermediate densities to make them tend to a black or white (1-0) solution. It is usually chosen between 2 and 4. Penalties less than 2 do not provide enough penalization, while those larger than 4 have a lower convergence rate. After optimization, elements with densities larger than a certain value (usually,  $\rho_i > 0.3$ ) are interpreted as elements with material, and the remaining as elements without material. The solution is called SIMP-convergent if the interpreted topology has a behavior close to the optimized artificial topology [10]. The ratio of elements with densities close to 0 or 1, to the total elements is used as a degree of SIMP-convergence.

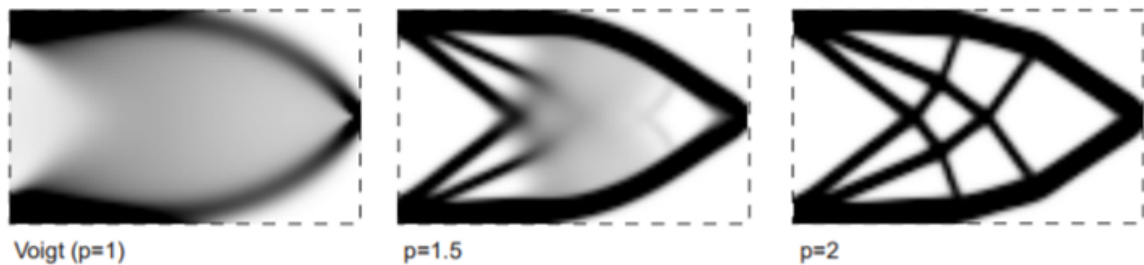


Figure 1.7: Solutions of minimum compliant cantilever beam problem for different penalties [9].

There are other artificial density interpolation schemes, such as Hashin-Shtrikman interpolation, and Reuss-Voigt interpolation [9]. SIMP is the most commonly used artificial material model, as it is simple and efficient. All topology optimizations performed in this research uses the SIMP interpolation.

There are two physical quantities dependent on the material distribution that are targeted by topology optimization. The first is the ratio of material volume to total volume, also called its volume fraction,  $V(x)$ . For constant elemental densities, the volume fraction is equal to the average of all the densities.

$$V(x) = \frac{1}{\Omega} \int_{\Omega} \rho_i d\Omega$$

The second is the effective elastic property of the meta-material,  $E_{ij}^M$ . It is evaluated either by asymptotic homogenization (homogenization), or field homogenization (volume averaging). The goal of topology optimization is to optimize the material distribution to make  $E_{ij}^M$  equal to the target  $E_{ij}^*$ .

The optimum micro-structure is the one which has the least volume while having an elastic behavior equal to the desired target. Hence, the optimization problem is formulated as:

$$\text{Minimize } V(x)$$

Subject to:

$$E_{ij}^M - E_{ij}^* = 0$$

$$0 \leq \rho_e \leq 1$$

This formulation can be modified by changing the linear constraint on  $E_{ij}^M$  to a quadratic constraint. The square of the linear constraint is constrained to be less than or equal to an engineering tolerance  $\delta$ . This problem would be:

$$\text{Minimize } V(x)$$

Subject to:

$$(E_{ij}^M - E_{ij}^*)^2 \leq \delta$$

$$0 \leq \rho_e \leq 1$$

Lastly, another variation of the problem would be to make the target on  $E_{ij}^M$  the objective of the formulation, while bounding the volume between target values.

$$\text{Minimize } (E_{ij}^M - E_{ij}^*)^2$$

Subject to:

$$V_1 \leq V(x) \leq V_2$$

$$0 \leq \rho_e \leq 1$$

These problems were formulated, and studied extensively by Dr. Czech. It was concluded that Formulations 1 and 2 both are able to converge to numerical and SIMP-convergent designs. Whereas, formulation 3 did not converge, both numerically and physically (SIMP-convergence).

## 1.2 Numerical Issues with Topology Optimization

Despite its advantages and broad applications, Topology optimization has several issues. These issues arise from its inherent numerical instability. Sigmund et. Al [11] identify three important numerical issues with TO.

### 1.2.1 Checker-boarding

Topology Optimization sometimes converges on results with alternating 1-0 densities, resulting in a checkerboard pattern. A check-boarding pattern is one where two elements with material are connected only by one node, surrounded by void elements, as observed in Figure 1.8b.

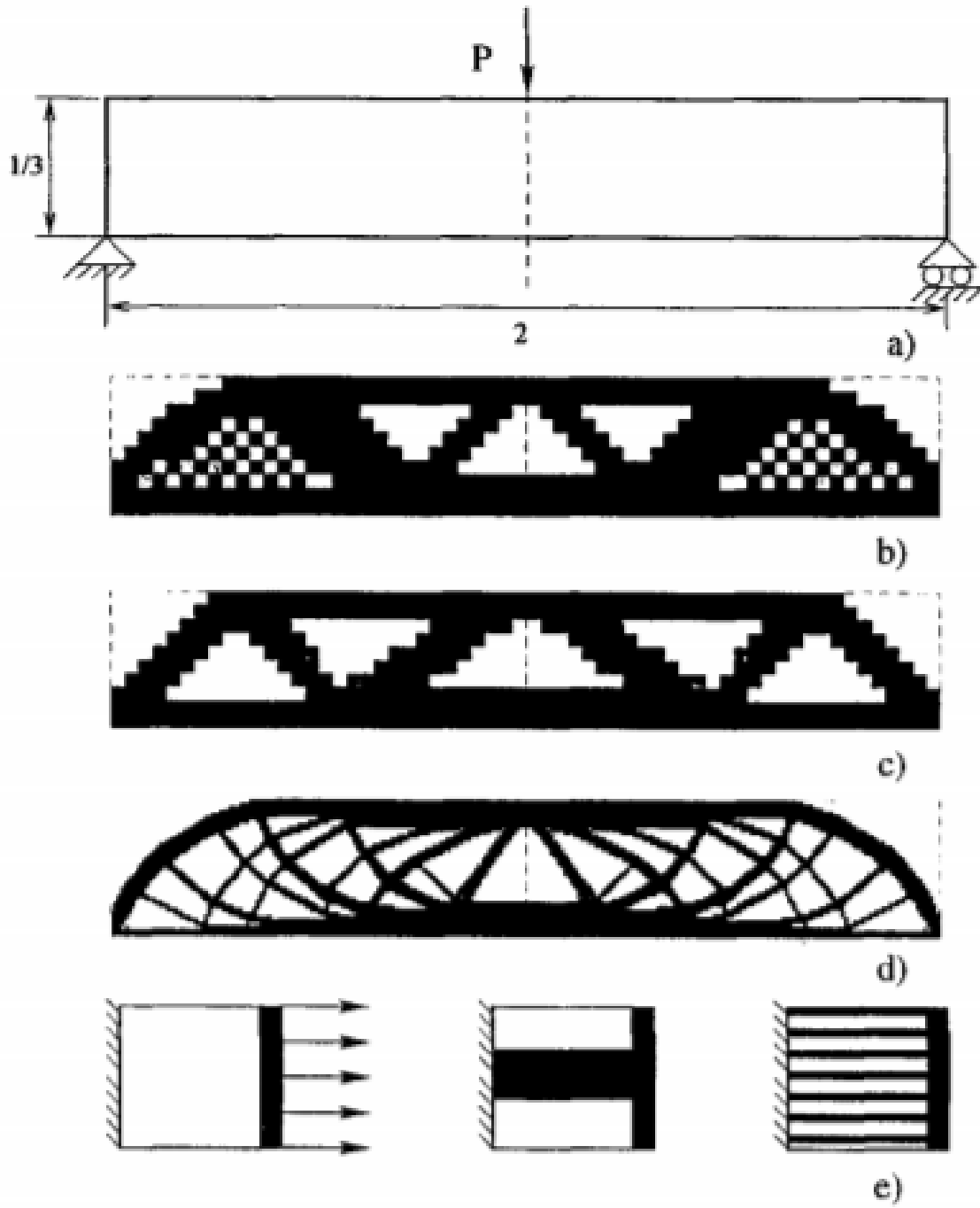


Figure 1.8: Numerical Issues with Topology Optimization. b) Checker-boarding. c-e) Mesh Dependence. [11]

Checker-boarding is an issue which is purely numerical in nature. Some suggest

ignoring the issue altogether, using image-processing algorithms to smooth out the output densities. This should be avoided as it ignores the underlying problem. The checkerboard numeric model is artificially stiffer than the corresponding post-processed numeric model [12].

To ensure non-checkerboard solutions, higher-order finite elements can be used. 8-node and 9-node elements have been proven to avoid checker-boarding. [12]. However, when using SIMP, 8-node and 9-node elements prevent checker-boarding only for small penalization [12]. Also, 8-node and 9-node elements unnecessarily make computation more expensive.

One can avoid 1-node hinges, by using element shapes where only 2-node connections are possible, such as hexagonal elements. Such elements have been proven to be feasible by Gibert et. al. [13]

The most popular and reliable way to avoid checker-boarding is to use image-processing filters, either on the densities themselves or on their sensitivities, during each iteration of the optimization algorithm. This method modifies the densities or the sensitivities using a weighted average of the original densities within a defined neighborhood.

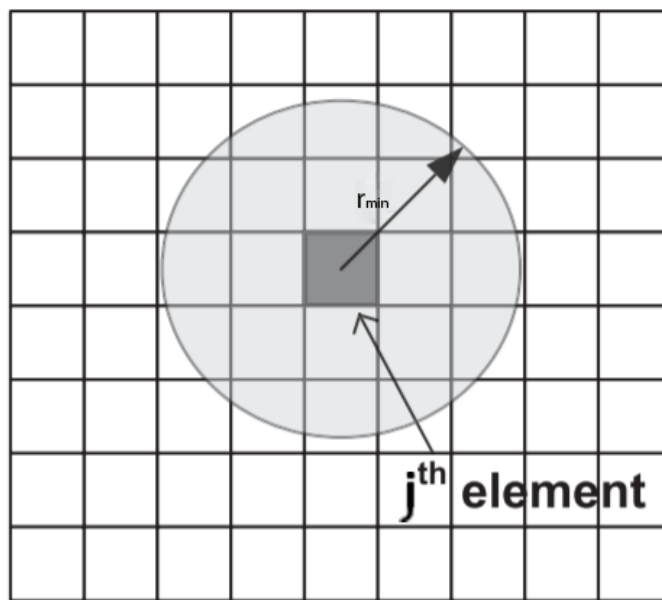


Figure 1.9: Defined neighborhood around element  $j$  for mesh-filtering. [11]



For the density filter, the new densities,  $\tilde{\rho}_j$  are calculated as follows [14] [15]:

$$\tilde{\rho}_j = \frac{\sum_{i \in S_j} \rho_i w_i}{\sum_{i \in S_j} w_i}$$

Where,

$\tilde{\rho}_j$  is the filtered density of element  $j$ .

$\rho_i$  is the density of element  $i$ .

$w_i$  is the value of the weighting function for element  $i$ .

$S_j$  is set of all elements inside the defined neighborhood around element  $j$ .

For the sensitivity filter, the new sensitivities,  $\widetilde{\frac{\partial E^M}{\partial \rho_j}}$  are calculated as follows [16] [11]:

$$\widetilde{\frac{\partial E^M}{\partial \rho_j}} = \frac{\sum_{i \in S_j} \frac{\partial E^M}{\partial \rho_i} \rho_i w_i}{\rho_j \sum_{i \in S_j} w_i}$$

Where,

$\widetilde{\frac{\partial E^M}{\partial \rho_j}}$  is the filtered derivative of modulus  $E^M$  wrt the density of element  $j$ .

$\frac{\partial E^M}{\partial \rho_j}$  is the original derivative of modulus  $E^M$  wrt the density of element  $j$ .

$\rho_i$  is the density of element  $i$ .

$w_i$  is the value of the weighting function for element  $i$ .

$S_j$  is set of all elements inside the defined neighborhood around element  $j$ .

There are multiple weighing functions which can be used [17]. The most commonly used one is a linear weighing function, where the weights are defined by  $w_j = r_{min} - r_j$ . Where,  $r_{min}$  is the radius of the defined neighborhood, and  $r_j$  is the distance between the center of the neighborhood and the center of element  $j$  [17]. Non-linear weighting functions can be used to push the solutions to a more 1-0 solution [17].

It is important to note that Topology Optimization will not obtain topologies with feature sizes less than the size of the defined neighborhood ( $2r_{min}$ ) [11] [18]. Hence, the

minimum achievable length scale in topology optimization can be controlled by the parameter  $r_{min}$ . This also means, that  $r_{min}$  has a lower limit imposed on it, which is equal to the minimum feature length achievable by the manufacturing process to be used for the meta-material. Also, for mesh-filtering to be effective, more than 1 element must be included in the neighborhood. For 4-node rectangular elements, this imposes the following constraint on  $r_{min}$ :  $r_{min} > h$ , where  $h$  is the element size.

### 1.2.2 Mesh Dependence

Mesh dependence of the solutions is another critical numerical issue with TO. The mesh-dependence issue is highlighted by Figures 1.8c-1.8e, where it can be observed that a finer mesh leads to a finer structure. This issue occurs due to the non-uniqueness of the TO solution. An example of a problem with non-unique solutions is a bar in uni-axial tension. A single thick bar is structurally equivalent to multiple finer bars. Mesh-dependence is usually not an issue when topology optimization is used for material optimization with tools like homogenization [11]. Hence, this issue does not need to be addressed for this research.

### 1.2.3 Local Minimums

Topology Optimization can converge to different solutions for the same discretization when different parameters are used. The two most commonly demonstrated TO problems in the literature are the cantilever beam and MBB beam minimum compliance problems. It can be observed in the literature, that many different solutions exist for the same problem, using the same discretization. i.e. TO converges to a local optimum. The TO process is highly sensitive to small changes in parameters, which include but are not limited to: the initial guess, the type of filtering, the value of  $r_{min}$ , the weighing function, the penalization parameter. [11]

A global optimization algorithm, such as genetic or evolutionary algorithms can be used, but they may not be able to handle the size of a typical topology optimization problem. There are various methods suggested in the literature to ensure a global solution.

The most common ones are continuation methods, which gradually change a particular TO parameter during optimization.

One such continuation method was suggested by Allaire and Francfort [19], which initially solves the TO optimization with no penalization, and after convergence, gradually increases the penalization to obtain a 1-0 solution.

Another continuation approach is to initially solve the TO problem with a large value of  $r_{min}$  and upon convergence gradually decrease it, until a near 1-0 solution is obtained. [11]

### 1.3 Asymptotic Homogenization (Homogenization)

Asymptotic Homogenization is an approach to calculate effective properties of a periodic, heterogeneous, structure. It converts a periodic, heterogeneous material model into a homogeneous material model. The approach is based on the mathematical theory of homogenization. It can be applied to various disciplines of engineering for example, heat transfer, fluid flow through a porous medium, electromagnetism, or elasticity.

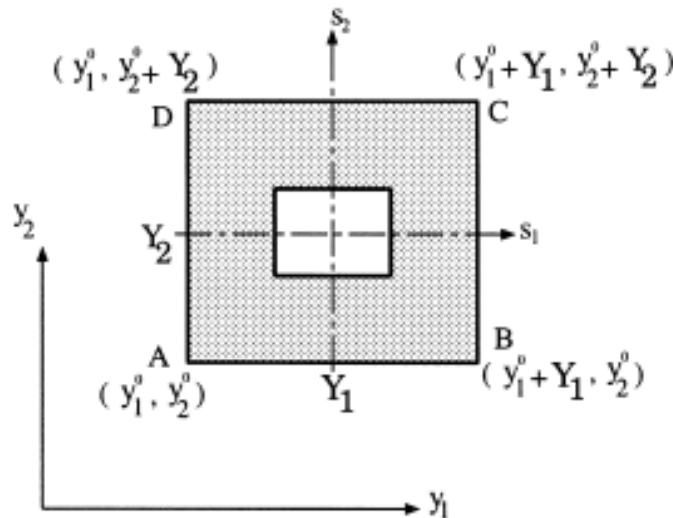


Figure 1.10: Local Design Domain for Homogenization [8].

The Y-periodicity conditions on displacements incur the following boundary condi-

tions on the base cell of the periodic micro-structure (Unit Cell).

$$\chi(y_1, y_2) = \chi(y_1 + Y_1, y_2) = \chi(y_1, y_2 + Y_2) = \chi(y_1 + Y_1, y_2 + Y_2)$$

Where,  $\chi(y_1, y_2)$  are the displacements at points  $(y_1, y_2)$ , on the boundary of the Unit Cell.

The local domain  $Y$  with the periodic conditions enforced is called the Repeated Unit Cell (RUC). The mathematical requirements of asymptotic homogenization require the widths  $Y_1$  and  $Y_2$  of the RUC to be very small compared to the global design domain.

Symmetric boundary conditions are applied on the boundary based on the direction of evaluation. For evaluating any normal moduli the normal displacements on the boundary of the RUC are restricted,  $\chi_n(y_1, y_2) = 0$ . For evaluating the shear modulus the tangential displacements on the boundary of the RUC are restricted,  $\chi_t(y_1, y_2) = 0$ .

A force  $F_e$  is applied to each element such that there is unit initial strain induced in the  $j^{th}$  direction.

$$F_e = \int_{\Omega} B d_j d\Omega$$

Where  $B$  is the strain-displacement matrix.

Using the finite element stiffness matrix,  $K$ , for solid 2-D, linear, isotropic elasticity, the displacement field  $u(y_1, y_2)$  (induced due to the global force,  $F$ ), is calculated as the solution for the linear system:

$$[K]\{u\} = \{F\}$$

The effective moduli of the periodic structure are calculated using the homogenization equation.

$$C_{ij}^H(\rho) = \frac{1}{\Omega} \int_{\Omega} (C_{ij} - d_i^T \epsilon(u)) d\Omega$$

Where,

$C_{ij}$  are the elastic moduli at any given point

$d_i^T$  are the  $i^{th}$  columns of elasticity matrix  $D_{ij}$

$\epsilon(u)$  is the strain due to displacement  $u$

$\Omega$  is the domain of the RUC

$u$  are the displacements induced in  $\Omega$ , due to the force  $F$ .

## 1.4 Field Homogenization (Volume Averaging)

Field Homogenization, also called Volume Averaging is an evaluation tool, originally developed for calculating the global elastic properties of conventional fiber composites by Drago et. al. [20]

Unlike asymptotic homogenization, the evaluation is performed on the Representative Volume Element (RVE) of the global domain, and not the RUC. The RVE is defined as the volume which accurately represents the properties of the global material. The smallest RVE which can be analyzed to accurately evaluate the global properties of the material is called the RVE limit. In the context of meta-materials, RVE limit can either be a single UC or a collection of UCs. [20] [5]

There are two sets of boundary conditions which can be applied to the design domain, homogeneous traction or homogeneous displacements. Homogeneous traction boundary conditions apply a uniform traction force,  $\sigma_{ij}^0$ , on the boundary of the domain. Homogeneous displacement boundary conditions enforce a uniform boundary deformation on the domain. [20] [5]

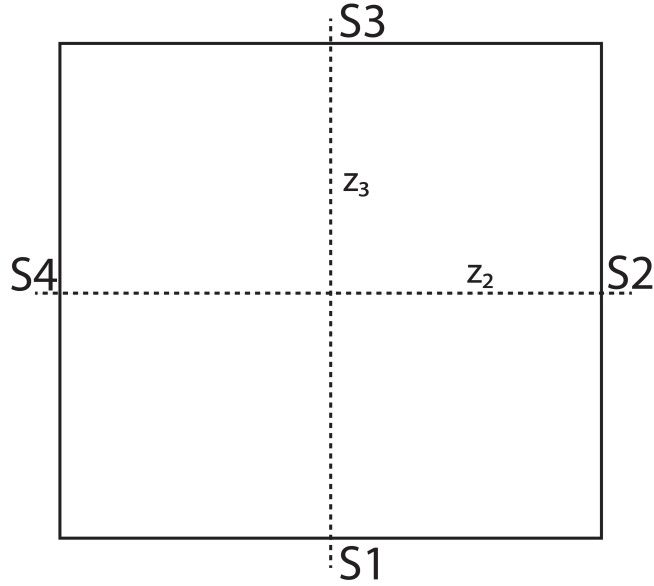


Figure 1.11: Representative Volume Element (RVE) [20]

The different Boundary Conditions that can be applied on the RVE boundaries, S [20] [5] are:

Traction BCs for Transverse Normal loading - For evaluation of  $E_{22}^T$  or  $E_{33}^T$

$$z \in \text{S1:} \quad \sigma_{22}(z) = 0 \quad \sigma_{33}(z) = 0$$

$$z \in \text{S2:} \quad \sigma_{22}(z) = \sigma_{22}^0 \quad \sigma_{33}(z) = 0$$

$$z \in \text{S3:} \quad \sigma_{22}(z) = 0 \quad \sigma_{33}(z) = 0$$

$$z \in \text{S4:} \quad \sigma_{22}(z) = -\sigma_{22}^0 \quad \sigma_{33}(z) = 0$$

Displacement BCs for Transverse Normal loading - For evaluation of  $E_{22}^U$  or  $E_{33}^U$

$$z \in \text{S:} \quad u_2(z) = \varepsilon_{22}^0 z_2 \quad u_3(z) = -\varepsilon_{33}^0 z_3$$

The unknown  $\varepsilon_{33}^0$  is determined subject to the integral constraint,  $\bar{\sigma}_{33} = 0$  on S2 and S3

Traction BCs for Transverse Shear loading - For evaluation of  $G_{23}^T$

$$z \in \text{S1:} \quad \sigma_{23}(z) = -\sigma_{23}^0 \quad \sigma_{33}(z) = 0$$

$$z \in \text{S2:} \quad \sigma_{23}(z) = \sigma_{23}^0 \quad \sigma_{22}(z) = 0$$

$$z \in \text{S3:} \quad \sigma_{23}(z) = \sigma_{23}^0 \quad \sigma_{33}(z) = 0$$

$$z \in \text{S4:} \quad \sigma_{23}(z) = -\sigma_{23}^0 \quad \sigma_{22}(z) = 0$$

Displacement BCs for Transverse Shear loading - For evaluation of  $G_{23}^U$

$$z \in \mathbf{S}: \quad u_2(z) = \varepsilon_{23}^0 z_3 \quad u_3(z) = \varepsilon_{23}^0 z_2$$

Using finite element stiffness matrix,  $K$ , for solid 2-D, linear, isotropic elasticity, the displacement field  $u(z_2, z_3)$  is calculated as the solution for the linear system [20] [5]:

$$[K]\{u\} = \{F\}$$

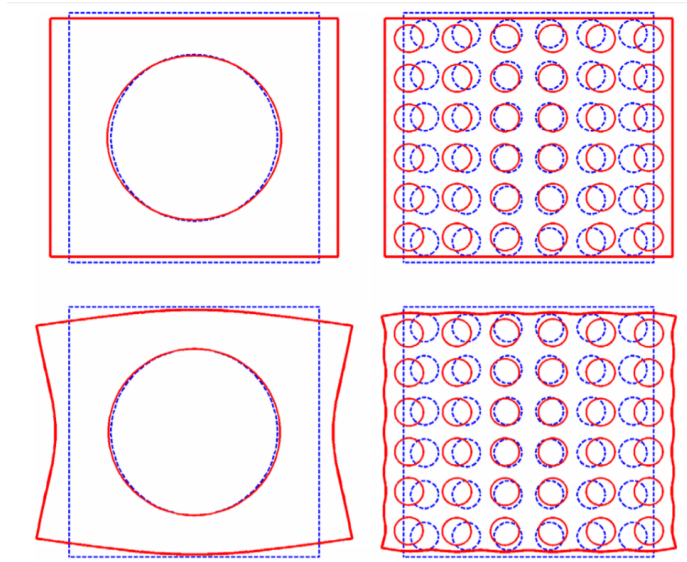


Figure 1.12: Single/Multiple Unit Cells deformed in normal loading using displacement(top) and traction(bottom) BCs [20]

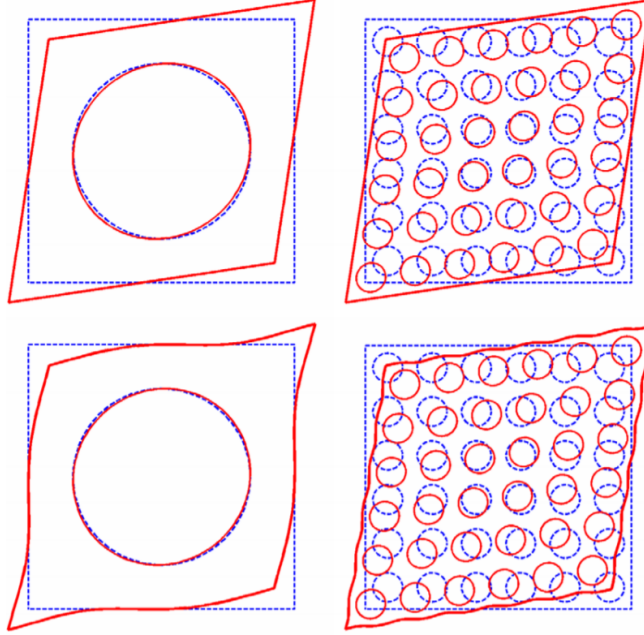


Figure 1.13: Single/Multiple Unit Cells deformed in shear loading using displacement(top) and traction(bottom) BCs [20]

The effective modulus of the periodic structure,  $E_{ij}^M$  is then calculated as the solution to:

$$\bar{\sigma}_i = E_{ij}^M \bar{\varepsilon}_j$$

Where,  $\bar{\varepsilon}$  is the average strain, and  $\bar{\sigma}$  is the average stress induced the RVE due to the displacement field  $u(z_2, z_3)$ . The average stresses and strains are calculated using the average stress and strain theorems [20] [5].

$$\bar{\varepsilon}_i = \frac{1}{V} \int_V \varepsilon_i dV$$

$$\bar{\sigma}_i = \frac{1}{V} \int_V \sigma_i dV$$

The average strain  $\bar{\varepsilon}_i$  in the RVE is equal to the boundary displacements  $\varepsilon_i^0$  in case of displacement BCs, and the average stress  $\bar{\sigma}_i$  is equal to the boundary traction  $\sigma_i^0$  in case of traction BCs. The RVE limit is reached when the strain energy is equivalent for any



boundary condition applied. [20] [5]

$$\frac{1}{2}\bar{\sigma}_i\bar{\varepsilon}_i = \frac{1}{2}\bar{\sigma}_i\varepsilon_i^0 = \frac{1}{2}\sigma_i^0\bar{\varepsilon}_i$$

The Volume Averaging method evaluates the meta-material using the RVE, rather than the RUC. This eliminates the sizing constraints on the UC that homogenization theory requires. This expands the meta-material design process to include problems in which meta-materials could not be designed by homogenization due to manufacturing constraints. If the system of the meta-material is small enough in one or more dimensions, a meta-material with UCs bound by homogenization's requirements would be too small to be manufactured.

[20] [5]

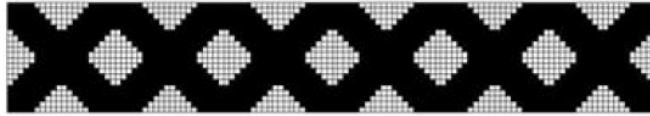


Figure 1.14: A meta-material which violates the homogenization requirements in the vertical direction [5]

## Chapter 2

# Motivation and Research Questions

As mentioned in chapter 1, this research focuses on the second step of the meta-material design process. i.e. using Topology Optimization to design a meta-material with a target effective material property. In this context, meta-material is a heterogeneous, periodic structure.

A typical meta-material is a regular periodic structure with square or rectangular unit cells. In principle, meta-material design using regular meso-structures can obtain the full spectrum of typologies, as Topology Optimization creates and shapes holes in the meso-structure as required. However, meta-materials with shapes like honeycombs or auxetic honeycombs cannot be obtained by the standard Topology Optimization process targeting elastic or shear modulus, as observed in the literature.

Diaz et al. used a parallelogram unit cell with regular periodicity to design meta-materials [21]. By using such parallelogram unit cells, with varying angles, they could obtain honeycomb shapes as the optimal design of the meta-material design process. A change in the parallelogram angle changes the shape of the global and local design domains. This requires re-discretization of the finite elements every time the angle changes.

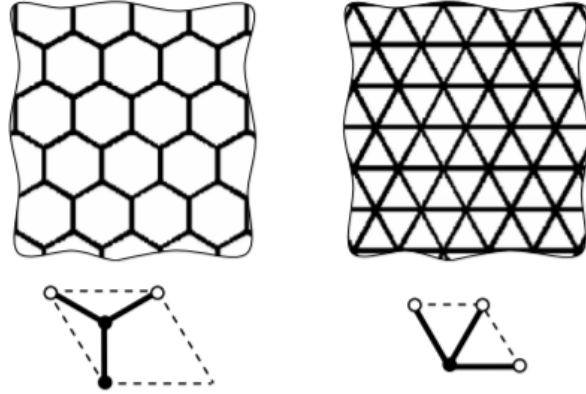


Figure 2.1: Example meso-structures using parallelogram unit cells [22].

Chris Czech proposed a way to obtain honeycomb or auxetic honeycomb shapes from the meta-material design process by using square unit cells with irregular periodicity [10]. Square or rectangular unit cells are tessellated in a staggered arrangement as shown in Figure 2.2. Changes in the staggered arrangement do not change the shape of the global and local design domains. Hence, such meso-structures have an advantage over parallelogram meso-structures, as they do not require re-discretization for every change in the topological connectivity. It was demonstrated that such irregular periodicities can lead to a broader class of meta-materials such as ones with auxetic honeycomb geometries [10].

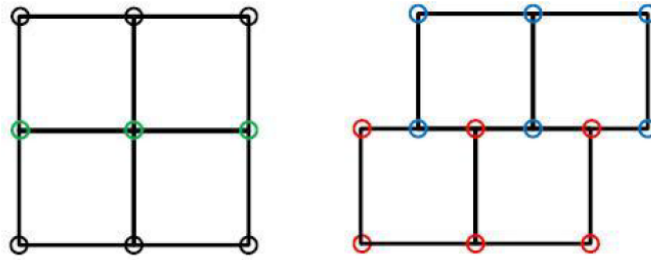


Figure 2.2: Left: Regular periodic unit cells; Right: Irregular periodic unit cells [10].

Chris Czech successfully obtained an auxetic honeycomb meta-material by using square unit cells with layers offset by a half-width of the unit cell. However, no research exists in the literature that uses arrangements with offsets other than zero and half-width of the unit cell. This research will investigate the meta-material shapes obtained by us-

ing tessellations with varying offsets. Such tessellations are expected to generate broader classes of meta-materials. Tessellations like these break the Y-periodicity requirements for asymptotic homogenization. Can volume averaging be used for this modified periodicity?

Typically, the meta-material design process aims to achieve one specific elastic property, like normal elastic modulus, or shear modulus. However, some design problems can demand a meta-material to have multiple specific properties simultaneously. For example, the design of a meta-material with a target shear modulus and a target normal elastic modulus. It needs to be researched whether the meta-material design using TO, can be used to design "extreme" meta-materials, which are extremely stiff in one deformation mode, and extremely compliant in another.

While the framework to solve multi-criteria problems exists, there have been no demonstrated meta-materials designed for multiple criteria using Topology Optimization [5]. Hashin et. al. have provided bounds for the bulk and shear moduli that a meta-material can achieve as a function of volume ratio [23]. There exists a physical bound on the Poisson's ratio of any linear homogeneous material ( $-1 \leq \nu \leq 0.5$ ). It was proven by Milton et. al. [24] that any positive-definite elasticity tensor can be obtained for heterogeneous structures, by using 1-point linkages. Such linkages are not physically practical, and will not be obtained by Topology Optimization. It needs to be investigated if there are any restrictions in the range of obtainable moduli.

## 2.1 Hypothesis and Research Questions

These are the questions this research tries to answer:

1. Will having offsets of unit cells other than none or half-widths lead to a broader class of meta-materials?
2. Must volume averaging be used to evaluate the effective behavior of offset meta-materials?
3. Is any combination of shear and elastic moduli achievable when using multi-

criteria design of meta-materials?

These research questions lead to the following hypothesis to be proposed.

The first hypothesis is that: *changing the periodicity of the meta-material will lead to a broader class of meta-materials as the solution of the design process.* It was demonstrated by Chris Czech that a half-width offset of unit cells lead to a different class of meta-materials [10]. It is therefore viable that different offsets could lead to broader classes of meta-materials.

The second hypothesis is that: *Volume Averaging must be used to evaluate the effective properties of meta-materials with offset periodicity.* By introducing offset, the Y-periodicity condition required for homogenization is broken. Volume Averaging was successfully used to evaluate meta-materials outside the scaling limit of homogenization, therefore it is feasible that it could be used to evaluate meta-materials which break the other condition required for homogenization.

The third hypothesis is that: *there exists a constraint on the range obtainable combinations of the effective properties of a meta-material* Hashin et al. have provided bounds on the bulk and shear moduli as a function of the volume ratio of a meta-material [25]. For homogeneous, linear isotropic or orthotropic materials, the shear modulus is a function of the normal moduli and Poisson's ratios.

## Chapter 3

# Meta-materials with Offset

## Periodicity

As mentioned before in chapter 1, meta-materials with hexagonal/auxetic-hexagonal shapes have not been observed as a result of TO (for targeting elastic/shear modulus) on regularly periodic square/rectangular UCs. One must use irregular UCs to obtain such shapes. One such irregular UC shape is a parallelogram UC. Such UCs have been demonstrated to achieve hexagon-shaped meta-materials. [26]

Another irregular UC is a simple rectangular cell tessellated with an offset of half-width. Chris Czech demonstrated that such offset topological connectivity can be used to obtain auxetic honeycomb shapes [5] [6] [10]. It needs to be seen how a generalized offset will affect the TO results.

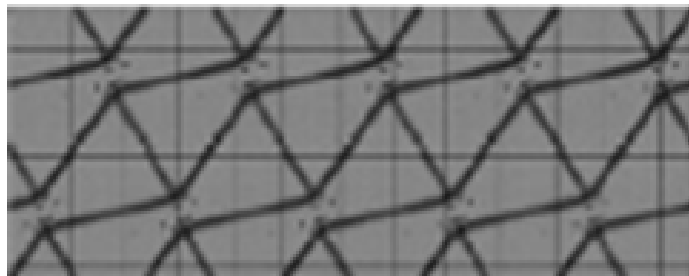


Figure 3.2: Meta-material designed using square unit cells offset by their half-widths [5]

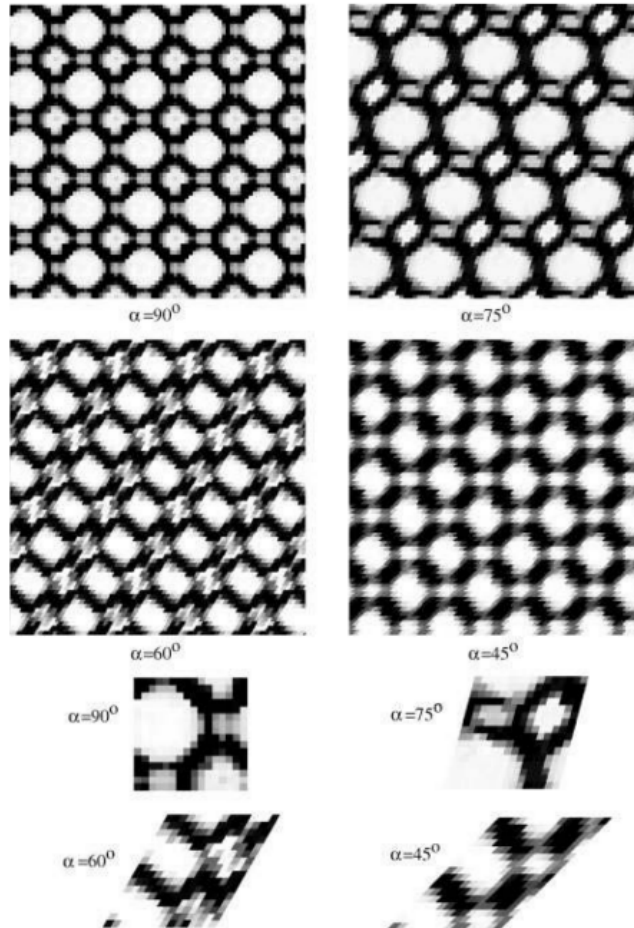


Figure 3.1: Meta-materials designed using parallelogram unit cells for different parallelogram angles  $\alpha$  [26]

This chapter discusses the modifications to the two meta-material analysis tools, homogenization and volume averaging. The modifications allow for an offset topological connectivity.

Further, a fictional meta-material design problem is solved to demonstrate the viability of the method and compare the results for different offsets. This example helps answer the first research question.

Lastly, the non-pneumatic wheels shear beam, as designed by Dr. Czech [5] is re-designed using different values of offset.

### 3.1 Overview of the Problem

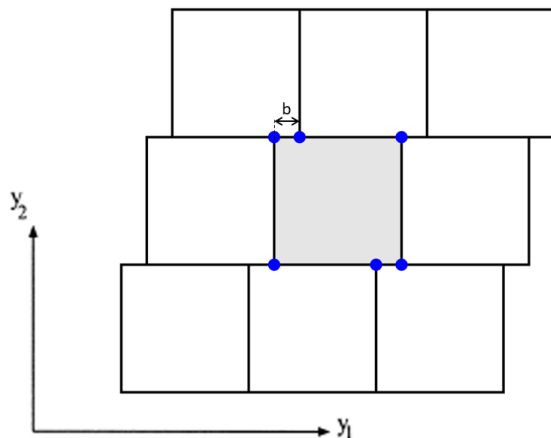


Figure 3.3: Square UC w/ offset tessellation

Consider the UC geometry in Figure 3.3. Layers in  $y_2$  are shifted by  $b$  relative to the previous layer. For simplicity and uniformity of the discretization, the offset parameter  $b$  is limited to be an integer multiple of  $h_2$  (the element size in  $y_2$ ). If  $b$  is continuous instead of discrete, the finite element discretization will not be uniform. An additional node per element would be required at the interface of two meta-material layers. This non-uniformity also means that the domain has to be re-discretized for every change in the offset.

Introducing offset between the layers of UC also results in a change in Y-periodicity condition. As defined in Chapter 1, the design domain  $Y$  is said to be Y-periodic if the elasticity tensor in the domain follows the periodicity equation  $C_{ijkl}(x + nY_1 + mY_2) = C_{ijkl}(x)$ , where  $n, m$  are arbitrary integers and  $Y_{1,2}$  are vectors defining the domain  $Y$ . i.e. for orthogonal Unit Cells, the meta-material has to be orthogonally periodic. Polygonal Unit Cells must be used for non-orthogonally periodic meta-materials for evaluation by homogenization [26]. For the Unit Cell in Figure 3.3.,  $Y_1 = [L, 0]^T$  and  $Y_2 = [b, W]^T$ , where  $L$ ,  $W$ , and  $b$  are the lengths, widths and the offsets of the UC respectively.



### 3.1.1 Discussion on Homogenization for Offset Periodicity

As discussed previously, homogenization cannot be used for evaluating offset meta-materials. To demonstrate this, homogenization with modified periodicity will be compared with Volume Averaging.

The modified periodicity boundary conditions are:

$$\chi(y_1, y_2) = \chi(y_1 + L, y_2)$$

$$\chi(y_1, y_2) = \chi(y_1 + b, y_2 + W)$$

The standard homogenization analysis (as established in Chapter 1) is then repeated.

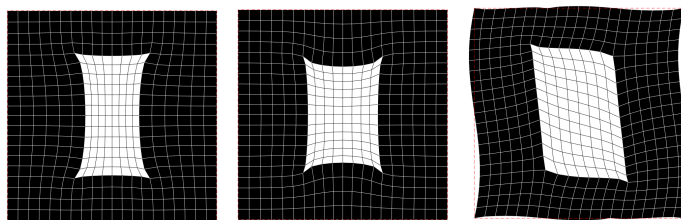


Figure 3.4: RUC with modified offset periodicity conditions in the three modes of deformation: Tension in  $Y_2$ , Tension in  $Y_1$  and Shear

It can be observed in the deformed RUCs in Figure 3.4, that the modified boundary conditions have no visible effect on the tensile deformation modes. It is therefore hypothesized that changing the periodicity, will not have any effect on the homogenized normal moduli. This can lead to geometries which are not physically continuous.

### 3.1.2 Modifications to Volume Averaging for Offset Meta-Materials

Unlike the RUC used in homogenization, the boundary conditions of the RVE used in Volume Averaging are not dependent on the periodicity of the UCs. Hence, no changes are required in the FEA for Volume Averaging analysis.

The RVE is generated from a single UC, while offsetting layers. Partial unit cells are used to ensure a rectangular shape of RVE as seen in Figure 3.5.

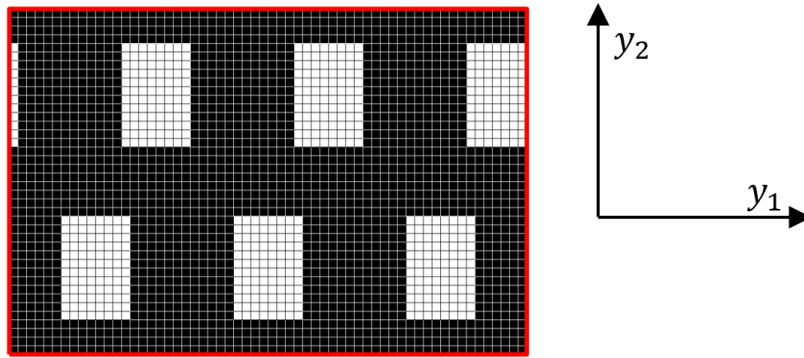


Figure 3.5: Rectangular RVE generated using partial unit cells

Volume Averaging analysis (as established in Chapter 1) is repeated while generating the RVE w/ offset unit cells.

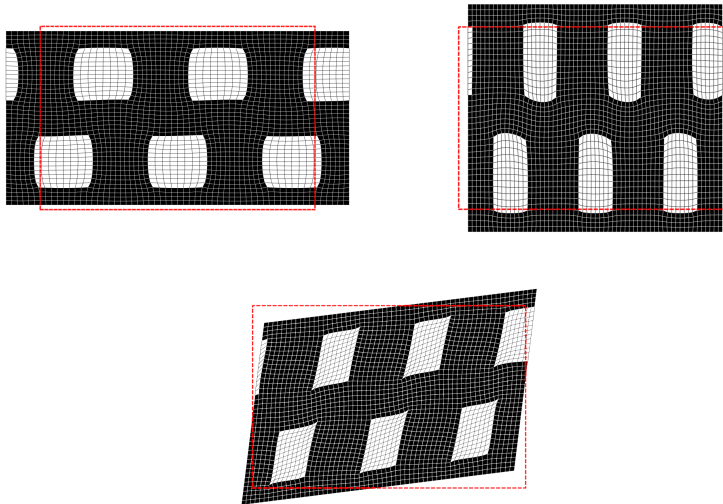


Figure 3.6: RVE with modified offset periodicity in the three modes of deformation, with the original shape shown in red

## 3.2 Comparison between Volume Averaging and Homogenization for Offset Periodicity

A program is developed on MATLAB to analyze any given geometry with offset-ed UCs. The development and validation of the program is explained in Appendix A.

Homogenization is compared against Volume Averaging. Volume Averaging for offset meta-materials is validated as described in Appendix A.

Two geometries are analyzed by volume averaging (RVE: 5x5 unit cells) and homogenization for offsets ranging from 0% to 50%. The discretization is 20x20 elements per UC. A fictional linear isotropic base material w/  $E=30\text{GPa}$  and  $\nu=0.3$  is chosen. The analyzed moduli are normalized and graphed.

As previously hypothesized, offsetting layers of unit cells has no effect on the Elastic Moduli as calculated by homogenization. For geometry A, which is always physically connected irrespective of offset, it can be observed that the moduli calculated using homogenization nearly match the moduli calculated by volume averaging. However, the normal moduli  $E_{22}$  becomes more inaccurate as the offset is increased. The normal moduli calculated by homogenization do not change significantly with a change in offset. This was also previously hypothesized.

This phenomenon can be more easily observed in the moduli calculated for geometry B. For offsets greater than 6 elements, the geometry is no longer physically connected. The moduli calculated by volume averaging agrees with this. After an offset of 6 elements,  $E_{22}^v$  and  $E_{12}^v$  drop to nearly zero. The normal moduli calculated by homogenization do not change significantly with a change in offset. This was also previously hypothesized and confirmed by the analysis of geometry A. The deviation between volume averaging and homogenization before and after offset of 6 elements, can be observed in Figure 3.12.

Based on the analysis of the two geometries, it can be concluded that by offsetting layers of UC, we break the necessary periodic condition required by homogenization, hence rendering it unusable.

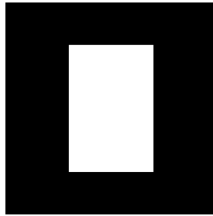


Figure 3.7: Geometry A

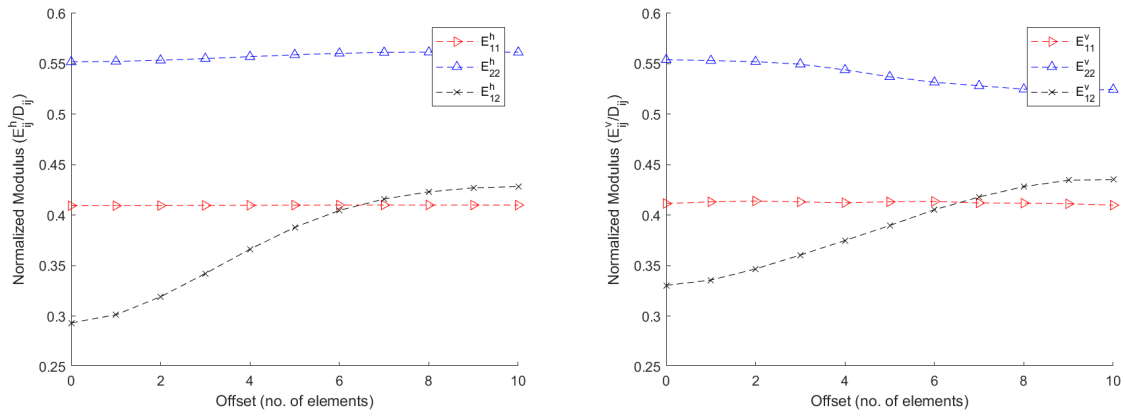


Figure 3.8: Normalized moduli for geometry A

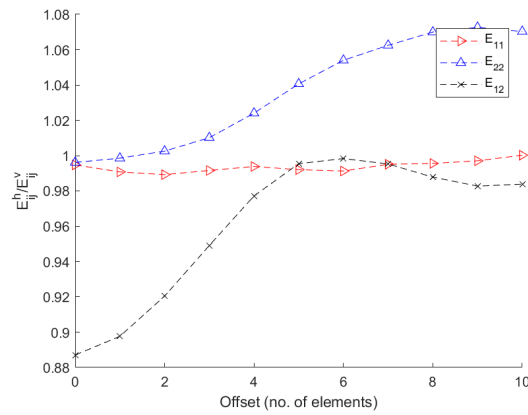


Figure 3.9: Comparison between homogenization and volume averaging for geometry A

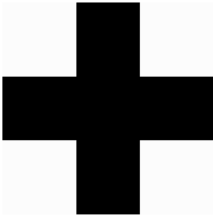


Figure 3.10: Geometry B

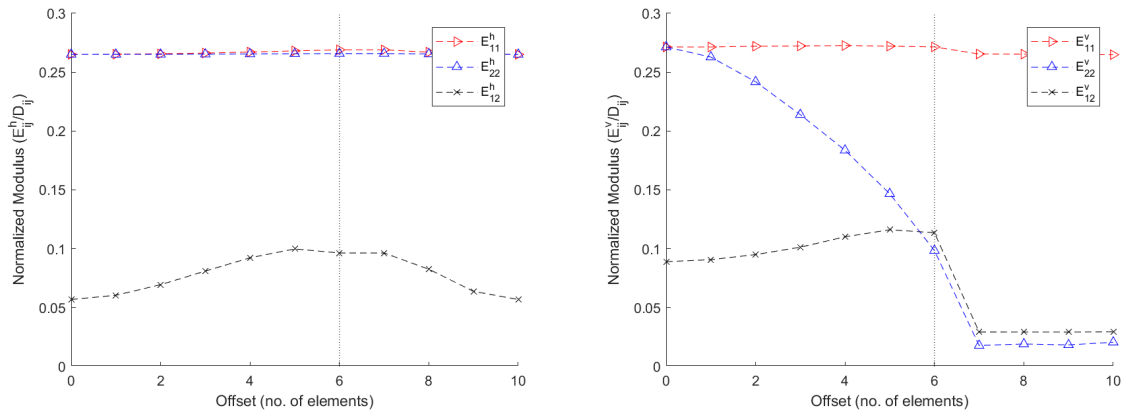


Figure 3.11: Normalized moduli for geometry B

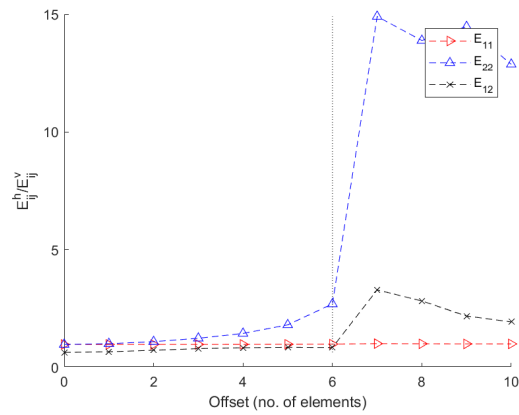


Figure 3.12: Comparison between homogenization and volume averaging for geometry B

### 3.3 Example Optimization for Different Offsets

Two meta-material optimizations are solved. One targets the effective normal elastic modulus, while the other targets the effective shear modulus. The UC is a square, with 20x20 element discretization. The optimization is solved using MATLABs SQP algorithm. Formulation 1 is used to solve the problem. An early termination parameter of 400 iterations is used. The base material is a fictional isotropic linear material with a Young’s modulus of 30 GPa and a Poisson’s ratio of 0.3.

The optimization problem is solved for normal moduli targets 3, 9, 15, and 21 GPa and Shear Modulus targets 1, 4, 5, and 7 GPa, and for offsets 0% to 50%, in 5% increments. Two different RVEs are considered. One with 6x2 unit cells and another with 3x3 unit cells.

This example serves as the demonstration for the first and second hypotheses discussed in Chapter 2. Along with the validation in Appendix A, this answers the first two research questions.

Table 3.1: Numerical results for  $E_{11}^t = 3$  GPa using volume averaging analysis for RVE containing 6x2 unit cells

Offset	V	Iterations	Function Evaluations	Active Constraints
0	0.1570	63	127	360
1	0.1410	111	229	396
2	0.1410	102	213	391
3	0.1450	111	238	394
4	0.1480	103	209	389
5	0.1540	93	198	384
6	0.1590	114	229	393
7	0.1670	110	221	390
8	0.1760	112	227	392
9	0.2180	124	262	375
10	0.2190	124	259	380

Table 3.2: Numerical results for  $E_{11}^t = 9$  GPa using volume averaging analysis for RVE containing 6x2 unit cells

Offset	V	Iterations	Function Evaluations	Active Constraints
0	0.3240	106	241	392
1	0.3220	135	287	395
2	0.3280	139	285	389
3	0.3360	132	272	388
4	0.3450	142	293	394
5	0.3580	135	272	390
6	0.4030	172	352	388
7	0.4060	114	240	373
8	0.3920	118	244	390
9	0.3870	82	182	378
10	0.3760	104	211	360

Table 3.3: Numerical results for  $E_{11}^t = 15$  GPa using volume averaging analysis for RVE containing 6x2 unit cells

Offset	V	Iterations	Function Evaluations	Active Constraints
0	0.4960	72	145	396
1	0.5000	96	227	390
2	0.5130	70	161	375
3	0.5200	78	163	388
4	0.5330	106	219	395
5	0.5610	114	258	389
6	0.5700	128	281	387
7	0.5670	105	260	378
8	0.5620	127	271	389
9	0.5790	76	161	337
10	0.5660	96	193	360



Table 3.4: Numerical results for  $E_{11}^t = 21$  GPa using volume averaging analysis for RVE containing 6x2 unit cells

Offset	V	Iterations	Function Evaluations	Active Constraints
0	0.8330	5	24	324
1	0.8330	5	25	323
2	0.8330	5	25	325
3	0.8330	5	25	328
4	0.8330	5	25	329
5	0.8330	5	25	328
6	0.8320	5	25	328
7	0.8320	5	25	328
8	0.8310	5	25	328
9	0.8310	5	25	328
10	0.8310	5	25	328

Table 3.5: Graphical results when targeting normal moduli, using volume averaging analysis for RVE containing 6x2 unit cells.

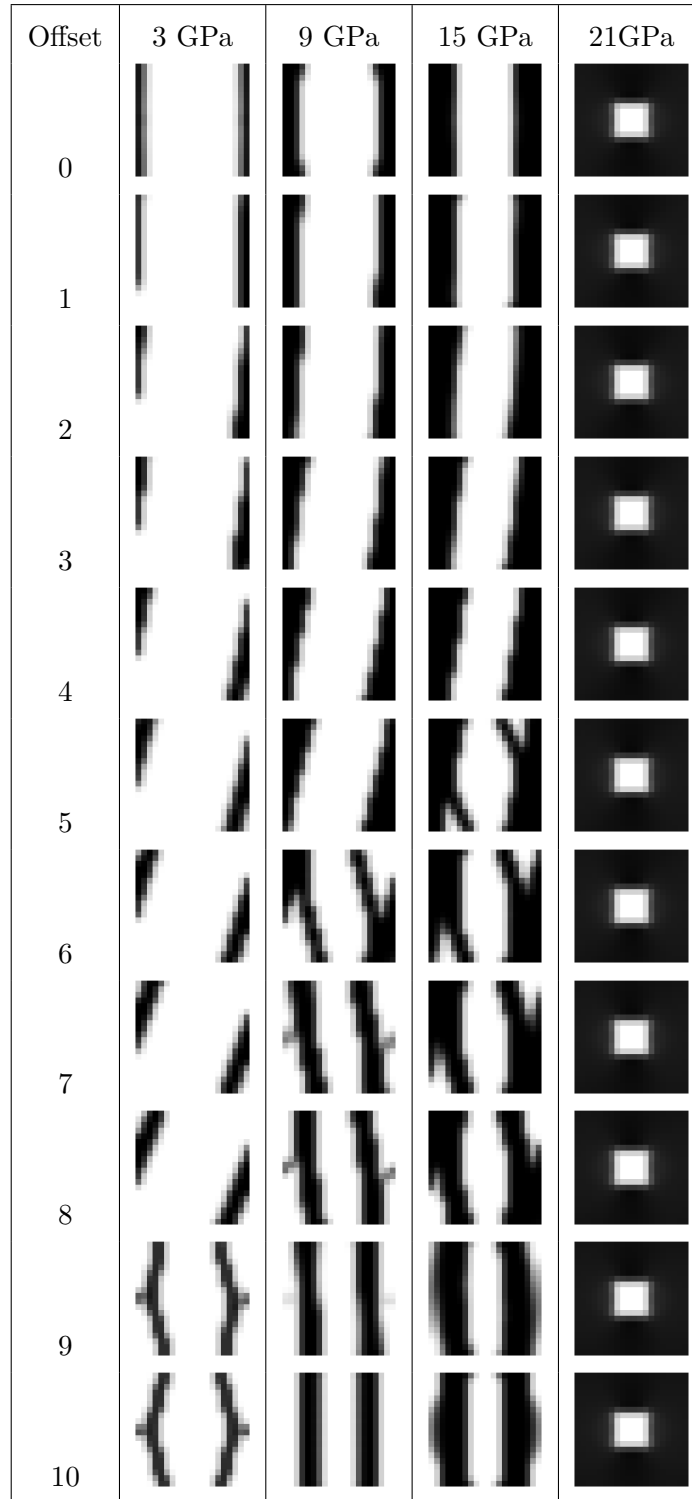


Table 3.6: Numerical results for  $E_{12}^t = 1$  GPa using volume averaging analysis for RVE containing 6x2 unit cells

Offset	V	Iterations	Function Evaluations	Active Constraints
0	0.3210	91	189	344
1	0.2820	177	355	396
2	0.2830	145	292	392
3	0.2830	170	350	391
4	0.2860	176	365	389
5	0.3170	167	341	389
6	0.2570	262	525	384
7	0.3080	139	285	369
8	0.3020	188	385	369
9	0.3110	176	360	373
10	0.3220	118	247	338

Table 3.7: Numerical results for  $E_{12}^t = 4$  GPa using volume averaging analysis for RVE containing 6x2 unit cells

Offset	V	Iterations	Function Evaluations	Active Constraints
0	0.5370	114	248	384
1	0.5350	143	312	389
2	0.5390	117	243	382
3	0.5400	110	238	387
4	0.5460	103	214	374
5	0.5520	124	262	380
6	0.5490	173	369	398
7	0.5630	174	379	394
8	0.5900	145	298	376
9	0.5850	151	373	379
10	0.5770	131	274	382

Table 3.8: Numerical results for  $E_{12}^t = 5$  GPa using volume averaging analysis for RVE containing 6x2 unit cells

Offset	V	Iterations	Function Evaluations	Active Constraints
0	0.8010	5	24	196
1	0.8000	5	24	190
2	0.8000	5	24	189
3	0.7980	5	24	187
4	0.7970	5	24	181
5	0.7950	5	24	179
6	0.7940	5	24	176
7	0.7920	5	24	166
8	0.7920	5	24	167
9	0.7910	5	24	164
10	0.7910	5	24	160

Table 3.9: Numerical results for  $E_{12}^t = 7$  GPa using volume averaging analysis for RVE containing 6x2 unit cells

Offset	V	Iterations	Function Evaluations	Active Constraints
0	0.8750	4	19	392
1	0.8740	4	19	393
2	0.8740	4	19	392
3	0.8730	4	19	392
4	0.8720	4	19	392
5	0.8710	4	19	392
6	0.8690	4	19	392
7	0.8680	4	19	392
8	0.8680	4	19	392
9	0.8680	4	19	392
10	0.8670	4	18	392

Table 3.10: Graphical results when targeting shear moduli, using volume averaging analysis for RVE containing 6x2 unit cells.

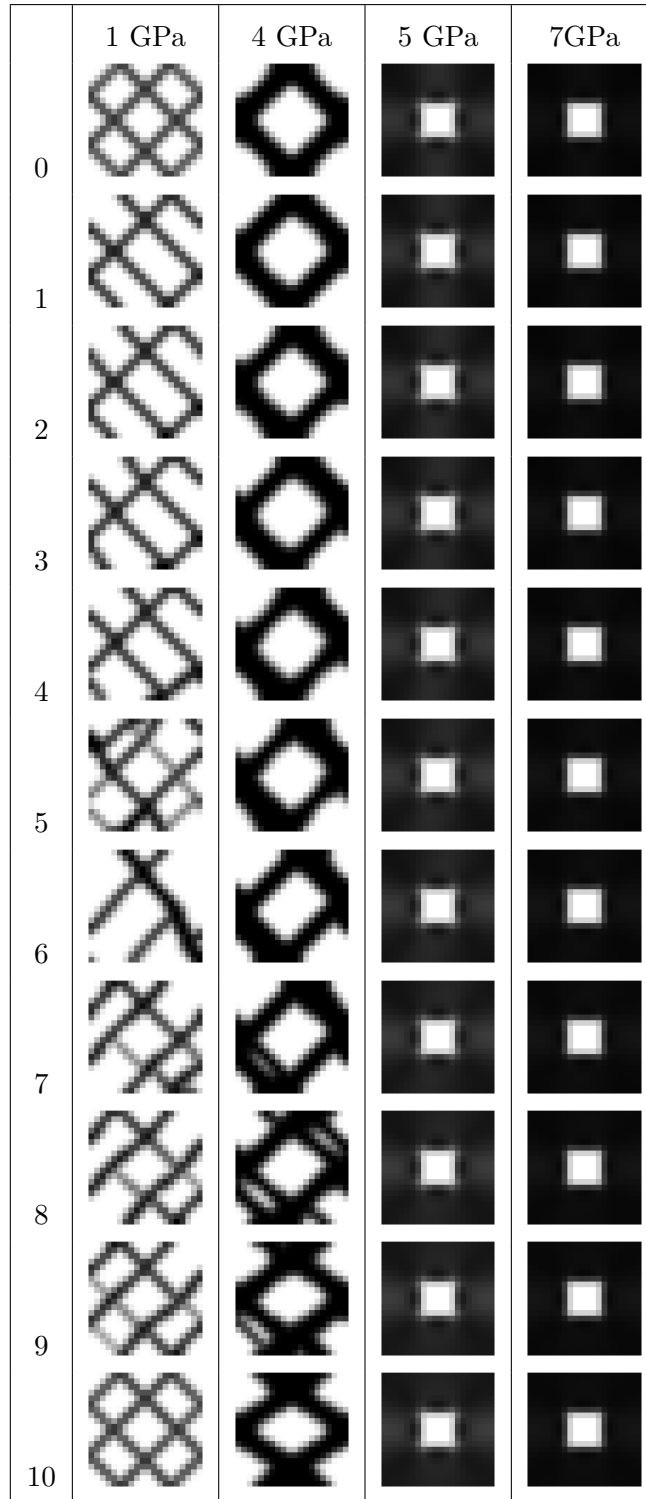


Table 3.11: Numerical results for  $E_{11}^t = 3$  GPa using volume averaging analysis for RVE containing 3x3 unit cells

Offset	V	Iterations	Function Evaluations	Active Constraints
0	0.1570	61	123	360
1	0.1350	105	221	396
2	0.1400	91	191	388
3	0.1460	92	194	388
4	0.1480	116	233	394
5	0.1530	119	239	391
6	0.1600	128	257	395
7	0.1670	119	239	393
8	0.1750	141	283	392
9	0.2210	163	337	388
10	0.2190	96	203	364



Table 3.12: Numerical results for  $E_{11}^t = 9$  GPa using volume averaging analysis for RVE containing 3x3 unit cells

Offset	V	Iterations	Function Evaluations	Active Constraints
0	0.3250	103	259	392
1	0.3230	120	258	391
2	0.3290	117	239	390
3	0.3370	118	252	388
4	0.3470	145	292	392
5	0.4100	147	296	375
6	0.4040	180	372	384
7	0.4090	100	213	373
8	0.3940	79	173	375
9	0.3770	86	185	378
10	0.3770	77	156	328

Table 3.13: Numerical results for  $E_{11}^t = 15$  GPa using volume averaging analysis for RVE containing 3x3 unit cells

Offset	V	Iterations	Function Evaluations	Active Constraints
0	0.5130	53	107	372
1	0.5060	69	153	379
2	0.5110	134	275	396
3	0.5240	72	156	387
4	0.5660	76	165	350
5	0.5700	109	230	380
6	0.5760	89	187	369
7	0.5660	126	260	386
8	0.5710	121	254	374
9	0.5700	113	235	370
10	0.5670	97	195	364

Table 3.14: Numerical results for  $E_{11}^t = 21$  GPa using volume averaging analysis for RVE containing 3x3 unit cells

Offset	V	Iterations	Function Evaluations	Active Constraints
0	0.8330	5	25	328
1	0.8330	5	25	328
2	0.8330	5	25	329
3	0.8320	5	25	324
4	0.8300	5	25	315
5	0.8290	5	25	309
6	0.8300	5	25	315
7	0.8310	5	25	322
8	0.8310	5	25	327
9	0.8310	5	25	326
10	0.8310	5	25	324

Table 3.15: Graphical results when targeting normal moduli, using volume averaging analysis for RVE containing 3x3 unit cells.

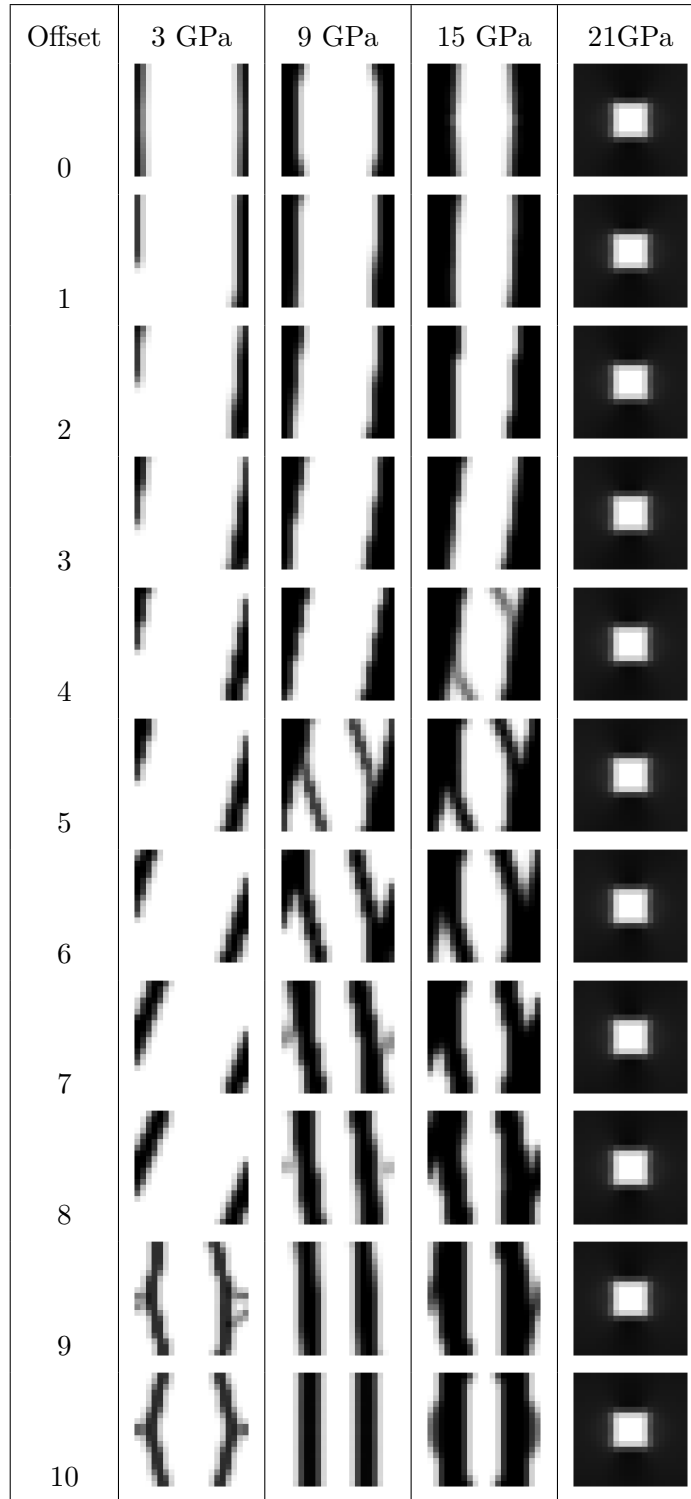


Table 3.16: Numerical results for  $E_{12}^t = 1$  GPa using volume averaging analysis for RVE containing 3x3 unit cells

Offset	V	Iterations	Function Evaluations	Active Constraints
0	0.3210	111	231	328
1	0.2830	131	275	393
2	0.2820	151	319	393
3	0.2830	169	350	393
4	0.2610	137	285	378
5	0.2420	238	489	387
6	0.3030	160	322	367
7	0.2870	164	335	385
8	0.3010	131	271	362
9	0.3190	191	428	373
10	0.3220	100	204	328

Table 3.17: Numerical results for  $E_{12}^t = 4$  GPa using volume averaging analysis for RVE containing 3x3 unit cells

Offset	V	Iterations	Function Evaluations	Active Constraints
0	0.5560	60	121	320
1	0.5350	150	327	389
2	0.5370	120	249	389
3	0.5460	87	180	365
4	0.5440	115	242	389
5	0.5530	100	209	375
6	0.5570	117	244	378
7	0.5590	191	402	398
8	0.5910	205	426	393
9	0.5940	197	409	394
10	0.5810	123	247	388

Table 3.18: Numerical results for  $E_{12}^t = 5$  GPa using volume averaging analysis for RVE containing 3x3 unit cells

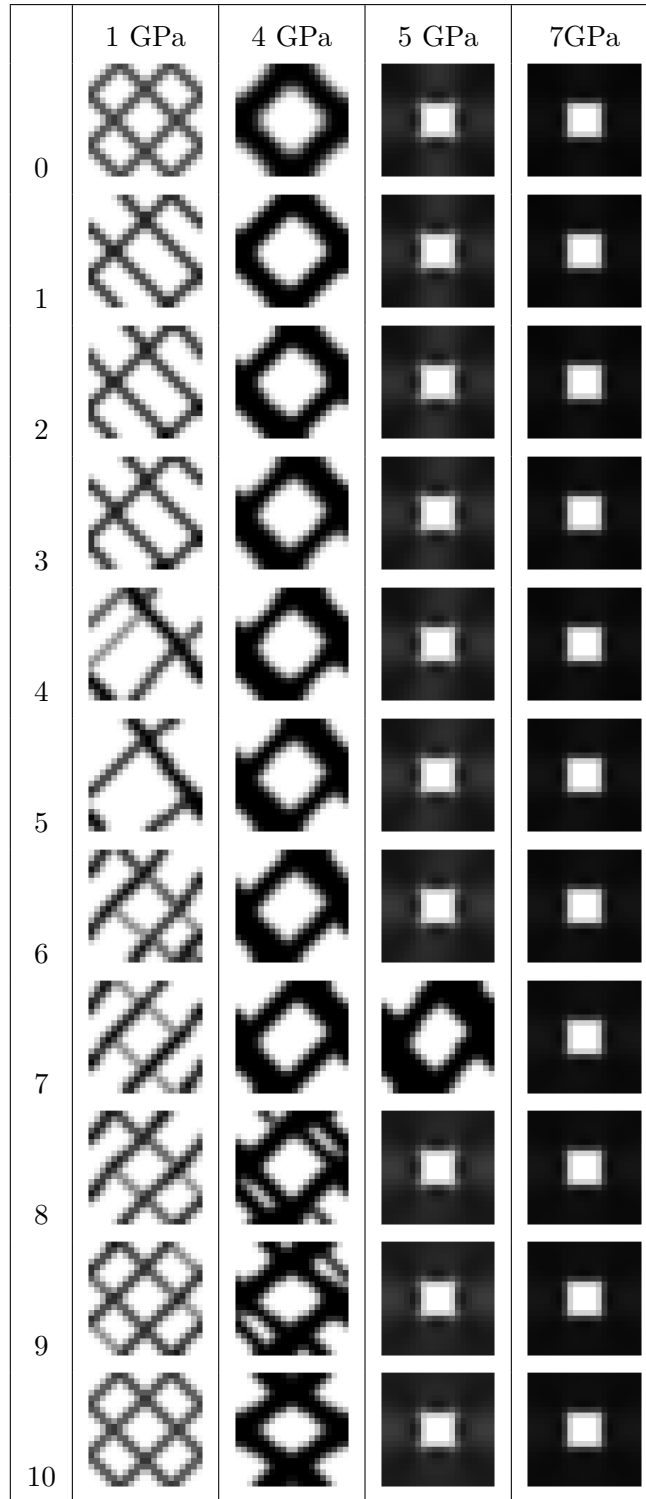
Offset	V	Iterations	Function Evaluations	Active Constraints
0	0.8000	5	24	204
1	0.7990	5	24	195
2	0.7970	5	24	188
3	0.7940	5	24	179
4	0.7930	5	24	173
5	0.7890	5	24	165
6	0.7870	5	24	152
7	0.6470	186	397	394
8	0.7850	5	24	125
9	0.7850	5	24	111
10	0.7840	5	24	104

Table 3.19: Numerical results for  $E_{12}^t = 7$  GPa using volume averaging analysis for RVE containing 3x3 unit cells

Offset	V	Iterations	Function Evaluations	Active Constraints
0	0.8740	4	19	392
1	0.8740	4	19	392
2	0.8730	4	19	392
3	0.8700	4	19	392
4	0.8690	4	19	392
5	0.8670	4	19	392
6	0.8650	4	18	392
7	0.8630	4	18	392
8	0.8640	4	18	392
9	0.8640	4	18	392
10	0.8640	4	18	392



Table 3.20: Graphical results when targeting shear moduli, using volume averaging analysis for RVE containing 3x3 unit cells.



### 3.3.1 Discussion

The visual and numeric solutions to the fictional Topology Optimization problems are shown in Tables 3.1 to 3.20. One can observe that the optimized volume fraction generally decreases with offset when target modulus is small compared to the base modulus, and then increases again near 50% offset.

For a larger target modulus, the volume fraction always increases with volume. It can be concluded that intermediate offsets can converge to a lower volume fraction than the extreme offsets (0% and 50%). i.e. It is beneficial to consider meta-materials with an intermediate offset periodicity.

One can also observe that the formulation used does not converge to practical meta-materials when targeting a very high modulus.

The optimization problem can be setup with the offset parameter,  $b$ , as an optimizable design variable. However,  $b$  is a discrete, integer parameter. To solve the modified problem, a global search meta-heuristic algorithm, such as NSGA-II, must be used. However, such algorithms are inefficient for the very large number of variables in a typical topology optimization problem.

### 3.4 Optimization of the Shear Beam for a Non-Pneumatic Wheel

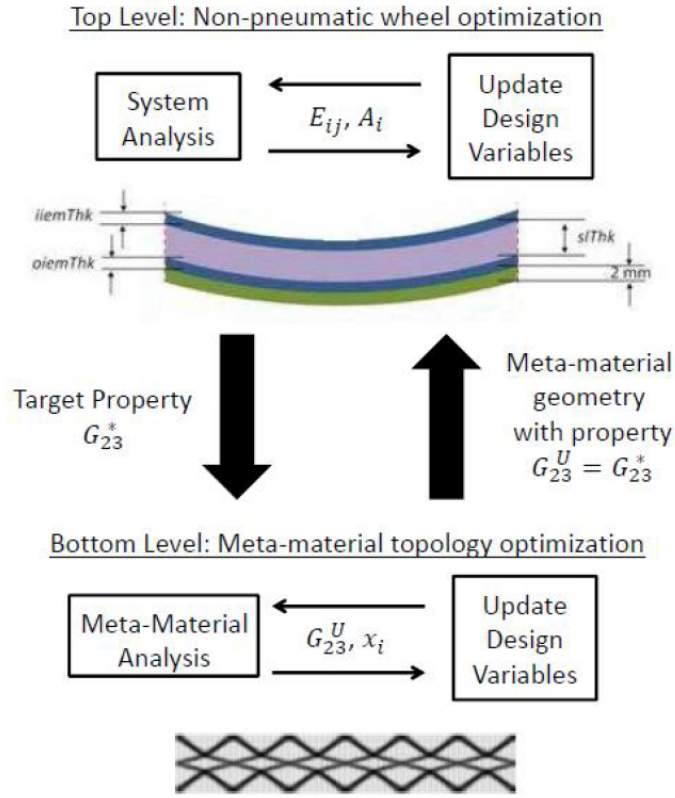


Figure 3.13: Two-level optimization process used for meta-material design of the shear beam of the non-pneumatic wheel [27]

The design of the shear beam of a non-pneumatic wheel consists of two steps. The top-level, or the system-level optimization is solved by Thyagaraja et. al. [27] The goal of this step is to identify the target moduli of the next step of optimization, aiming to reduce the hysteresis losses in the beam. Sensitivity analysis on the design variables identified the shear beam thickness,  $sl_{Thk}$  and shear modulus  $G_{23}$  as the most influential variables for the system-level optimization. The solution to the optimization problem was found to lie on the curve:

$$G_{23} \cdot sl_{Thk} = 67 \text{MPa} \cdot \text{mm}$$

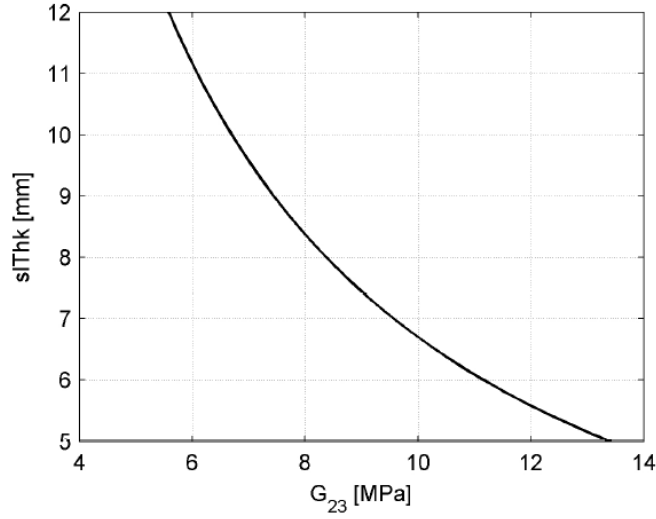


Figure 3.14: Solution to the top-level optimization for design of the shear beam of the non-pneumatic wheel [27] [5]

### 3.4.1 Topology Optimization of the Shear Layer

The solution to the top-level optimization establishes the targets of the bottom-level optimization (i.e. Topology Optimization). The bottom-level optimization was solved by Dr. Czech, for meta-materials with half-width offset periodicity [5]. The base material chosen was Poly-carbonate (PC) with  $E=2.7$  GPa and  $\nu=0.42$ . The physical constraints on the shear layer require a meta-material outside the homogenization scaling limit, hence volume averaging analysis was required to calculate the effective meta-material moduli. A high-resolution mesh of 40x40 was chosen.

The optimization problem was formulated as:

$$\text{Minimize } V(x)$$

Subject to:

$$G_{23}^v - G_{23}^t = 0$$

$$0 \leq x_e \leq 1$$

The Topology Optimization is repeated while using unit cells with offset periodicity. The offsets range from 0%(0 element) to 50%(20 element) in 5%(2 element) increments.

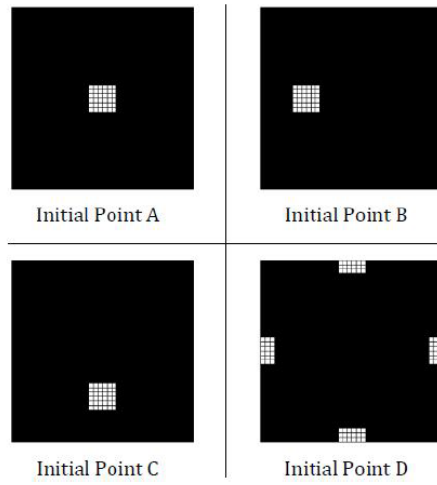


Figure 3.15: Different initial points used for the Topology Optimization of the shear beam of the non-pneumatic wheel [5]

$t_{sz}$ [mm]	$G_{23}^U$ [MPa]	$V$	Geometry
<b>Initial Point A</b>			
6	11.17	0.117	
7	9.57	0.102	
12	5.58	0.054	
<b>Initial Point B</b>			
5	13.40	0.080	
7	9.57	0.121	
8	8.42	0.064	
12	5.58	0.104	
<b>Initial Point C</b>			
5	13.39	0.072	
8	8.38	0.115	

Figure 3.16: Selected solutions to Topology Optimization of the shear beam of the non-pneumatic wheel as produced by Dr. Czech [5]

Table 3.21: Optimization results for  $sl_{Thk} = 6$  mm, initial point A.

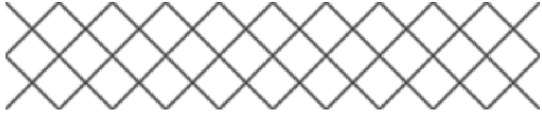










Offset	V	Meta-Material
0	0.1062	
2	0.0662	
4	0.0660	
6	0.0651	
8	0.0646	
10	0.0644	
12	0.1074	
14	0.1017	
16	0.1021	
18	0.1039	
20	0.1259	

Table 3.22: Optimization results for  $sl_{Thk} = 7$  mm, initial point A.








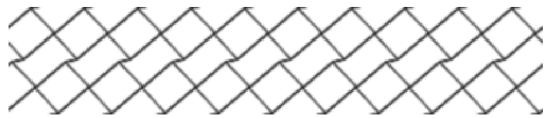



Offset	V	Meta-Material
0	0.1000	
2	0.0628	
4	0.0653	
6	0.0617	
8	0.0614	
10	0.0609	
12	0.0611	
14	0.1024	
16	0.0958	
18	0.0993	
20	0.1204	



Table 3.23: Optimization results for  $sl_{Thk} = 12$  mm, initial point A.












Offset	V	Meta-Material
0	0.0859	
2	0.0529	
4	0.0521	
6	0.0539	
8	0.0514	
10	0.0509	
12	0.0509	
14	0.0890	
16	0.0881	
18	0.0886	
20	0.1039	

Table 3.24: Optimization results for  $sl_{Thk} = 5$  mm, initial point B.

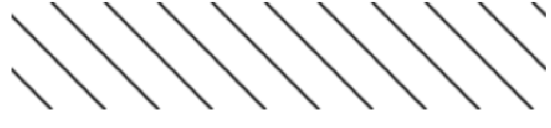
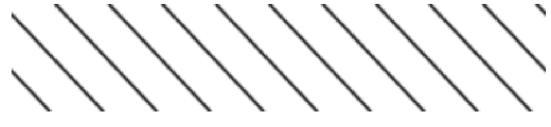
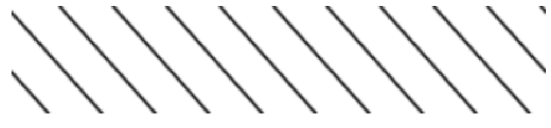
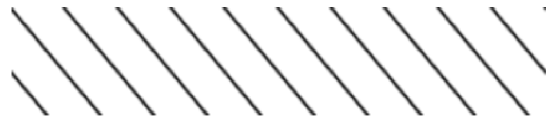
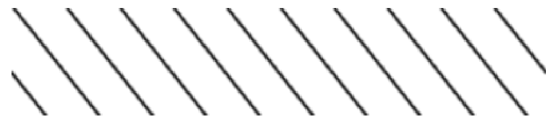




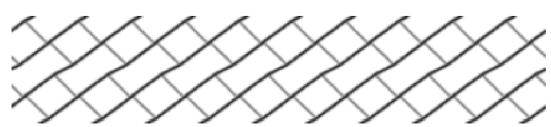
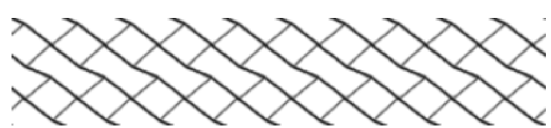
Offset	V	Meta-Material
0	0.0706	
2	0.0710	
4	0.0698	
6	0.0693	
8	0.0683	
10	0.0684	
12	0.1105	
14	0.1075	
16	0.1043	
18	0.1094	
20	0.1160	

Table 3.25: Optimization results for  $sl_{Thk} = 7$  mm, initial point B.












Offset	V	Meta-Material
0	0.0941	
2	0.0632	
4	0.0624	
6	0.0616	
8	0.0610	
10	0.0608	
12	0.0604	
14	0.1022	
16	0.0996	
18	0.1002	
20	0.1066	

Table 3.26: Optimization results for  $sl_{Thk} = 8$  mm, initial point B.






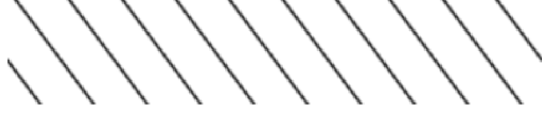

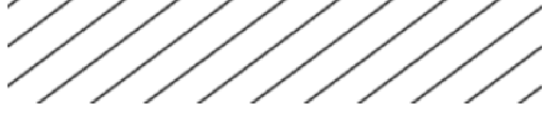



Offset	V	Meta-Material
0	0.0910	
2	0.0603	
4	0.0599	
6	0.0589	
8	0.0583	
10	0.0580	
12	0.0998	
14	0.0704	
16	0.0970	
18	0.0977	
20	0.1017	

Table 3.27: Optimization results for  $sl_{Thk} = 12$  mm, initial point B.












Offset	V	Meta-Material
0	0.0879	
2	0.0527	
4	0.0521	
6	0.0512	
8	0.0508	
10	0.0541	
12	0.0538	
14	0.0886	
16	0.0867	
18	0.0880	
20	0.0912	

Table 3.28: Optimization results for  $sl_{Thk} = 5$  mm, initial point C.









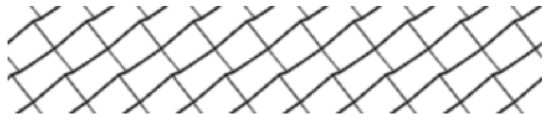
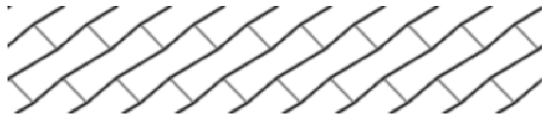
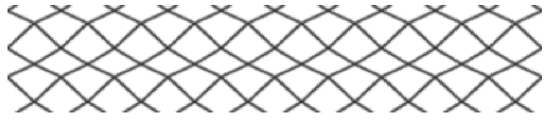











Offset	V	Meta-Material
0	0.1078	
2	0.0707	
4	0.0697	
6	0.0694	
8	0.0684	
10	0.0683	
12	0.0687	
14	0.0702	
16	0.1120	
18	0.0997	
20	0.1341	

Table 3.29: Optimization results for  $sl_{Thk} = 8$  mm, initial point C.

Offset	V	Meta-Material
0	0.0939	
2	0.0601	
4	0.0594	
6	0.0589	
8	0.0585	
10	0.0581	
12	0.0583	
14	0.0582	
16	0.0589	
18	0.0970	
20	0.1172	

### 3.4.2 Discussion on Topology Optimization Results

Selected results to the Topology Optimization problem are shown in Table B.2 to Table 3.29. Complete results are listed in Appendix B. Numerical results are listed in Appendix C. It can be observed that for problems with zero offset, the result obtained are meta-materials with a cross X-like geometry. It is a well known fact that such structures are the stiffest in shear when minimizing the volume fraction [28].

Another class of meta-material is obtained for intermediate offsets (from  $>0$  elements to 12 elements). These meta-materials have a bristle /-like geometry. These meta-materials have the lowest volume among all the different classes of meta-materials obtained, however, such meta-materials can buckle when loaded in compression.

For offsets  $>12$  elements, the meta-materials have a staggered x-like geometry, which consists of alternating layers of auxetic hexagons and crosses. These geometries have a lower volume fraction than pure x-like geometries, without any obvious buckling issue.

Some problems yield a near auxetic honeycomb structure, such as offset 12 problems with starting point 'D'. These meta-materials are quite close to the auxetic honeycomb obtained by Dr. Czech [5] as seen in Figure 3.16.

The conclusions from the optimization of the fictional problem earlier in Chapter 3, are reaffirmed. It is not necessary that extreme offsets of zero or half-width will converge to lower volume fractions than intermediate ones.

The results obtained by Dr. Czech for an offset of 20 elements are not reproduced. However, one must note that the volume fractions of the results produced are generally lower than the volume fractions of the meta-materials produced by Dr. Czech. Also, if optimization is attempted with the meta-material produced by Dr. Czech as the initial point, it returns the same meta-material without performing any iterations. These are the characteristics of a local minimum (Existence of solutions with lower objective function value, and zero gradient at the point). Such local minimum issues are quite common for a Topology Optimization problem as discussed in Chapter 1. Local minima for this problem can be caused by TO parameters like the filter size  $r_{min}$ , and/or the numerical optimization



algorithm used. It should be noted that the numerical optimization used by Dr. Czech was the native SQP algorithm of Matlab 2011, while the one used for this thesis is the native SQP algorithm of Matlab 2017.

To prevent such local minima issues, continuation methods as explained in Chapter 1 can be used. The results shown in Table B.2 to Table 3.29 have been obtained by using continuation method on the filter size  $r_{min}$  (reduced gradually from 3 elements to 1.5 elements).

### 3.5 Summary

Modified asymptotic homogenization and volume averaging methods were proposed. It was concluded that the modified periodicity invalidates the Y-periodicity condition required for homogenization, and hence invalidates homogenization as a tool to evaluate the modulus of offset meta-materials.

By optimizing the fictional problem it was established that intermediate offsets may or may not have the most optimum designs. This conclusion was re-affirmed by the Topology Optimization results for the design of the shear beam of a non-pneumatic wheel. The non-pneumatic wheel problem also showed that it is indeed possible to obtain different classes of meta-materials based on the offset parameter.

This chapter answered the first two research questions and validates the first two hypotheses.

## Chapter 4

# Multi-criteria design of meta-materials

This chapter demonstrates the formulations discussed in Chapter 1 for multi-criteria design. It also establishes the restriction on the obtainable range of different moduli, if any exist. Most meta-material design problems in the literature require targeting of one modulus [5]. However, there may be design problems which may require design of meta-materials for multiple moduli simultaneously. Multi-criteria design solutions for homogenization exists in the literature [28], but none exist for volume averaging. The formulations (developed by Dr. Czech [5]) discussed in chapter 1, can be used for the multi-criteria design.

### 4.1 Optimization Formulation Studies

The formulations discussed in chapter 1 are:

Formulation 1:

*Minimize*  $V(x)$

Subject to:

$$h_k: E_k^M - E_k^* = 0$$

$$0 \leq \rho_e \leq 1$$

Formulation 2:

$$\text{Minimize } V(x)$$

Subject to:

$$h_k: (E_k^M - E_k^*)^2 \leq \delta$$

$$0 \leq \rho_e \leq 1$$

For formulation 3, the objective is to design a meta-material closest to the target moduli. For multi-criteria design, the objective is changed to the weighted summation of the square of differences between meta-material moduli and the target moduli. The weights are the relative importance of the objectives.

Formulation 3:

$$\text{Minimize } \sum_k (w_k)(E_k^M - E_k^*)^2$$

Subject to:

$$V_1 \leq V(x) \leq V_2$$

$$0 \leq \rho_e \leq 1$$

For single criteria design, formulation 3 does not converge either numerically or for SIMP convergence, as observed by Dr. Czech [5]. Hence, it is not considered for multi-criteria design. To study the other formations, each are used to optimize for different targets on the elastic modulus and shear modulus. Both homogenization and volume averaging are used to evaluate the modulus. For Volume Averaging, the RVE is chosen to contain 3x3 unit cells. The UC is a square, with 20x20 discretization. Optimization is solved using MATLABs SQP algorithm. Early termination parameters of 400 iterations is used. Base material is a fictional isotropic linear material with Young's modulus 30 GPa and Poisson's ratio 0.3.

The formulations are also compared using the degrees of numerical convergence and SIMP convergence. The design is said to be numerically converged when it's effective modulus is very close to the target modulus. The number of active constraints ( $e \in \rho_e \geq 0.9$  or  $\leq 0.3$ ) are used as the degree of SIMP convergence.

The optimization problem is solved for all pairings of normal moduli targets 3, 9,

and 15 GPa and Shear Modulus targets 1, 3, and 5 GPa. For formulation 2, optimization is performed for  $\delta = 0.1, 1$  and 10.

Table 4.1: Numerical results for multi-criteria design, formulation 1, using Homogenization

$E_{22}$	$E_{12}$	V	Iterations	Function Evaluations	Active Constraints
3.0000	1.0000	0.3288	347	139608	0.9675
3.0000	3.0000	0.5768	73	29675	0.9500
3.0624	4.4848	0.8459	30	12119	0.9500
9.0000	1.0001	0.5076	114	46141	0.9300
9.0000	3.0000	0.5680	124	50125	0.9700
8.9999	4.9999	0.6576	53	21654	0.9100
14.9994	0.9992	0.6368	92	37304	0.8300
15.0009	3.0000	0.6603	104	42115	0.8900
15.0000	5.0000	0.7579	40	16441	0.5800

Table 4.2: Numerical results for multi-criteria design, formulation 2,  $\delta = 0.1$ , using Homogenization

$E_{22}$	$E_{12}$	V	Iterations	Function Evaluations	Active Constraints
2.9999	0.9999	0.3607	136	54943	0.8975
3.0001	2.9966	0.5874	35	14044	0.8900
3.0233	4.5439	0.8354	27	10899	1.0000
8.9951	1.0001	0.5682	87	34988	0.6500
9.0002	3.0001	0.7388	5	2013	0.3100
8.9872	4.9855	0.6691	41	16452	0.8800
15.0007	1.0000	0.6815	50	20074	0.6800
14.9990	3.0002	0.7523	32	12910	0.3600
15.0000	4.9999	0.7579	45	18455	0.5800

Table 4.3: Numerical results for multi-criteria design, formulation 2,  $\delta = 1$ , using Homogenization

$E_{22}$	$E_{12}$	V	Iterations	Function Evaluations	Active Constraints
2.9988	0.9985	0.3592	114	46120	0.8700
3.0010	2.9990	0.5730	70	28472	0.9500
0.0000	0.0000	0.0010	32	12901	1.0000
8.9857	1.0016	0.5815	52	20905	0.5550
8.9990	2.9990	0.5693	137	55353	0.9600
8.9902	4.9896	0.6603	43	17251	0.9000
15.0047	1.0045	0.7431	5	2012	0.5400
15.0008	2.9988	0.7825	5	2011	0.4700
14.9991	4.9990	0.7579	42	17243	0.5800

Table 4.4: Numerical results for multi-criteria design, formulation 2,  $\delta = 10$ , using Homogenization

$E_{22}$	$E_{12}$	V	Iterations	Function Evaluations	Active Constraints
2.9895	0.9897	0.3646	114	46127	0.8700
3.0100	2.9900	0.5730	57	23258	0.9500
3.0572	4.9716	0.8814	57	23041	0.9875
8.9900	0.9900	0.5008	111	44918	0.9200
8.9900	2.9900	0.5666	135	54551	0.9900
9.0100	4.9900	0.6575	53	21654	0.9100
14.9900	0.9900	0.5870	163	65764	0.9475
14.9900	2.9900	0.6611	112	45327	0.9000
14.9900	4.9900	0.7576	42	17243	0.5800

Table 4.5: Graphical results for multi-criteria design, formulation 1, using Homogenization

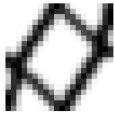



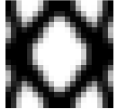
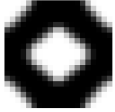
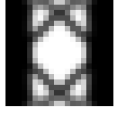
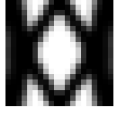
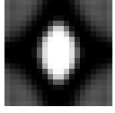
$E_{22}^t \backslash E_{12}^t$	$E_{12}^t$	1 GPa	3 GPa	5 GPa
3 GPa				
	9 GPa			
	15 GPa			

Table 4.6: Graphical results for multi-criteria design, formulation 2,  $\delta = 0.1$ , using Homogenization

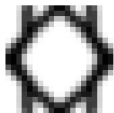
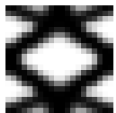



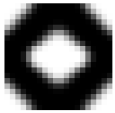
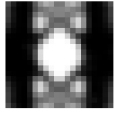

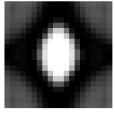
$E_{22}^t \backslash E_{12}^t$	$E_{12}^t$	1 GPa	3 GPa	5 GPa
3 GPa				
	9 GPa			
	15 GPa			

Table 4.7: Graphical results for multi-criteria design, formulation 2,  $\delta = 1$ , using Homogenization

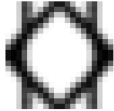



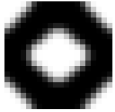
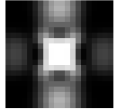
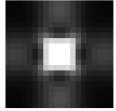
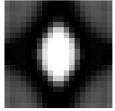
$E_{22}^t \backslash E_{12}^t$	$E_{12}^t$	1 GPa	3 GPa	5 GPa
3 GPa				
9 GPa				
15 GPa				

Table 4.8: Graphical results for multi-criteria design, formulation 2,  $\delta = 10$ , using Homogenization

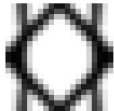



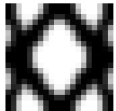
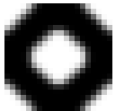

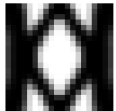
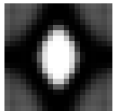
$E_{22}^t \backslash E_{12}^t$	$E_{12}^t$	1 GPa	3 GPa	5 GPa
3 GPa				
9 GPa				
15 GPa				

Table 4.9: Numerical results for multi-criteria design, formulation 1, using Volume Averaging

$E_{22}$	$E_{12}$	V	Iterations	Function Evaluations	Active Constraints
3.0002	0.9998	0.3447	105	108	0.9500
2.9947	2.9888	0.5817	51	64	0.9400
3.0265	4.1661	0.8255	23	69	1.0000
8.9916	1.0001	0.5304	99	104	0.8700
8.9993	2.9997	0.5796	122	123	0.8600
8.9974	4.9993	0.6583	54	66	0.9500
15.0030	0.9996	0.6330	94	95	0.8900
14.9996	2.9989	0.6801	117	208	0.9200
14.9989	4.9997	0.7417	87	88	0.7300

Table 4.10: Numerical results for multi-criteria design, formulation 2,  $\delta = 0.1$ , using Volume Averaging

$E_{22}$	$E_{12}$	V	Iterations	Function Evaluations	Active Constraints
2.9717	0.9967	0.5771	14	69	0.1600
3.0000	2.9989	0.7010	19	63	0.7100
3.3818	4.3418	0.8326	15	59	0.9775
9.0001	0.9990	0.5308	95	107	0.8200
8.9978	2.9916	0.5812	140	167	0.8500
8.9949	4.9940	0.6788	30	41	0.8800
14.9866	0.9872	0.6278	92	116	0.8900
14.9945	2.9982	0.7742	6	20	0.4700
15.0002	4.9999	0.7498	79	89	0.6700



Table 4.11: Numerical results for multi-criteria design, formulation 2,  $\delta = 1$ , using Volume Averaging

$E_{22}$	$E_{12}$	V	Iterations	Function Evaluations	Active Constraints
2.9940	0.9997	0.5677	18	58	0.1500
2.9987	2.9881	0.7012	16	55	0.7100
3.3763	4.1995	0.8482	24	90	0.9550
8.9961	0.9981	0.5352	91	105	0.8000
8.9977	2.9927	0.5819	116	157	0.8200
8.9937	4.9966	0.6713	35	45	0.9100
14.9990	0.9989	0.6306	84	111	0.9000
14.9923	2.9963	0.7739	6	20	0.4700
14.9977	4.9988	0.6925	144	163	0.9700

Table 4.12: Numerical results for multi-criteria design, formulation 2,  $\delta = 10$ , using Volume Averaging

$E_{22}$	$E_{12}$	V	Iterations	Function Evaluations	Active Constraints
2.9852	0.9999	0.6259	9	29	0.1400
3.0070	2.9865	0.6005	50	73	0.8500
3.4079	4.3535	0.8397	23	85	0.9125
8.9745	0.9885	0.5295	102	132	0.8100
8.9830	2.9860	0.5513	107	117	0.9300
8.9796	4.9729	0.6685	38	45	0.9300
14.9900	0.9888	0.6270	95	107	0.9000
14.9902	2.9900	0.6835	90	103	0.8100
14.9891	4.9897	0.7502	66	71	0.6700

Table 4.13: Graphical results for multi-criteria design, formulation 1, using Volume Averaging

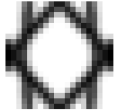




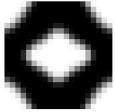



$E_{22}^t \backslash E_{12}^t$	1 GPa	3 GPa	5 GPa
3 GPa			
9 GPa			
15 GPa			

Table 4.14: Graphical results for multi-criteria design, formulation 2,  $\delta = 0.1$ , using Volume Averaging

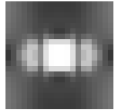






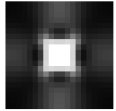

$E_{22}^t \backslash E_{12}^t$	1 GPa	3 GPa	5 GPa
3 GPa			
9 GPa			
15 GPa			

Table 4.15: Graphical results for multi-criteria design, formulation 2,  $\delta = 1$ , using Volume Averaging

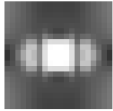




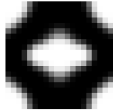

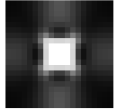
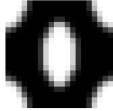
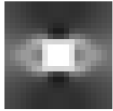



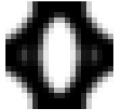
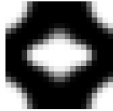

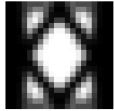
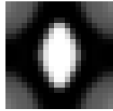
$E_{22}^t \backslash E_{12}^t$	1 GPa	3 GPa	5 GPa
3 GPa			
9 GPa			
15 GPa			

Table 4.16: Graphical results for multi-criteria design, formulation 2,  $\delta = 10$ , using Volume Averaging

$E_{22}^t \backslash E_{12}^t$	1 GPa	3 GPa	5 GPa
3 GPa			
9 GPa			
15 GPa			

#### 4.1.1 Discussion on Results

The results for the different optimization problems are listed in Tables 4.9 to 4.8.

Firstly it is observed that the problems do not converge to numerically feasible

solutions while targeting  $E_{22}^t = 3$  GPa and  $E_{12}^t = 5$  GPa. It is also observed that formulation 1 generally has better numerically and SIMP converged results. It can also be observed that for high values of both  $E_{22}^t$  and  $E_{12}^t$ , the solutions have numerically converged, but have not SIMP-converged. Apart from the exception cases, all other problems converge to well resolved meta-materials.

This study serves as the demonstration of the use of multi-criteria formulations while designing meta-materials using homogenization and volume averaging. It should be noted that solutions for multi-criteria problems using homogenization exists in the literature [28].

## 4.2 Range of Obtainable Moduli

For a two-phase composite material, there exists a rigorous bound on the effective moduli, as a function of the volume fraction of the constituent phases. Meta-materials can be seen as a two-phase composite material with one phase being the base material and the other being void.

The shear modulus is bounded by Hashin-Shtrikman bounds [25], which are:

$$G^+ = G_2 + \frac{1 - V}{(G_1 - G_2)^{-1} + \frac{2V(K_2 + 2G_2)}{5G_2(K_2 + 1.3333G_2)}}$$

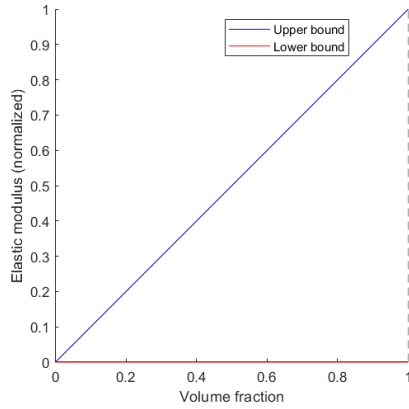
$$G^- = G_1 + \frac{V}{(G_2 - G_1)^{-1} + \frac{2(1-V)(K_1 + 2G_1)}{5G_1(K_1 + 1.3333G_1)}}$$

The elastic modulus is bounded by Voight-Reuss bounds [29], which are:

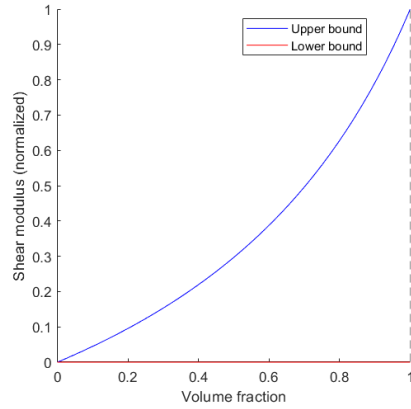
$$E^+ = (1 - V)E_1 + VE_2$$

$$E^- = \left( \frac{1 - V}{E_1} + \frac{V}{E_2} \right)^{-1}$$

For 1-phase meta-materials, consider a base material with Young's Modulus  $E_0$ , shear modulus  $G_0$ . The corresponding moduli for void is taken as  $\phi$  ( $\phi \ll E_0, G_0$ ).



(a) Bounds on Elastic Modulus



(b) Bounds on Shear Modulus

Figure 4.1: Bounds on the Elastic and Shear Moduli

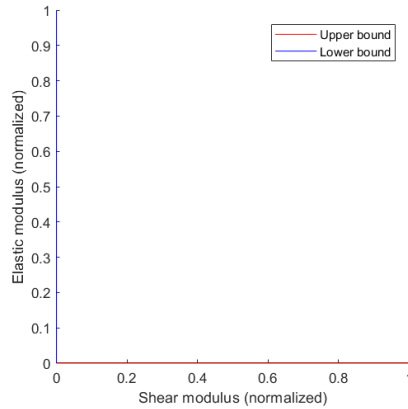


Figure 4.2: Bounds on moduli, plotted against each other

The normalized bounds for the effective moduli of the meta-material are shown in Figures 4.1a to 4.1b. The bounds are plotted against each other as a parametric function of the volume fraction, as seen in Figure 4.2. Figure 4.2 shows that there should be no bounds between the shear and elastic moduli.

It should be noted that these bounds do not consider the fact that the optimization formulations discussed earlier, will not converge to “un-connected” meta-materials (where a chunk of material is surrounded completely by void). In experience, as observed during the formulation studies, optimization does not converge when targeting extreme combinations

of moduli. (high shear modulus, very small elastic modulus target, or vice versa).

Such extreme meta-materials are possible, as proven by Milton et. al [24]. By using 1-node connections and origami meta-materials, one can design materials stiff in one deformation mode, but will collapse in other [24]. For continuum-like meta-materials as discussed by this thesis, the bounds may or may not be the same.

To find the bounds between obtainable moduli for meta-materials designed using TO, the following optimization problems are formulated.

$$\text{Minimize } E_{22}^M$$

Subject to:

$$E_{12}^M - E_{12}^* = 0$$

$$0 \leq \rho_e \leq 1$$

$$\text{Minimize } E_{12}^M$$

Subject to:

$$E_{22}^M - E_{22}^* = 0$$

$$0 \leq \rho_e \leq 1$$

An RVE of 3x3 Unit cells is chosen, with 20x20 mesh for each UC. The two formulations are run for  $E_{12}^* = (0, 0.1, 0.2, \dots, 1) * D_{12}$  and  $E_{22}^* = (0, 0.1, 0.2, \dots, 1) * D_{22}$ . Standard meta-material design parameters as used, as mentioned while performing the fictional material optimization in Chapter 3.

The results are shown in Figure 4.3.

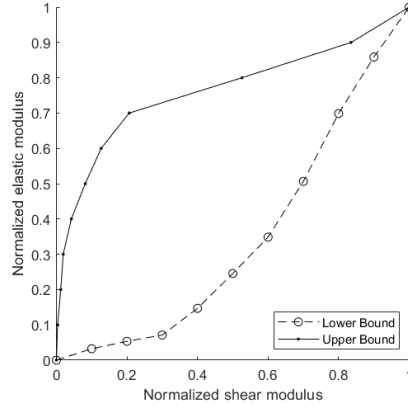


Figure 4.3: Obtained bounds for 20x20 mesh, 3x3 UCs, 0 offset problem

It can be clearly seen in Figure 4.3, that not all combinations of  $E^{22}$  and  $E^{12}$  can be achieved for meta-materials designed using Topology Optimization.

To further investigate and understand this phenomenon, the formulations are run for multiple times while changing TO parameters like number of variables, number of unit cells in the RVE. This is done to study the effects of the parameters on the bounding. The offset periodicity, as explained in Chapter 3 is introduced, and the formulations are repeated for different offsets to see how the modified periodicity may affect the bounds.

#### 4.2.1 Effect of number of design variables

The number of design variables are inversely proportional to the size of the finite elements used. The minimum obtainable feature length is  $2r_{min}$ , while  $r_{min}$  has to be at least  $2h$  for proper mesh filtering [18]. This means at-most the minimum feature length would be  $4 * h$ . This restricts the number of obtainable meta-materials. By using a finer mesh, smaller feature lengths can be obtained, which expands the design space. The initial hypothesis is that, this expanded design space would relax the bounds. i.e. The degree of restriction of obtainable combinations of shear and elastic modulus is inversely proportional to the mesh size used, and directly proportional to the square root of the number of design variables).

To test this hypothesis, the optimization formulations are solved for a coarser mesh size of 20x20 and a finer mesh size of 50x50. The results obtained are shown in Figure 4.4.

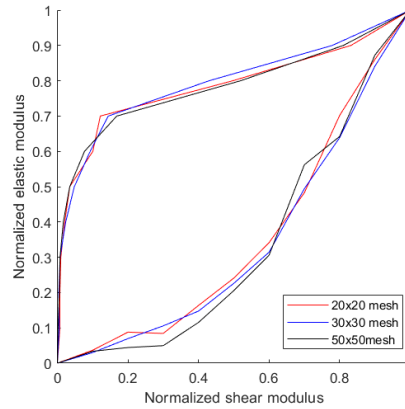


Figure 4.4: Obtained bounds for different mesh sizes

As seen in Figure 4.4, the mesh size does not affect the degree of restriction of obtainable combinations of moduli. The initial hypothesis is rejected. By doing this study, it is concluded that the bounding phenomenon does not occur due to the smaller design space of a coarse mesh. An even finer mesh could be used to test this. However, the current hardware limitations do not allow this. (Each optimization for 50x50 mesh size takes around 45 hours.)

#### 4.2.2 Effect of number of UCs in the RVE

Generally speaking, the smaller the RVE, the stiffer is the meta-material [5]. The studies on different geometries and different RVEs performed by Dr. Czech corroborates this [5]. An example of this is shown in Figure 4.5.



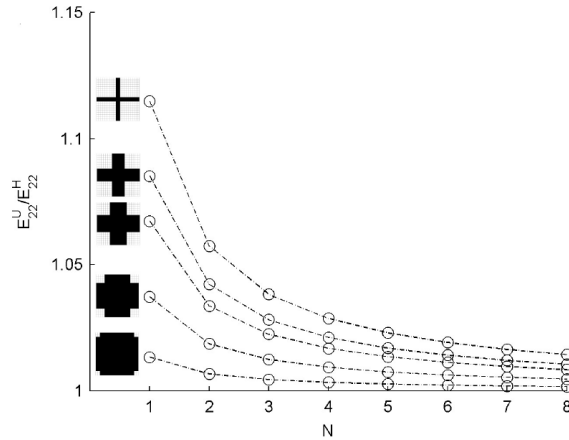


Figure 4.5: Elastic modulus for different RVEs ( $N \times N$ ), as calculated by Dr. Czech [5]

The initial hypothesis is that, because of this “additional” stiffness for meta-materials with small RVEs, the range of obtainable combinations of the moduli is inversely proportional to the number of UCs in the RVE.

To test this hypothesis, the optimization formulations are solved for RVEs containing  $3 \times 3$ , and  $5 \times 5$  UCs. The optimization is also solved using asymptotic homogenization, which is effectively considering a meta-material with nearly  $\infty \times \infty$  UCs.

The formulations are also run for single layer meta-materials with RVE containing  $3 \times 1$ ,  $5 \times 1$ ,  $1 \times 3$  and  $1 \times 5$  UCs. This is to test the effect of RVE size on layered meta-materials like the ones used for the shear beam of non-pneumatic wheels, in Chapter 3. The results obtained are shown in Figures 4.6- 4.7.

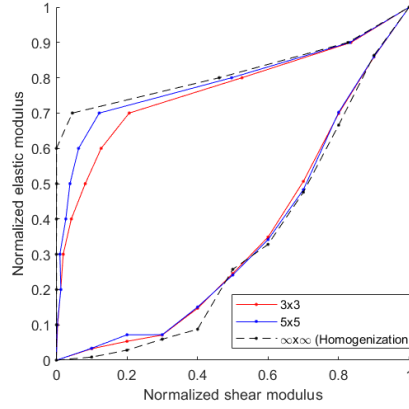


Figure 4.6: Obtained bounds for different RVEs ( $N \times N$ )

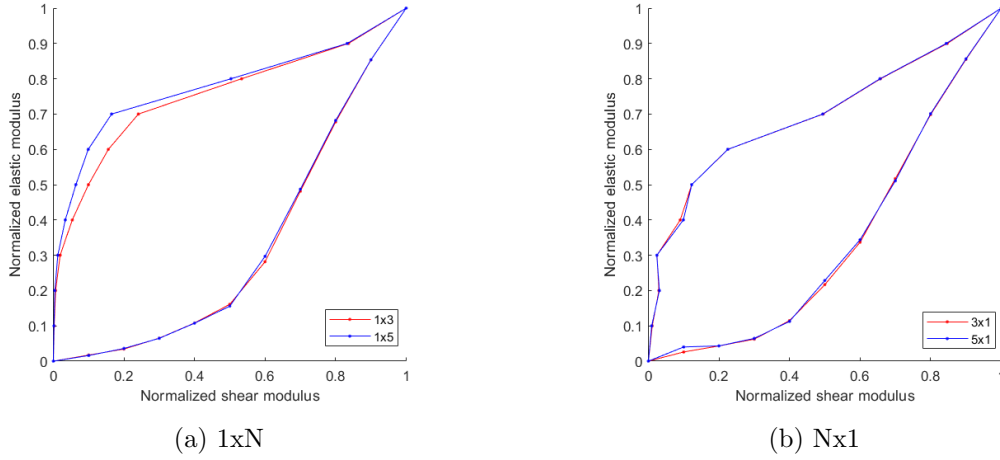


Figure 4.7: Obtained bounds for different RVEs

It can be observed from Figure 4.6 that the upper bound on  $E_{22}$  relaxes as the number of UCs are increased in the RVE. Figures 4.7a- 4.7a, show that the number of UCs in the  $j^{th}$  direction is what contributes to the relaxation on the upper bound on  $E_{jj}$ , for a certain  $E_{12}$ .

Note that the lower bound on  $E_{22}$  for a certain  $E_{12}$ , is not affected by the number of UCs in the RVE.

The initial hypothesis is concluded to be true for upper bound (of  $E_{22}$  for a certain  $E_{12}$ ), and false for lower bounds (of  $E_{22}$  for a certain  $E_{12}$ ).

### 4.2.3 Effect of Offset

As observed in chapter 3, The stiffness and offset parameter may or may not have any direct co-relation. Offset periodicity changes the topological connectivity, which introduces new classes of materials, but renders other as unobtainable. As seen in chapter 3, different offsets can lead to different classes of optimum meta-materials. Will this have an effect on the degree of restriction of the bounds between the moduli? Because there is no direct co-relation between stiffness and offset, it is difficult to hypothesize any specific effect of offset on the degree of restriction on the bounds.

To find the effect of offset on the bounds (if any), the original bounding optimization is performed for offsets 0, quarter-widths and half-widths. The results obtained are shown in Figure 4.8.

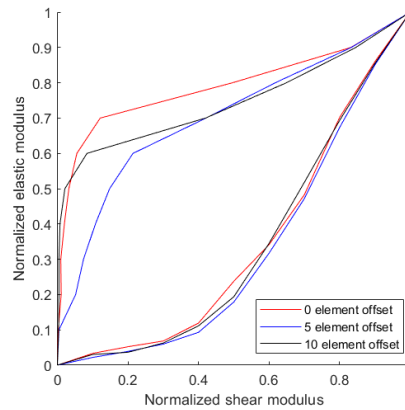


Figure 4.8: Obtained bounds for different offsets

Figure 4.8 shows that offset has a significant impact on the degree of restriction on the upper bounds (of  $E_{22}$  for a certain  $E_{12}$ ), while no effect on the lower bound (of  $E_{22}$  for a certain  $E_{12}$ ).

## 4.3 Summary

This chapter established the feasibility of the formulations discussed in chapter 1, for multi-criteria design of meta-materials using Volume Averaging.

It was discovered that TO for meta-material design cannot design “extreme” meta-materials, which are stiff in one mode of deformation, while totally compliant in another. This will help designers using this method to add constraints to the system-level optimization step of meta-material design, to avoid such extreme materials.

Physically, there is no known restriction on the range of obtainable moduli. It is hypothesized that the restriction in obtainable combinations of moduli are due to the shortcomings of Topology Optimization method for designing meta-materials. Further research is needed to confirm or reject this.

Effect of different TO parameters on the degree of restriction of bounds was determined and discussed. This will help designers choose the different parameters as required for the specific design case.

# Chapter 5

## Concluding Remarks

### 5.1 Answering Research Questions

The research questions posed in Chapter 2 are listed below.

1. Will having offsets of unit cells other than none or half-widths lead to a broader class of meta-materials?
2. Must volume averaging be used to evaluate the effective behavior of offset meta-materials?
3. Is any combination of shear and elastic moduli achievable when using multi-criteria design of meta-materials?

Each of these questions are addressed below.

#### 5.1.1 Answering Question 1

The question was posed as an extension to Dr. Czech's research in half-width offset meta-materials. That research was the first time an auxetic honeycomb shaped meta-material was observed as the solution of Topology Optimization targeting effective shear modulus. It demonstrated that half-width offsets can lead Topology Optimization to output a different classes of meta-materials.

The same optimization problem (design of the shear beam of a non-pneumatic wheel) was solved for different offsets in Chapter 3. Based on the optimization results it was

observed that it is indeed possible to converge on differently shaped meta-materials for different offsets.

Based on the fictional material optimization in Chapter 3, it was observed that it is not necessary that either of the offsets can obtain meta-materials with the least volume.

### 5.1.2 Answering Question 2

It was initially hypothesized that homogenization cannot be used for evaluating the effective properties of an offset meta-material. This was because of the violation of Y-periodicity requirement of asymptotic homogenization. Previously, Dr. Czech had developed and demonstrated that Volume Averaging can be used to design meta-materials which break the other essential requirement for homogenization (scaling limit).

This question was partially answered by Dr. Czech's research into half-width offset meta-materials. In Chapter 3, it was demonstrated that homogenization cannot be used for offset meta-materials. Also in Chapter 3, by optimizing the fictional material problem and the shear beam of a non-pneumatic wheel, it was demonstrated that volume averaging can be used to design offset meta-materials with any value of offset parameters. The validation study in Appendix A, confirms that the analysis is accurate to within acceptable tolerances.

### 5.1.3 Answering Question 3

Extreme materials are meta-materials with high stiffness in one deformation mode, and low stiffness in another. Can such meta-materials be designed using Topology Optimization? By running the optimization problems formulated in Chapter 4, it was observed that such meta-materials could not be obtained as a result of Topology Optimization problem.

The range of obtainable moduli was established in chapter 4, and effects of different TO parameters were noted.

It was earlier proven in the literature that there are no physical limitations to the range of moduli for two-phase materials with one sufficiently stiff phase and one sufficiently compliant phase. It is currently hypothesized that the range of obtainable moduli estab-

lished in Chapter 4 are a limitation of the Topology Optimization method. Further research is needed to confirm or deny this.

## 5.2 Contributions

The contributions of this research to the science and engineering community are listed below.

- Demonstrated that homogenization cannot be used to design offset meta-materials.
- Demonstrated the use of Volume Averaging for design of meta-materials with offsets other than zero or half-width.
- Demonstrated for the first time, the use of Topology Optimization with Volume Averaging for multi-criteria design of meta-materials.
- Potentially identified a drawback of Topology Optimization for design of meta-materials: It cannot be used for the design of extreme meta-materials.
- Established the range of obtainable moduli that can be obtained using the current Topology Optimization method for the design of meta-materials.
- Established the effect of parameters such as mesh size, number of UCs in RVE, and offset, on the range of obtainable moduli.
- Discussed the bounds on the shear modulus as a function of elastic modulus, for 1-phase continuous structures (with a minimum feature length) for the first time.

## 5.3 Future Research

### 5.3.1 Variable offset parameters

The problems posed in this research were for a constant offset parameter. The goal of considering offset meta-materials was to find the optimum meta-material across different

offset values. Optimization of the meta-material for all offsets possible, and then choosing the design with the least volume, is computationally inefficient.

Instead, the offset parameter  $b$ , can be considered a design variable. This complicates the optimization formulation, because  $b$  is a discrete parameter. To avoid re-discretization of the domain,  $b$  is limited to integer multiples of element size  $h$ .

For a variable  $b$ , one must consider a continuous  $b$ , or use optimization algorithms that can handle integer variables, such as NSGA-II. The feasibility and disadvantages of each of these directions needs to be looked into.

### **5.3.2 Further investigation into the range of obtainable effective properties of meta-materials**

This research established the range combinations of shear and elastic moduli that can be obtained using the current Topology Optimization method for design of meta-materials. It is hypothesized that this is a drawback of the Topology Optimization method for design of meta-materials. Further investigation is needed to confirm or deny this.

The effect of more parameters on the range of obtainable moduli, such as filter size  $r_{min}$ , SIMP penalty  $s$ , etc. needs to be investigated.

The range of different obtainable properties needs to be established. This research only considered shear and elastic moduli. Other elastic properties which can be considered are the different effective Poisson's ratio and effective bulk modulus.

### **5.3.3 Non-linear meta-materials**

The meta-materials designed in this thesis have a targeted linear elastic behaviour. Some design problems may desire meta-materials with a prescribed non-linear behaviour.

A method can be developed to design non-linear meta-materials, using Topology Optimization with volume averaging. Both homogenization and volume averaging needs to be modified for geometric non-linearity (large displacements).



#### **5.3.4 Inclusion of failure properties**

All optimization problems in this research deals only with the effective properties of the meta-materials. The designed meta-materials, especially ones with low volume fractions, are susceptible to failures due to Von-Mises stresses or buckling stresses. A constraint can be added to the optimization formulations to prevent such failures.

# Appendices

# Appendix A

## Code Development and Validation

All modulus evaluation analysis and optimization in this thesis are developed on MATLAB 2017b. This appendix deals with the development and validation of the written programs.

### A.1 Program development

#### A.1.1 Setting up parameters and optimization

The main program defines and generates the input files, and set-ups the optimization problem. The matlab function used for optimization is `fmincon`, or the constrained non-linear optimization function. Variable tolerances and initial point for optimization are input into the function, along with the volume and analysis functions.

`fmincon` communicates with the volume and analysis functions. It inputs the current design variables  $\rho$  to the functions, which evaluate the volume, moduli and their gradients with respect to  $\rho$ . `fmincon` uses these outputs for its SQP algorithm to calculate the next design variables. If converged, `fmincon` returns the optimized design variables.

The analysis function also requires 4 input files. `input.mat` lists the parameters required for Topology Optimization. `nodes.dat`, `elements.dat` and `centroids.dat` are the mesh files, which list all the nodes, and elements. The data flow between `fmincon` and the

volume and analysis functions can be visualized in Figure A.1.

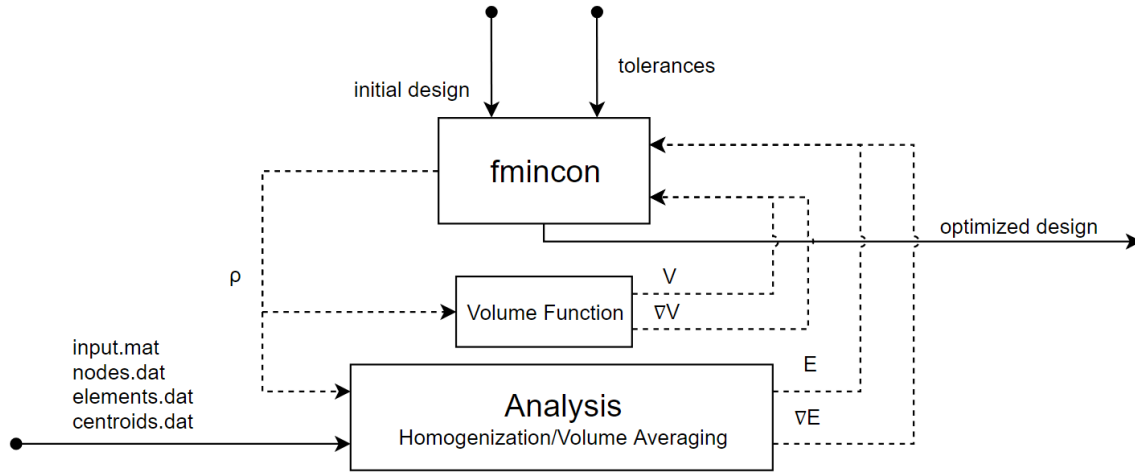


Figure A.1: Flow of data between Matlab’s fmincon, volume and analysis functions.

### A.1.2 Homogenization program

The homogenization programs requires the input files and densities  $\rho$ . First, the densities are filtered using the simple density filter discussed in Chapter 1. These filtered densities are used for SIMP, to generate material matrices for each element and then, the local FEA stiffness matrices for the corresponding element. The densities are also used to calculate the local FEA Force vectors. Global matrices  $K$  and  $F$  are assembled. Periodic and Symmetric boundary conditions, as explained in chapter 1 are enforced using the Lagrange Multiplier method. Nodal displacements are calculated as the solution to the equation  $[K]\{u\} = \{F\}$ . The displacements are used to calculate the strains in each element and hence the effective meta-material moduli  $E$ . Numerical finite differences methods are used to estimate the gradients of  $E$  w.r.t the densities.

### A.1.3 Volume Averaging program

Requires the input files and densities  $\rho$ . First, the densities are filtered using the simple density filter discussed in Chapter 1. These filtered densities are used for SIMP, to generate material matrices for each element and then, the local FEA stiffness matrices for

the corresponding element. Global stiffness matrix  $K$  is assembled. Boundary conditions are enforced using the direct elimination method. Nodal displacements are calculated as the solution to the equation  $[K]u = F$ . The displacements are used to calculate the strains and stresses in each element and hence average stresses and strains in the domain. Effective meta-material moduli are calculated as ratio of average stress to average strain. The analytical gradients are then calculated as explained in Chapter 1.

## A.2 Validation of Modulus for non-offset Meta-Materials.

The homogenization and Volume Averaging codes are validated against the calculations done by Bendsoe et. al [1]. The design evaluated by Bendsoe et. al. is a square UC with a rectangular hole in the center, as shown in Figure A.2.

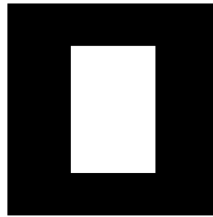


Figure A.2: Geometry evaluated [1]

The base material used has the following properties:  $E_{1111} = 30$ ,  $E_{2222} = 30$ ,  $E_{1122} = 10$ ,  $E_{1212} = 10$ . The effective modulus of the eometry evaluated by Bendsoe et. al. are:

$$E_{1111}^M = 13.015,$$

$$E_{1122}^M = 3.241,$$

$$E_{2222}^M = 17.552,$$

$$E_{1212}^M = 2.785 [1].$$

The moduli calculated by homogenization code developed are:

$$E_{1111}^H = 13.0148,$$

$$E_{2222}^H = 17.5523,$$

$$E_{1212}^H = 2.7849.$$

The moduli calculated by volume averaging (RVE=5x5 unit cells) code developed are:

$$E_{1111}^V = 12.6388,$$

$$E_{2222}^V = 17.0812,$$

$$E_{1212}^V = 2.6550.$$

Since the calculated moduli are within 5% of the moduli calculated by Bendsoe et. al [1], the program developed is validated.

The gradient of the modulus w.r.t the design variables is validated against Matlab's finite difference gradient. The difference between calculated gradient and the finite differences gradient within  $10^{-5}\%$ , the gradient is validated.

### A.3 Validation of Modulus for offset Meta-Materials.

It has been established in chapter 3 that only Volume Averaging can be used to evaluate the effective properties of offset meta-materials. To validate the Volume Averaging program, two FEA problems are setup, one for tensile loading and one for shear loading.

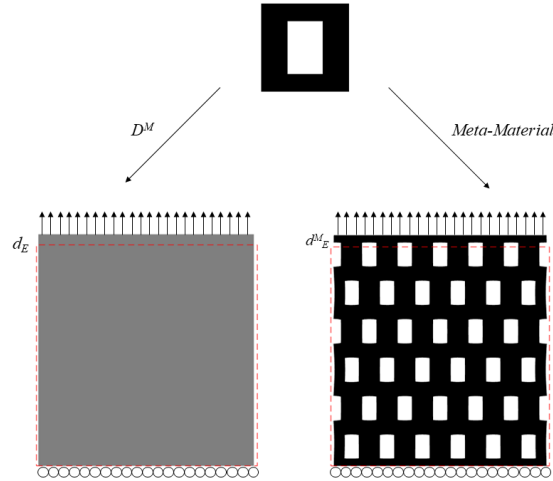


Figure A.3: Validation analysis for elastic modulus; here  $d_E$  is the vertical displacement of the top edge

First, the meta-material is loaded with the boundary conditions shown in Fig-

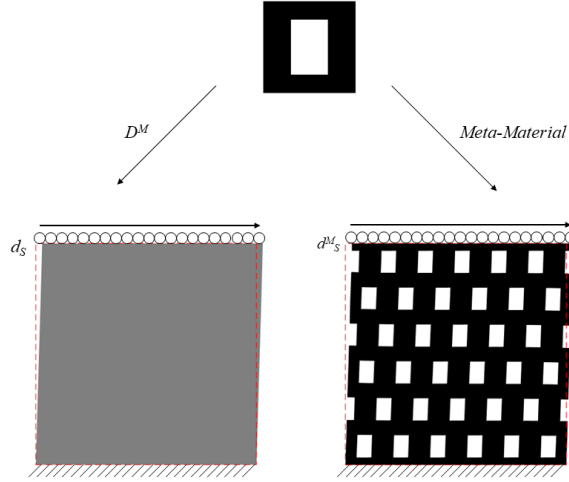


Figure A.4: Validation analysis for shear modulus; here  $d_S$  is the horizontal displacement of the top edge

ures A.3& A.4, and displacements  $d_S^M$  and  $d_E^M$  are calculated.

Then, the effective material matrix  $D^M$  is calculated using volume averaging. A homogeneous material with properties  $D^M$  is loaded with the same boundary conditions, and the displacements  $d_S$  and  $d_E$  are calculated.

The displacements for the meta-material,  $d_S^M$  and  $d_E^M$ , are compared with the displacements for the homogeneous material,  $d_S$  and  $d_E$ . If they results match within a certain amount of error, we can conclude that the effective material matrix  $D^M$  is valid.

The relative error between  $d$  and  $d^M$  for the meta-material shown in Figure A.2 for different offsets are displayed in Table A.1.

The gradient of the modulus w.r.t the design variables is validated against Matlab's finite difference gradient. The difference between calculated gradient and the finite differences gradient within  $10^{-5}\%$ , the gradient is validated.

Table A.1: Relative difference between displacements for meta-material and corresponding homogeneous material

Offset	% error in $d_E$	% error in $d_S$
0	0.60	4.47
2	1.91	4.93
4	2.53	4.64
6	3.79	4.16
8	3.09	3.56
10	2.91	2.42



## Appendix B

# Geometric Results - Shear Beam of a Non-Pneumatic Wheel

Table B.1: Optimization results for  $sl_{Thk} = 5$  mm, initial point A.

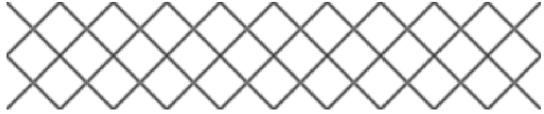










Offset	V	Meta-Material
0	0.1116	
2	0.0706	
4	0.0701	
6	0.0692	
8	0.0688	
10	0.0690	
12	0.1125	
14	0.1086	
16	0.1068	
18	0.1109	
20	0.1324	

Table B.2: Optimization results for  $sl_{Thk} = 6$  mm, initial point A.

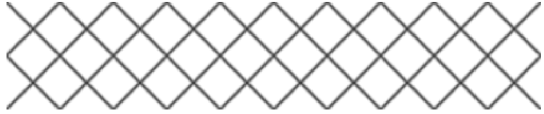










Offset	V	Meta-Material
0	0.1062	
2	0.0662	
4	0.0660	
6	0.0651	
8	0.0646	
10	0.0644	
12	0.1074	
14	0.1017	
16	0.1021	
18	0.1039	
20	0.1259	

Table B.3: Optimization results for  $sl_{Thk} = 7$  mm, initial point A.

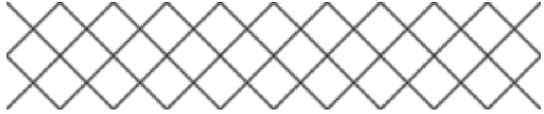










Offset	V	Meta-Material
0	0.1000	
2	0.0628	
4	0.0653	
6	0.0617	
8	0.0614	
10	0.0609	
12	0.0611	
14	0.1024	
16	0.0958	
18	0.0993	
20	0.1204	

Table B.4: Optimization results for  $sl_{Thk} = 8$  mm, initial point A.

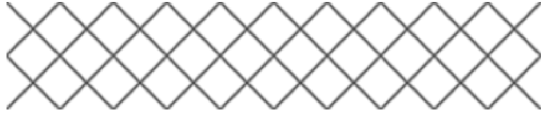










Offset	V	Meta-Material
0	0.0974	
2	0.0603	
4	0.0596	
6	0.0590	
8	0.0591	
10	0.0584	
12	0.0583	
14	0.0987	
16	0.0974	
18	0.0975	
20	0.1165	

Table B.5: Optimization results for  $sl_{Thk} = 9$  mm, initial point A.

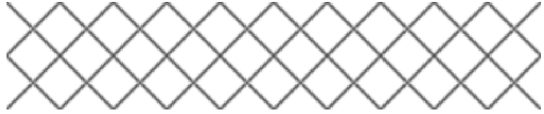









Offset	V	Meta-Material
0	0.0964	
2	0.0577	
4	0.0000	<div style="border: 1px solid black; padding: 5px; text-align: center;"><i>did not converge</i></div>
6	0.0567	
8	0.0563	
10	0.0567	
12	0.0562	
14	0.0974	
16	0.0891	
18	0.0959	
20	0.1123	

Table B.6: Optimization results for  $sl_{Thk} = 10$  mm, initial point A.

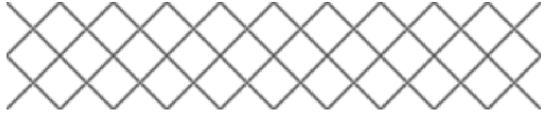










Offset	V	Meta-Material
0	0.0935	
2	0.0558	
4	0.0555	
6	0.0547	
8	0.0543	
10	0.0541	
12	0.0541	
14	0.0945	
16	0.0926	
18	0.0939	
20	0.1095	

Table B.7: Optimization results for  $sl_{Thk} = 11$  mm, initial point A.

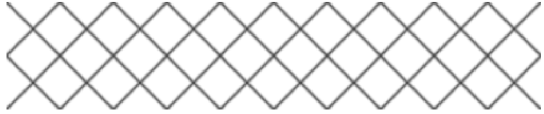










Offset	V	Meta-Material
0	0.0878	
2	0.0540	
4	0.0537	
6	0.0531	
8	0.0526	
10	0.0560	
12	0.0523	
14	0.0912	
16	0.0902	
18	0.0907	
20	0.1068	



Table B.8: Optimization results for  $sl_{Thk} = 12$  mm, initial point A.












Offset	V	Meta-Material
0	0.0859	
2	0.0529	
4	0.0521	
6	0.0539	
8	0.0514	
10	0.0509	
12	0.0509	
14	0.0890	
16	0.0881	
18	0.0886	
20	0.1039	

Table B.9: Optimization results for  $sl_{Thk} = 5$  mm, initial point B.

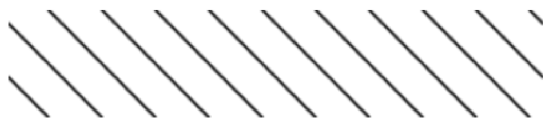


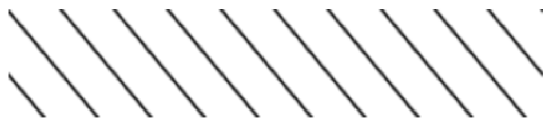


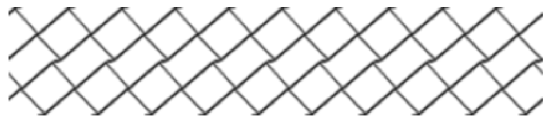
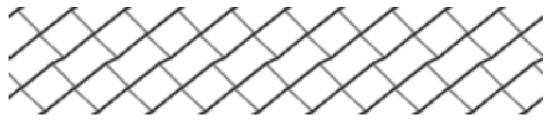

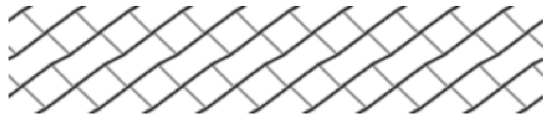

Offset	V	Meta-Material
0	0.0706	
2	0.0710	
4	0.0698	
6	0.0693	
8	0.0683	
10	0.0684	
12	0.1105	
14	0.1075	
16	0.1043	
18	0.1094	
20	0.1160	

Table B.10: Optimization results for  $sl_{Thk} = 6$  mm, initial point B.


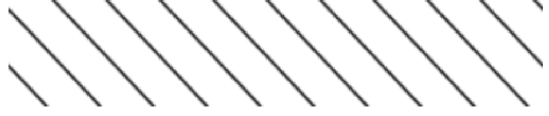
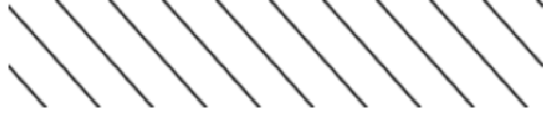

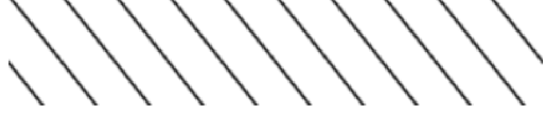
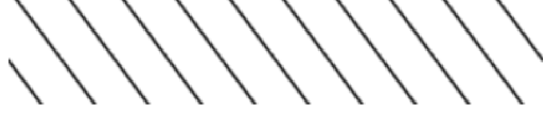





Offset	V	Meta-Material
0	0.1019	
2	0.0665	
4	0.0656	
6	0.0650	
8	0.0644	
10	0.0640	
12	0.1069	
14	0.1057	
16	0.0967	
18	0.1036	
20	0.1268	

Table B.11: Optimization results for  $sl_{Thk} = 7$  mm, initial point B.












Offset	V	Meta-Material
0	0.0941	
2	0.0632	
4	0.0624	
6	0.0616	
8	0.0610	
10	0.0608	
12	0.0604	
14	0.1022	
16	0.0996	
18	0.1002	
20	0.1066	

Table B.12: Optimization results for  $sl_{Thk} = 8$  mm, initial point B.


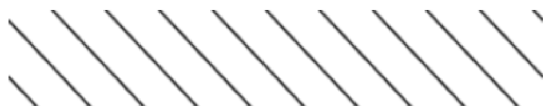
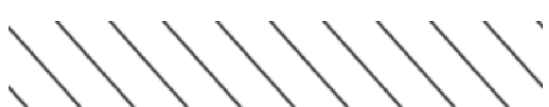
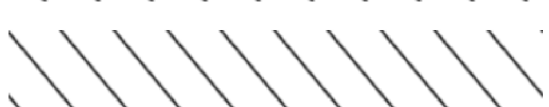







Offset	V	Meta-Material
0	0.0910	
2	0.0603	
4	0.0599	
6	0.0589	
8	0.0583	
10	0.0580	
12	0.0998	
14	0.0704	
16	0.0970	
18	0.0977	
20	0.1017	

Table B.13: Optimization results for  $sl_{Thk} = 9$  mm, initial point B.




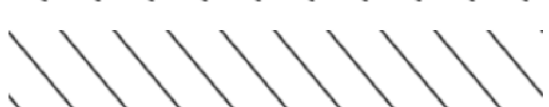







Offset	V	Meta-Material
0	0.0883	
2	0.0579	
4	0.0574	
6	0.0565	
8	0.0561	
10	0.0559	
12	0.0558	
14	0.0934	
16	0.0938	
18	0.0953	
20	0.0966	

Table B.14: Optimization results for  $sl_{Thk} = 10$  mm, initial point B.


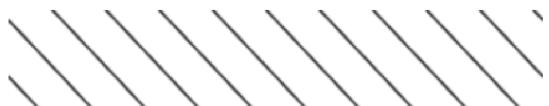

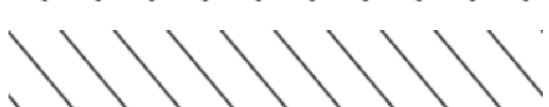







Offset	V	Meta-Material
0	0.0919	
2	0.0559	
4	0.0562	
6	0.0546	
8	0.0545	
10	0.0543	
12	0.0539	
14	0.0908	
16	0.0904	
18	0.0932	
20	0.0970	

Table B.15: Optimization results for  $sl_{Thk} = 11$  mm, initial point B.












Offset	V	Meta-Material
0	0.0857	
2	0.0539	
4	0.0536	
6	0.0529	
8	0.0526	
10	0.0523	
12	0.0523	
14	0.0912	
16	0.0886	
18	0.0904	
20	0.0932	



Table B.16: Optimization results for  $sl_{Thk} = 12$  mm, initial point B.




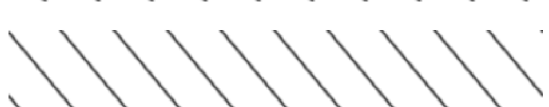







Offset	V	Meta-Material
0	0.0879	
2	0.0527	
4	0.0521	
6	0.0512	
8	0.0508	
10	0.0541	
12	0.0538	
14	0.0886	
16	0.0867	
18	0.0880	
20	0.0912	

Table B.17: Optimization results for  $sl_{Thk} = 5$  mm, initial point C.










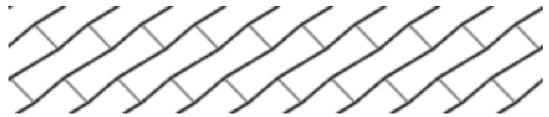

Offset	V	Meta-Material
0	0.1078	
2	0.0707	
4	0.0697	
6	0.0694	
8	0.0684	
10	0.0683	
12	0.0687	
14	0.0702	
16	0.1120	
18	0.0997	
20	0.1341	

Table B.18: Optimization results for  $sl_{Thk} = 6$  mm, initial point C.












Offset	V	Meta-Material
0	0.1004	
2	0.0663	
4	0.0655	
6	0.0649	
8	0.0643	
10	0.0640	
12	0.0645	
14	0.0648	
16	0.1115	
18	0.1036	
20	0.1266	

Table B.19: Optimization results for  $sl_{Thk} = 7$  mm, initial point C.


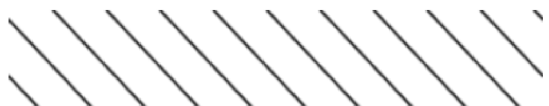

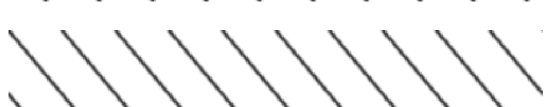


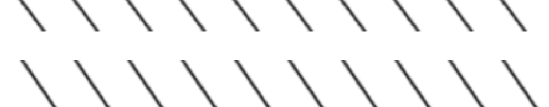




Offset	V	Meta-Material
0	0.0961	
2	0.0629	
4	0.0621	
6	0.0653	
8	0.0610	
10	0.0607	
12	0.0609	
14	0.0614	
16	0.1058	
18	0.0979	
20	0.1207	

Table B.20: Optimization results for  $sl_{Thk} = 8$  mm, initial point C.












Offset	V	Meta-Material
0	0.0939	
2	0.0601	
4	0.0594	
6	0.0589	
8	0.0585	
10	0.0581	
12	0.0583	
14	0.0582	
16	0.0589	
18	0.0970	
20	0.1172	

Table B.21: Optimization results for  $sl_{Thk} = 9$  mm, initial point C.












Offset	V	Meta-Material
0	0.0941	
2	0.0578	
4	0.0578	
6	0.0567	
8	0.0561	
10	0.0563	
12	0.0557	
14	0.0559	
16	0.0566	
18	0.0923	
20	0.1144	

Table B.22: Optimization results for  $sl_{Thk} = 10$  mm, initial point C.












Offset	V	Meta-Material
0	0.0865	
2	0.0560	
4	0.0553	
6	0.0545	
8	0.0542	
10	0.0537	
12	0.0541	
14	0.0538	
16	0.0972	
18	0.1009	
20	0.1100	

Table B.23: Optimization results for  $sl_{Thk} = 11$  mm, initial point C.












Offset	V	Meta-Material
0	0.0862	
2	0.0542	
4	0.0535	
6	0.0530	
8	0.0523	
10	0.0523	
12	0.0524	
14	0.0552	
16	0.0936	
18	0.0903	
20	0.1084	



Table B.24: Optimization results for  $sl_{Thk} = 12$  mm, initial point C.












Offset	V	Meta-Material
0	0.0827	
2	0.0527	
4	0.0518	
6	0.0513	
8	0.0510	
10	0.0505	
12	0.0556	
14	0.0505	
16	0.0924	
18	0.0902	
20	0.1048	

Table B.25: Optimization results for  $sl_{Thk} = 5$  mm, initial point D.



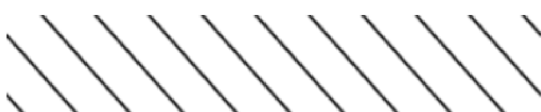

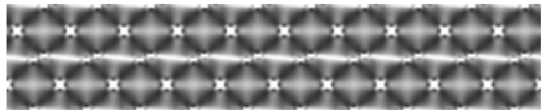

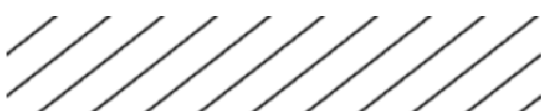
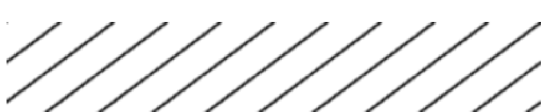


Offset	V	Meta-Material
0	0.1102	
2	0.0728	
4	0.0700	
6	0.0889	
8	0.5044	
10	0.0791	
12	0.0805	
14	0.0822	
16	0.0000	<div style="border: 1px solid black; padding: 5px; text-align: center;"><i>did not converge</i></div>
18	0.1001	
20	0.1328	

Table B.26: Optimization results for  $sl_{Thk} = 6$  mm, initial point D.






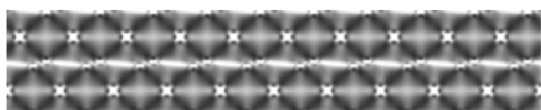





Offset	V	Meta-Material
0	0.1046	
2	0.0685	
4	0.0658	
6	0.0729	
8	0.0726	
10	0.4971	
12	0.0976	
14	0.0993	
16	0.0794	
18	0.0937	
20	0.1249	

Table B.27: Optimization results for  $sl_{Thk} = 7$  mm, initial point D.




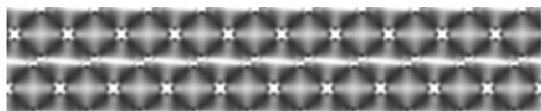






Offset	V	Meta-Material
0	0.1041	
2	0.0651	
4	0.0624	
6	0.4903	
8	0.0690	
10	0.0000	<div style="border: 1px solid black; padding: 5px; text-align: center;"><i>did not converge</i></div>
12	0.0719	
14	0.0739	
16	0.0751	
18	0.0859	
20	0.1203	

Table B.28: Optimization results for  $sl_{Thk} = 8$  mm, initial point D.








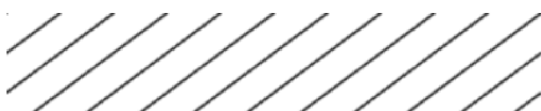
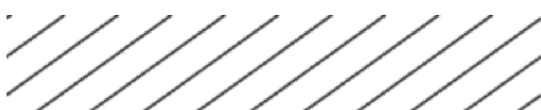

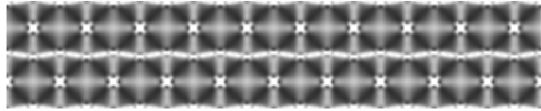
Offset	V	Meta-Material
0	0.0964	
2	0.0622	
4	0.0592	
6	0.0587	
8	0.0663	
10	0.0673	
12	0.0687	
14	0.0703	
16	0.0718	
18	0.0829	
20	0.5019	

Table B.29: Optimization results for  $sl_{Thk} = 9$  mm, initial point D.












Offset	V	Meta-Material
0	0.0600	
2	0.0597	
4	0.0575	
6	0.0565	
8	0.0633	
10	0.0646	
12	0.0706	
14	0.0753	
16	0.0789	
18	0.0897	
20	0.1120	

Table B.30: Optimization results for  $sl_{Thk} = 10$  mm, initial point D.












Offset	V	Meta-Material
0	0.0605	
2	0.0577	
4	0.0552	
6	0.0548	
8	0.0613	
10	0.0624	
12	0.0638	
14	0.0653	
16	0.0884	
18	0.0995	
20	0.4930	

Table B.31: Optimization results for  $sl_{Thk} = 11$  mm, initial point D.



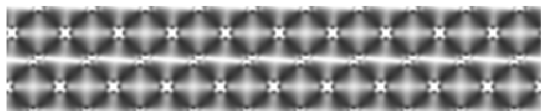







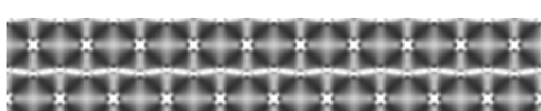


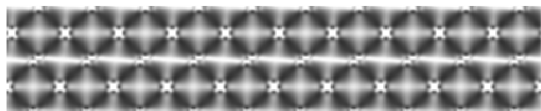








Offset	V	Meta-Material
0	0.0879	
2	0.0559	
4	0.4686	
6	0.0586	
8	0.0593	
10	0.0607	
12	0.0618	
14	0.0881	
16	0.0739	
18	0.0876	
20	0.4898	



Table B.32: Optimization results for  $sl_{Thk} = 12$  mm, initial point D.

Offset	V	Meta-Material
0	0.0891	
2	0.0545	
4	0.4651	
6	0.0565	
8	0.0578	
10	0.0591	
12	0.0869	
14	0.0851	
16	0.0857	
18	0.0861	
20	0.1038	

## Appendix C

# Numerical Results - Shear Beam of a Non-Pneumatic Wheel

Table C.1: Numerical results for  $sl_{Thk} = 5$  mm, initial point A.

Offset	$G_{12}$	V	Iterations	Function Evaluations	Active Constraints
0	12.9373	0.1116	203	408	0.8675
2	13.3927	0.0706	219	439	0.9731
4	13.3953	0.0701	248	504	0.9738
6	13.3983	0.0692	240	483	0.9800
8	13.3962	0.0688	223	452	0.9794
10	13.4001	0.0690	400	801	0.9769
12	13.3239	0.1125	223	448	0.9731
14	13.4007	0.1086	313	638	0.9419
16	13.3129	0.1068	212	428	0.9594
18	13.3240	0.1109	244	493	0.9506
20	13.4019	0.1324	227	454	0.9688

Table C.2: Numerical results for  $sl_{Thk} = 6$  mm, initial point A.

Offset	$G_{12}$	V	Iterations	Function Evaluations	Active Constraints
0	10.9263	0.1062	187	375	0.8625
2	11.1699	0.0662	220	441	0.9744
4	11.1703	0.0660	192	385	0.9712
6	11.1744	0.0651	246	504	0.9788
8	11.1652	0.0646	267	551	0.9794
10	11.1791	0.0644	299	610	0.9812
12	11.1061	0.1074	250	513	0.9637
14	11.1519	0.1017	400	801	0.9337
16	11.1453	0.1021	242	490	0.9406
18	11.0935	0.1039	248	500	0.9681
20	11.1238	0.1259	251	503	0.9425

Table C.3: Numerical results for  $sl_{Thk} = 7$  mm, initial point A.

Offset	$G_{12}$	V	Iterations	Function Evaluations	Active Constraints
0	9.5699	0.1000	180	361	0.9050
2	9.5730	0.0628	204	408	0.9775
4	9.5219	0.0653	193	390	0.9294
6	9.5694	0.0617	202	410	0.9769
8	9.5702	0.0614	233	476	0.9762
10	9.5572	0.0609	257	517	0.9769
12	9.5732	0.0611	400	801	0.9806
14	9.5133	0.1024	214	432	0.9575
16	9.5020	0.0958	346	695	0.9556
18	9.4765	0.0993	290	592	0.9513
20	9.5638	0.1204	228	458	0.9413

Table C.4: Numerical results for  $sl_{Thk} = 8$  mm, initial point A.

Offset	$G_{12}$	V	Iterations	Function Evaluations	Active Constraints
0	8.1484	0.0974	180	361	0.8725
2	8.3753	0.0603	223	446	0.9712
4	8.3800	0.0596	192	389	0.9788
6	8.3797	0.0590	206	426	0.9825
8	8.3810	0.0591	237	482	0.9769
10	8.3791	0.0584	225	459	0.9756
12	8.3776	0.0583	400	816	0.9838
14	8.3234	0.0987	215	431	0.9613
16	8.3245	0.0974	286	575	0.9494
18	8.3672	0.0975	231	464	0.9513
20	8.3791	0.1165	195	392	0.9287

Table C.5: Numerical results for  $sl_{Thk} = 9$  mm, initial point A.

Offset	$G_{12}$	V	Iterations	Function Evaluations	Active Constraints
0	7.4385	0.0964	161	372	0.8600
2	7.4385	0.0577	191	411	0.9769
4	0.0000	0.0000	0	0	0.0000
6	7.4394	0.0567	167	358	0.9781
8	7.4338	0.0563	178	366	0.9850
10	7.4398	0.0567	212	452	0.9719
12	7.4383	0.0562	389	801	0.9769
14	7.4398	0.0974	192	391	0.9444
16	7.3904	0.0891	400	896	0.9650
18	7.3854	0.0959	211	425	0.9425
20	7.4230	0.1123	189	381	0.9350

Table C.6: Numerical results for  $sl_{Thk} = 10$  mm, initial point A.

Offset	$G_{12}$	V	Iterations	Function Evaluations	Active Constraints
0	6.6987	0.0935	164	332	0.8600
2	6.7003	0.0558	202	409	0.9800
4	6.6901	0.0555	203	408	0.9781
6	6.6984	0.0547	210	420	0.9819
8	6.6977	0.0543	236	483	0.9862
10	6.6976	0.0541	255	512	0.9881
12	6.6988	0.0541	305	622	0.9856
14	6.6989	0.0945	226	458	0.9469
16	6.6533	0.0926	234	473	0.9475
18	6.6358	0.0939	210	424	0.9325
20	6.6856	0.1095	188	378	0.9400

Table C.7: Numerical results for  $sl_{Thk} = 11$  mm, initial point A.

Offset	$G_{12}$	V	Iterations	Function Evaluations	Active Constraints
0	6.0906	0.0878	174	349	0.9075
2	6.0582	0.0540	207	416	0.9806
4	6.0892	0.0537	217	435	0.9788
6	6.0908	0.0531	234	469	0.9800
8	6.0890	0.0526	229	466	0.9881
10	6.0668	0.0560	255	515	0.9437
12	6.0558	0.0523	287	582	0.9881
14	6.0523	0.0912	205	416	0.9506
16	6.0567	0.0902	222	451	0.9475
18	6.0558	0.0907	231	467	0.9431
20	6.0761	0.1068	174	352	0.9287

Table C.8: Numerical results for  $sl_{Thk} = 12$  mm, initial point A.

Offset	$G_{12}$	V	Iterations	Function Evaluations	Active Constraints
0	5.3373	0.0859	165	336	0.9000
2	5.5693	0.0529	210	420	0.9775
4	5.5701	0.0521	210	421	0.9838
6	5.5428	0.0539	227	464	0.9394
8	5.5789	0.0514	233	477	0.9775
10	5.5787	0.0509	295	599	0.9881
12	5.5791	0.0509	348	702	0.9862
14	5.5472	0.0890	189	383	0.9506
16	5.5668	0.0881	211	425	0.9494
18	5.5710	0.0886	242	495	0.9444
20	5.5491	0.1039	205	412	0.9337

Table C.9: Numerical results for  $sl_{Thk} = 5$  mm, initial point B.

Offset	$G_{12}$	V	Iterations	Function Evaluations	Active Constraints
0	13.4000	0.0706	207	420	0.9769
2	13.4020	0.0710	244	489	0.9700
4	13.4009	0.0698	259	545	0.9731
6	13.3969	0.0693	294	604	0.9781
8	13.3966	0.0683	252	506	0.9819
10	13.3954	0.0684	400	801	0.9806
12	13.3765	0.1105	244	493	0.9463
14	13.3080	0.1075	348	704	0.9469
16	13.3948	0.1043	302	621	0.9556
18	13.3981	0.1094	262	527	0.9481
20	13.3146	0.1160	314	636	0.9500

Table C.10: Numerical results for  $sl_{Thk} = 6$  mm, initial point B.

Offset	$G_{12}$	V	Iterations	Function Evaluations	Active Constraints
0	11.1703	0.1019	189	381	0.9475
2	11.1699	0.0665	206	412	0.9731
4	11.1708	0.0656	218	438	0.9738
6	11.1746	0.0650	244	490	0.9794
8	11.1640	0.0644	269	540	0.9806
10	11.1698	0.0640	315	642	0.9775
12	11.1133	0.1069	381	767	0.9650
14	11.1121	0.1057	221	444	0.9537
16	11.1062	0.0967	299	608	0.9831
18	11.0987	0.1036	272	549	0.9450
20	11.1647	0.1268	269	542	0.9244

Table C.11: Numerical results for  $sl_{Thk} = 7$  mm, initial point B.

Offset	$G_{12}$	V	Iterations	Function Evaluations	Active Constraints
0	9.5533	0.0941	177	360	0.9888
2	9.5708	0.0632	217	434	0.9731
4	9.5691	0.0624	200	403	0.9738
6	9.5650	0.0616	227	460	0.9806
8	9.5704	0.0610	246	493	0.9781
10	9.5696	0.0608	261	529	0.9794
12	9.5159	0.0604	400	801	0.9900
14	9.5131	0.1022	282	570	0.9531
16	9.5101	0.0996	243	490	0.9500
18	9.4239	0.1002	233	469	0.9306
20	9.5686	0.1066	244	494	0.9688

Table C.12: Numerical results for  $sl_{Thk} = 8$  mm, initial point B.

Offset	$G_{12}$	V	Iterations	Function Evaluations	Active Constraints
0	8.3656	0.0910	175	353	0.9750
2	8.3795	0.0603	204	419	0.9731
4	8.3779	0.0599	194	402	0.9706
6	8.3768	0.0589	234	474	0.9812
8	8.3791	0.0583	241	493	0.9788
10	8.3379	0.0580	265	538	0.9850
12	8.3360	0.0998	197	398	0.9487
14	8.3815	0.0704	400	801	0.9806
16	8.3332	0.0970	268	541	0.9531
18	8.3082	0.0977	220	445	0.9500
20	8.3423	0.1017	207	433	0.9625

Table C.13: Numerical results for  $sl_{Thk} = 9$  mm, initial point B.

Offset	$G_{12}$	V	Iterations	Function Evaluations	Active Constraints
0	7.4378	0.0883	175	353	0.9575
2	7.4329	0.0579	203	408	0.9819
4	7.4375	0.0574	175	365	0.9756
6	7.3978	0.0565	176	392	0.9825
8	7.4396	0.0561	211	466	0.9812
10	7.4399	0.0559	225	459	0.9838
12	7.4435	0.0558	400	829	0.9819
14	7.4389	0.0934	400	801	0.9456
16	7.4078	0.0938	214	431	0.9644
18	7.3987	0.0953	218	438	0.9381
20	7.4004	0.0966	400	811	0.9537



Table C.14: Numerical results for  $sl_{Thk} = 10$  mm, initial point B.

Offset	$G_{12}$	V	Iterations	Function Evaluations	Active Constraints
0	6.5055	0.0919	186	378	0.8662
2	6.6976	0.0559	229	459	0.9838
4	6.7004	0.0562	199	398	0.9656
6	6.6997	0.0546	230	463	0.9838
8	6.6999	0.0545	235	492	0.9738
10	6.6972	0.0543	228	463	0.9744
12	6.6949	0.0539	324	651	0.9825
14	6.6664	0.0908	400	801	0.9587
16	6.6479	0.0904	400	817	0.9506
18	6.6607	0.0932	253	508	0.9381
20	6.6671	0.0970	296	596	0.9563

Table C.15: Numerical results for  $sl_{Thk} = 11$  mm, initial point B.

Offset	$G_{12}$	V	Iterations	Function Evaluations	Active Constraints
0	6.0609	0.0857	175	352	0.9550
2	6.0859	0.0539	237	482	0.9838
4	6.0896	0.0536	204	415	0.9844
6	6.0892	0.0529	202	405	0.9856
8	6.0861	0.0526	250	514	0.9775
10	6.0899	0.0523	267	541	0.9869
12	6.0879	0.0523	302	617	0.9825
14	6.0466	0.0912	251	506	0.9419
16	6.0570	0.0886	265	533	0.9656
18	6.0768	0.0904	196	397	0.9381
20	6.0603	0.0932	264	532	0.9594

Table C.16: Numerical results for  $sl_{Thk} = 12$  mm, initial point B.

Offset	$G_{12}$	V	Iterations	Function Evaluations	Active Constraints
0	5.4963	0.0879	170	343	0.8738
2	5.5800	0.0527	227	456	0.9838
4	5.5793	0.0521	199	399	0.9819
6	5.5516	0.0512	208	416	0.9869
8	5.5582	0.0508	213	435	0.9856
10	5.5629	0.0541	275	554	0.9394
12	5.5691	0.0538	394	790	0.9400
14	5.5424	0.0886	205	415	0.9456
16	5.5550	0.0867	218	439	0.9669
18	5.5693	0.0880	226	454	0.9331
20	5.5566	0.0912	245	490	0.9644

Table C.17: Numerical results for  $sl_{Thk} = 5$  mm, initial point C.

Offset	$G_{12}$	V	Iterations	Function Evaluations	Active Constraints
0	13.3972	0.1078	229	458	0.9487
2	13.4002	0.0707	201	408	0.9750
4	13.3961	0.0697	211	430	0.9762
6	13.3993	0.0694	198	410	0.9719
8	13.3813	0.0684	213	432	0.9819
10	13.3999	0.0683	240	488	0.9869
12	13.4004	0.0687	231	477	0.9812
14	13.4003	0.0702	400	801	0.9744
16	13.3256	0.1120	305	622	0.9637
18	13.2787	0.0997	345	699	0.9556
20	13.3999	0.1341	241	483	0.9375

Table C.18: Numerical results for  $sl_{Thk} = 6$  mm, initial point C.

Offset	$G_{12}$	V	Iterations	Function Evaluations	Active Constraints
0	11.1164	0.1004	211	422	0.9800
2	11.1707	0.0663	201	405	0.9738
4	11.1688	0.0655	201	413	0.9744
6	11.1684	0.0649	182	378	0.9750
8	11.1684	0.0643	209	418	0.9831
10	11.1736	0.0640	242	490	0.9875
12	11.1677	0.0645	178	373	0.9781
14	11.1683	0.0648	279	571	0.9831
16	11.1251	0.1115	285	580	0.9681
18	11.1153	0.1036	260	523	0.9506
20	11.1231	0.1266	259	524	0.9625

Table C.19: Numerical results for  $sl_{Thk} = 7$  mm, initial point C.

Offset	$G_{12}$	V	Iterations	Function Evaluations	Active Constraints
0	9.5316	0.0961	212	426	0.9712
2	9.5705	0.0629	205	418	0.9744
4	9.5642	0.0621	194	396	0.9750
6	9.5163	0.0653	214	445	0.9350
8	9.5720	0.0610	189	387	0.9775
10	9.5698	0.0607	204	413	0.9819
12	9.5676	0.0609	203	418	0.9812
14	9.5692	0.0614	259	526	0.9812
16	9.5261	0.1058	283	570	0.9644
18	9.5100	0.0979	274	551	0.9469
20	9.5299	0.1207	237	476	0.9600

Table C.20: Numerical results for  $sl_{Thk} = 8$  mm, initial point C.

Offset	$G_{12}$	V	Iterations	Function Evaluations	Active Constraints
0	8.3750	0.0939	192	390	0.9463
2	8.3718	0.0601	196	398	0.9775
4	8.3782	0.0594	193	390	0.9794
6	8.3773	0.0589	188	390	0.9756
8	8.3827	0.0585	181	400	0.9719
10	8.3792	0.0581	177	364	0.9781
12	8.3797	0.0583	192	427	0.9750
14	8.3798	0.0582	221	443	0.9844
16	8.3755	0.0589	384	792	0.9869
18	8.3213	0.0970	287	578	0.9544
20	8.3739	0.1172	243	487	0.9313

Table C.21: Numerical results for  $sl_{Thk} = 9$  mm, initial point C.

Offset	$G_{12}$	V	Iterations	Function Evaluations	Active Constraints
0	7.4211	0.0941	191	407	0.8838
2	7.4334	0.0578	213	470	0.9819
4	7.4397	0.0578	178	364	0.9712
6	7.4397	0.0567	210	425	0.9762
8	7.4370	0.0561	198	401	0.9806
10	7.4399	0.0563	278	569	0.9756
12	7.4404	0.0557	192	385	0.9812
14	7.4390	0.0559	241	490	0.9812
16	7.4405	0.0566	400	801	0.9894
18	7.3797	0.0923	400	834	0.9487
20	7.4377	0.1144	235	472	0.9213

Table C.22: Numerical results for  $sl_{Thk} = 10$  mm, initial point C.

Offset	$G_{12}$	V	Iterations	Function Evaluations	Active Constraints
0	6.6942	0.0865	205	429	0.9437
2	6.6984	0.0560	184	369	0.9769
4	6.6976	0.0553	213	426	0.9762
6	6.6990	0.0545	207	426	0.9825
8	6.6999	0.0542	252	514	0.9881
10	6.6997	0.0537	236	496	0.9875
12	6.6998	0.0541	220	442	0.9781
14	6.6984	0.0538	273	554	0.9856
16	6.6702	0.0972	259	520	0.9625
18	6.7008	0.1009	400	801	0.8769
20	6.6707	0.1100	248	497	0.9463

Table C.23: Numerical results for  $sl_{Thk} = 11$  mm, initial point C.

Offset	$G_{12}$	V	Iterations	Function Evaluations	Active Constraints
0	6.0888	0.0862	175	354	0.8988
2	6.0895	0.0542	199	398	0.9819
4	6.0853	0.0535	198	397	0.9806
6	6.0891	0.0530	137	300	0.9812
8	6.0540	0.0523	207	417	0.9806
10	6.0900	0.0523	237	481	0.9812
12	6.0880	0.0524	256	539	0.9825
14	6.0886	0.0552	310	666	0.9500
16	6.0617	0.0936	280	564	0.9594
18	6.0452	0.0903	232	470	0.9387
20	6.0085	0.1084	245	498	0.8912

Table C.24: Numerical results for  $sl_{Thk} = 12$  mm, initial point C.

Offset	$G_{12}$	V	Iterations	Function Evaluations	Active Constraints
0	5.5777	0.0827	176	354	0.9038
2	5.5799	0.0527	196	395	0.9838
4	5.5499	0.0518	213	427	0.9800
6	5.5800	0.0513	237	484	0.9862
8	5.5511	0.0510	234	472	0.9856
10	5.5806	0.0505	244	522	0.9906
12	5.5838	0.0556	256	513	0.9350
14	5.5798	0.0505	242	494	0.9900
16	5.5760	0.0924	252	506	0.9525
18	5.5768	0.0902	234	473	0.9294
20	5.5763	0.1048	200	404	0.9425

Table C.25: Numerical results for  $sl_{Thk} = 5$  mm, initial point D.

Offset	$G_{12}$	V	Iterations	Function Evaluations	Active Constraints
0	13.3994	0.1102	265	530	0.9050
2	13.3952	0.0728	400	801	0.9744
4	13.3959	0.0700	315	646	0.9781
6	13.3985	0.0889	351	709	0.9781
8	13.2664	0.5044	7	35	0.1656
10	13.4027	0.0791	400	803	0.9725
12	13.3655	0.0805	400	830	0.9762
14	13.3955	0.0822	400	807	0.9819
16	0.0000	0.0000	0	0	0.0000
18	13.4008	0.1001	264	530	0.9594
20	13.3390	0.1328	294	589	0.9575

Table C.26: Numerical results for  $sl_{Thk} = 6$  mm, initial point D.

Offset	$G_{12}$	V	Iterations	Function Evaluations	Active Constraints
0	11.1694	0.1046	235	471	0.9050
2	11.1719	0.0685	306	614	0.9762
4	11.1686	0.0658	330	665	0.9725
6	11.1146	0.0729	400	802	0.9788
8	11.1661	0.0726	288	585	0.9744
10	11.0283	0.4971	8	35	0.1756
12	11.1203	0.0976	281	573	0.9738
14	11.1174	0.0993	249	502	0.9825
16	11.1692	0.0794	400	801	0.9706
18	11.0965	0.0937	258	525	0.9525
20	11.1236	0.1249	276	555	0.9631

Table C.27: Numerical results for  $sl_{Thk} = 7$  mm, initial point D.

Offset	$G_{12}$	V	Iterations	Function Evaluations	Active Constraints
0	9.5759	0.1041	203	409	0.8575
2	9.5644	0.0651	284	573	0.9719
4	9.5686	0.0624	381	773	0.9712
6	9.3156	0.4903	7	37	0.2000
8	9.5684	0.0690	253	522	0.9712
10	0.0000	0.0000	0	0	0.0000
12	9.5696	0.0719	350	711	0.9781
14	9.5679	0.0739	400	804	0.9725
16	9.5643	0.0751	400	801	0.9812
18	9.5706	0.0859	400	813	0.9575
20	9.5262	0.1203	295	594	0.9563

Table C.28: Numerical results for  $sl_{Thk} = 8$  mm, initial point D.

Offset	$G_{12}$	V	Iterations	Function Evaluations	Active Constraints
0	8.3787	0.0964	214	429	0.9025
2	8.3760	0.0622	257	515	0.9756
4	8.3790	0.0592	381	767	0.9806
6	8.3819	0.0587	394	794	0.9788
8	8.3757	0.0663	396	810	0.9744
10	8.3776	0.0673	263	534	0.9738
12	8.3782	0.0687	316	642	0.9812
14	8.3805	0.0703	400	804	0.9769
16	8.3800	0.0718	400	817	0.9831
18	8.3234	0.0829	330	663	0.9706
20	8.2493	0.5019	7	35	0.1737

Table C.29: Numerical results for  $sl_{Thk} = 9$  mm, initial point D.

Offset	$G_{12}$	V	Iterations	Function Evaluations	Active Constraints
0	7.4400	0.0600	316	634	0.9500
2	7.4399	0.0597	250	508	0.9800
4	7.4363	0.0575	393	791	0.9756
6	7.4386	0.0565	211	431	0.9800
8	7.3984	0.0633	227	469	0.9806
10	7.4398	0.0646	258	519	0.9875
12	7.3934	0.0706	276	557	0.9244
14	7.3761	0.0753	378	764	0.9663
16	7.4295	0.0789	300	609	0.9644
18	7.3650	0.0897	236	476	0.9513
20	7.4398	0.1120	197	399	0.9513



Table C.30: Numerical results for  $sl_{Thk} = 10$  mm, initial point D.

Offset	$G_{12}$	V	Iterations	Function Evaluations	Active Constraints
0	6.6941	0.0605	310	620	0.9263
2	6.6998	0.0577	282	572	0.9812
4	6.6991	0.0552	347	709	0.9794
6	6.6992	0.0548	400	800	0.9794
8	6.6898	0.0613	249	505	0.9800
10	6.6722	0.0624	330	676	0.9794
12	6.6982	0.0638	365	734	0.9888
14	6.6710	0.0653	400	803	0.9800
16	6.6687	0.0884	266	537	0.9613
18	6.6949	0.0995	267	545	0.9131
20	6.5970	0.4930	7	35	0.1913

Table C.31: Numerical results for  $sl_{Thk} = 11$  mm, initial point D.

Offset	$G_{12}$	V	Iterations	Function Evaluations	Active Constraints
0	6.0695	0.0879	205	419	0.9125
2	6.0856	0.0559	284	571	0.9812
4	5.8629	0.4686	8	28	0.2369
6	6.0870	0.0586	288	577	0.9731
8	6.0907	0.0593	239	485	0.9812
10	6.0898	0.0607	309	618	0.9756
12	6.0848	0.0618	400	813	0.9888
14	6.0515	0.0881	241	492	0.9469
16	6.0583	0.0739	400	801	0.9725
18	6.0540	0.0876	312	633	0.9606
20	5.9961	0.4898	7	37	0.2037

Table C.32: Numerical results for  $sl_{Thk} = 12$  mm, initial point D.

Offset	$G_{12}$	V	Iterations	Function Evaluations	Active Constraints
0	5.5788	0.0891	172	348	0.8600
2	5.5800	0.0545	273	555	0.9800
4	5.3793	0.4651	8	28	0.2462
6	5.5800	0.0565	254	509	0.9838
8	5.5542	0.0578	265	543	0.9812
10	5.5800	0.0591	400	801	0.9744
12	5.4648	0.0869	234	469	0.8906
14	5.5429	0.0851	301	610	0.9456
16	5.5462	0.0857	232	468	0.9631
18	5.5469	0.0861	290	582	0.9606
20	5.5605	0.1038	286	579	0.9450

# References

- [1] M Bendsoe and Noboru Kikuchi. Generating optimal topologies in structural design using a homogenization method. *Comput Methods Appl Mech Eng*, 71:197–224, 1998.
- [2] O Sigmund. A 99 line topology optimization code written in Matlab. *Struct Multidisc Optim*, 21:120–127, 2001.
- [3] G. C. A. DeRose Jr. and A. R. Díaz. Solving three-dimensional layout optimization problems using fixed scale wavelets. *Computational Mechanics*, 25(2-3):274–285, 2000.
- [4] Rodger M. Walser. Electromagnetic metamaterials. volume 4467, page 1. International Society for Optics and Photonics, 7 2001.
- [5] Christopher Czech. Design of Meta-Materials Outside the Homogenization Limit Using Multiscale Analysis and Topology Optimization. *Ph.D. Dissertation, Clemson University*, pages 10–13, 2012.
- [6] Christopher Czech, Paolo Guarneri, James Gibert, and Georges Fadel. On the accurate analysis of linear elastic meta-material properties for use in design optimization problems. *Composites Science and Technology*, 72:580–586, 2012.
- [7] B Hassani and E Hinton. A review of homogenization and topology optimization I homogenization theory for media with periodic structure. *Computers & Structures*, 69(6):707–717, 1998.
- [8] B. Hassani and E. Hinton. A review of homogenization and topology optimization II analytical and numerical solution of homogenization equations. *Computers & Structures*, 69(6):719–738, 12 1998.
- [9] M. P. Bendsøe and O Sigmund. Material interpolation schemes in topology optimization. *Archive of Applied Mechanics (Ingenieur Archiv)*, 69(9-10):635–654, 1999.
- [10] Christopher Czech, Paolo Guarneri, and Georges Fadel. Meta-Material Design of the Shear Layer of a Non-Pneumatic Wheel Using Topology Optimization. In *Volume 3: 38th Design Automation Conference, Parts A and B*, page 893. ASME, 8 2012.
- [11] O. Sigmund and J. Petersson. Numerical instabilities in topology optimization: A survey on procedures dealing with checkerboards, mesh-dependencies and local minima. *Structural Optimization*, 16(1):68–75, 8 1998.

- [12] A. Díaz and O. Sigmund. Checkerboard patterns in layout optimization. *Structural Optimization*, 10(1):40–45, 8 1995.
- [13] James M. Gibert and Georges M. Fadel. Numerical Experiments in Using Voronoi Cell Finite Elements for Topology Optimization. In *Volume 5: 35th Design Automation Conference, Parts A and B*, pages 1307–1314. ASME, 2009.
- [14] Blaise Bourdin. Filters in topology optimization. Technical Report 9, 2001.
- [15] Tyler E. Bruns and Daniel A. Tortorelli. Topology optimization of non-linear elastic structures and compliant mechanisms. *Computer Methods in Applied Mechanics and Engineering*, 190(26-27):3443–3459, 3 2001.
- [16] Ole Sigmund. On the design of compliant mechanisms using topology optimization. *Mechanics of Structures and Machines*, 25(4):493–524, 1997.
- [17] Ole Sigmund. Morphology-based black and white filters for topology optimization. *Structural and Multidisciplinary Optimization*, 33(4-5):401–424, 2007.
- [18] J. K. Guest, J. H. Prévost, and T. Belytschko. Achieving minimum length scale in topology optimization using nodal design variables and projection functions. *International Journal for Numerical Methods in Engineering*, 61(2):238–254, 2004.
- [19] G Allaire and GA Francfort. A numerical algorithm for topology and shape optimization. In *Topology design of structures*, pages 239–248. Springer Netherlands, Dordrecht, 1993.
- [20] Anthony Drago and Marek Jerzy Pindera. Micro-macromechanical analysis of heterogeneous materials: Macroscopically homogeneous vs periodic microstructures. *Composites Science and Technology*, 67(6):1243–1263, 2007.
- [21] Alejandro R Diaz and Andre Benard. Designing materials with prescribed elastic properties using polygonal cells. *INTERNATIONAL JOURNAL FOR NUMERICAL METHODS IN ENGINEERING Int. J. Numer. Meth. Engng*, 57:301–314, 2003.
- [22] Fabian Lipperman, Moshe B. Fuchs, and Michael Ryvkin. Stress localization and strength optimization of frame material with periodic microstructure. *Computer Methods in Applied Mechanics and Engineering*, 197(45-48):4016–4026, 8 2008.
- [23] Z. Hashin and S. Shtrikman. A variational approach to the theory of the elastic behaviour of multiphase materials. *Journal of the Mechanics and Physics of Solids*, 11(2):127–140, 3 1963.
- [24] Graeme W. Milton and Andrej V. Cherkaev. Which Elasticity Tensors are Realizable? *Journal of Engineering Materials and Technology*, 117(4):483, 10 1995.
- [25] Z. Hashin and S. Shtrikman. A variational approach to the theory of the elastic behaviour of polycrystals. *Journal of the Mechanics and Physics of Solids*, 10(4):343–352, 3 1962.

- [26] Alejandro R. Diaz and Andr Bénard. Designing materials with prescribed elastic properties using polygonal cells. *International Journal for Numerical Methods in Engineering*, 57(3):301–314, 5 2003.
- [27] Niranjana Thyagaraja, Prabhu Shankar, Georges Fadel, and Paolo Guarneri. Optimizing the shear beam of a non-pneumatic wheel for low rolling resistance. In *Volume 5: 37th Design Automation Conference, Parts A and B*, pages 33–42. ASME, 1 2011.
- [28] Weihong Zhang, Gaoming Dai, Fengwen Wang, Shiping Sun, and Hicham Bassir. Using strain energy-based prediction of effective elastic properties in topology optimization of material microstructures. *Acta Mechanica Sinica/Lixue Xuebao*, 23(1):77–89, 2007.
- [29] DoITPoMS - TLP Library Mechanics of Fibre-Reinforced Composites - Stiffness of long fibre composites, 2008.